FE272911

NTIS
One Source. One Search. One Solution.

ALLOY CATALYSTS WITH MONOLITH SUPPORTS FOR METHANATION OF COAL-DERIVED GASES. FINAL TECHNICAL PROGRESS REPORT, SEPTEMBER 20, 1977-SEPTEMBER 20, 1980

BRIGHAM YOUNG UNIV.
PROVO, UT

05 OCT 1980

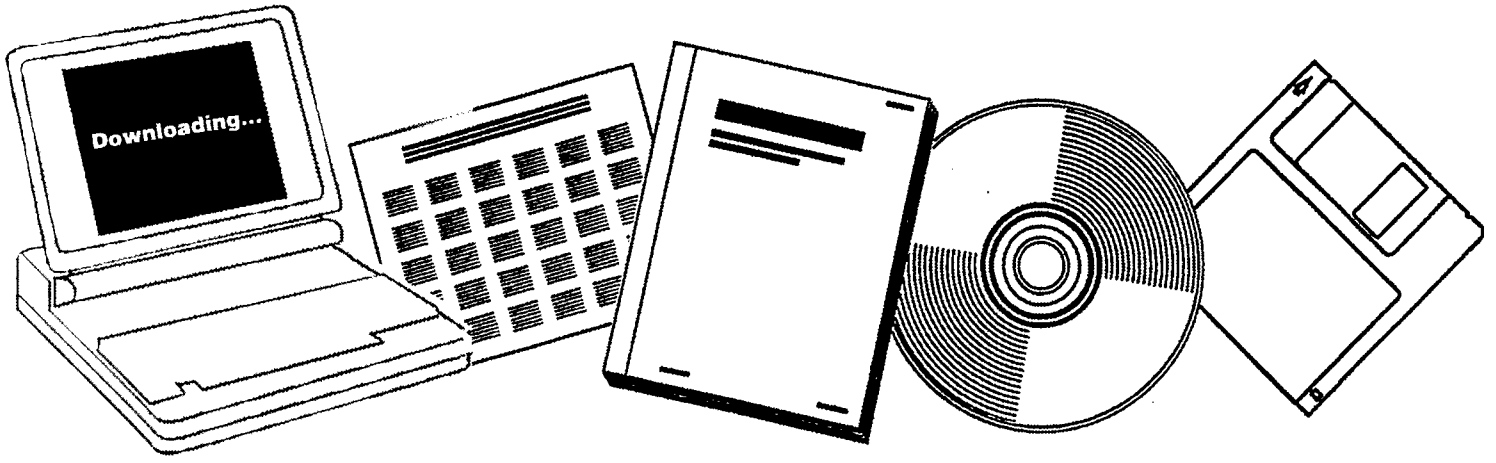

U.S. Department of Commerce
National Technical Information Service

One Source. One Search. One Solution.

NTIS

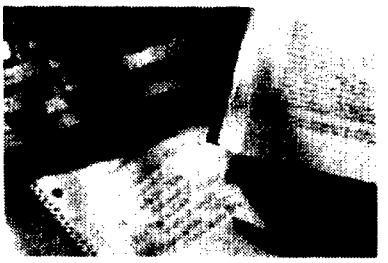

Providing Permanent, Easy Access to U.S. Government Information

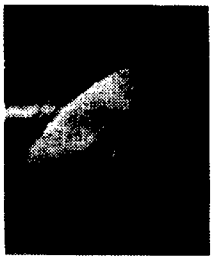

National Technical Information Service is the nation's largest repository and disseminator of government-initiated scientific, technical, engineering, and related business information. The NTIS collection includes almost 3,000,000 information products in a variety of formats: electronic download, online access, CD-ROM, magnetic tape, diskette, multimedia, microfiche and paper.

Search the NTIS Database from 1990 forward

NTIS has upgraded its bibliographic database system and has made all entries since 1990 searchable on **www.ntis.gov.** You now have access to information on more than 600,000 government research information products from this web site.

Link to Full Text Documents at Government Web Sites

Because many Government agencies have their most recent reports available on their own web site, we have added links directly to these reports. When available, you will see a link on the right side of the bibliographic screen.

Download Publications (1997 - Present)

NTIS can now provides the full text of reports as downloadable PDF files. This means that when an agency stops maintaining a report on the web, NTIS will offer a downloadable version. There is a nominal fee for each download for most publications.

For more information visit our website:

www.ntis.gov

U.S. DEPARTMENT OF COMMERCE
Technology Administration
National Technical Information Service
Springfield, VA 22161

FE-2729-11
Distribution Category UC-90c

FE272911

ALLOY CATALYSTS WITH MONOLITH SUPPORTS FOR METHANATION OF COAL-DERIVED GASES

Final Technical Progress Report
For Period September 20, 1977 to September 20, 1980

Calvin H. Bartholomew
Brigham Young University
Provo, Utah 84602

Date Published -- October 5, 1980

PREPARED FOR THE UNITED STATES
DEPARTMENT OF ENERGY

Under Contract No. EF-77-S-01-2729

FOREWORD

This report summarizes technical progress during a three-year study (September 20, 1977 to September 20, 1980) conducted for the Department of Energy (DOE) under Contract No. EF-77-S-01-2729. The principal investigator for this work was Dr. Calvin H. Bartholomew; Dr. Paul Scott and Mr. Henry Pennline were technical representatives for DOE.

The following students contributed to the technical accomplishments and to this report: Graduates - Erek Erekson, Ed Sughrue, Gordon Weatherbee, and Donald Mustard and Undergraduates - Kevin Mayo, John Watkins, Paul Moote, Clair James, and Richard Bowman. Karen Barrett, Janine Boyer, Lorelei Swingle and Victor Ramos provided typing and drafting services. The assistance of Dr. Phil Reucroft of the University of Kentucky and of Dr. Charles Pitt of the University of Utah in providing x-ray data and of Dr. Wilford Hess in obtaining transmission electron microscopy data is gratefully acknowledged.

TABLE OF CONTENTS

LIST OF TABLES

LIST OF TABLES (Cont.)

LIST OF FIGURES

LIST OF FIGURES (Cont.)

ABSTRACT

The activity, selectivity and stability of alumina-supported nickel and nickel bimetallics in methanation of CO was investigated. Support geometry, *in situ* H_2S poisoning tests, and carbon deposition tests initiated during the previous contract were completed. The results show that: (1) at high conversions and high through-put conditions monolithic supported catalysts are more active than pellet supported catalysts; (2) Ni-MoO_3 is more active and sulfur resistant than Ni, and (3) in carbon deposition tests Ni-Pt and Ni-Co maintain catalytic activity longer than Ni. High temperature reactor tests reveal that catalysts prepared in this laboratory are more active and in some cases more thermally stable than commercial catalysts and that carbon deposition is a major factor but not the only factor causing deactivation at high temperatures. A comprehensive investigation of methanation kinetics over nickel (and to a lesser extent ruthenium) and deactivation by carbon was conducted. The results provide significant insights into the mechanisms of the reaction and the deactivation by carbon. Effects of temperature, H_2S concentration, and other reaction variables on the sulfur poisoning rate of nickel during methanation were also investigated. The results provide a basis for modeling the deactivation process and predicting catalyst life. These and other significant results are presented and discussed. An account of technical communications with other workers and visits to other laboratories is also included.

I. OBJECTIVES AND SCOPE

A. Background

Natural gas is a highly desirable fuel because of its high heating value and nonpolluting combustion products. In view of the expanding demand for and depletion of domestic supplies of clean fuels, economic production of synthetic natural gas (SNG) from coal ranks high on the list of national priorities.

Presently there are several gasification processes under development directed toward the production of SNG. Although catalytic methanation of coal synthesis gas is an important cost item in each process, basic technological and design principles for this step are not well advanced. Extensive research and development are needed before the process can realize economical, reliable operation. Specifically, there appear to be important economical advantages in the development of more efficient, stable catalysts.

From the literature (1,2), three major catalyst problems are apparent which relate to stability: (i) sulfur poisoning, (ii) carbon deposition with associated plugging, and (iii) sintering. Our understanding of these problems is at best sorely inadequate, and the need to develop new and better catalyst technology is obvious. Nevertheless, there has been very little research dealing with new catalyst concepts such as bimetallic (alloy) or monolithic-supported catalysts for methanation. This study deals specifically with sulfur poisoning, carbon deposition, and the effects of support (monolith and pellet) geometry on the performance of alloy methanation catalysts.

B. Objectives

The general objectives of this research program are (i) to study the kinetics of methanation for a few selected catalysts tested during the earlier contract,(ii) to investigate these catalysts for resistance to deactivation due to sulfur poisoning and thermal degradation. The work is divided into five tasks.

Task 1. Characterize the surface, bulk and phase compositions, surface areas, and metal crystallite sizes for alumina-supported Ni, Ni-Co, Ni-MoO_3, Ni-Pt, Ni-Ru and Ru catalysts.

Task 2. Continue activity testing and support geometry studies of Ni and Ni-bimetallic catalysts initiated during the first two years. The tests include (i) conversion vs. temperature runs at low and high pressures, (ii) steady-state carbon deposition tests, (iii) *in situ* H_2S tolerance tests, and (iv) support geometry comparisons.

Task 3. Perform kinetic studies to find intrinsic rate data for alumina-supported Ni and Ru catalysts over a range of pressures and feed compositions. Detailed rate expressions for each catalyst will be determined at low and high pressure. Effectiveness factors

for monolithic and pellet-supported nickel on alumina will be obtained by comparing specific rates to those of finely powdered nickel on alumina.

Task 4. Determine H_2S poisoning rates, thermal deactivation rates, and operating temperature limits for Ni, Ni-Co, Ni-MoO_3, Ni-Pt, Ni-Ru, and Ru catalysts.

Task 5. Continue laboratory visits and technical communications. Interact closely with industrial and governmental representatives to promote large scale testing and development of the two or three best monolithic or pelleted alloy catalysts from this study.

C. Technical Approach

The technical approach was initially outlined in a statement of work dated May 20, 1977. The main features of that approach are reviewed here along with more specific details and modifications which have evolved as a result of progress.

Task 1: Catalyst Characterization

A comprehensive examination of alumina-supported Ni, Ni-Co, Ni-MoO_3, Ni-Pt, Ni-Ru, and Ru catalysts will be carried out to determine surface, bulk, and phase compositions, surface areas, and metal crystallite sizes using the following techniques: chemisorption, x-ray diffraction, chemical analysis, ESCA and SIMS spectroscopy, Auger spectroscopy and transmission electron microscopy.

Hydrogen chemisorption uptakes will be measured using a conventional volumetric apparatus before each reactor test and before and after deactivation tests. X-ray diffraction measurements will be carried out to determine the active metallic phases and metal crystallite size where possible. Selected "aged" samples from Task 4 will be analyzed (by x-ray, chemical analysis, and perhaps ESCA) to determine carbon content and possible changes in phase composition or particle size. Also, transmission electron micrographs will be made to determine particle size distributions for catalyst samples.

Task 2: Activity Testing and Support Geometry Design

Methanation activity and sulfur tolerance measurements initiated during the previous two years of study (3) will be completed. Pellet and monolithic alumina-supported Ni, Ni-Co, Ni-MoO_3, Ni-Pt, Ni-Ru, and Ru catalysts, (both high and low metal loadings) will be activity tested over a range of temperatures, pressures, and H_2S concentrations. A comparison of steady state conversions for nickel on different pellet and monolith supports of varying geometry will be made. Low pressure activity and sulfur tolerance tests will also be made for pelleted Co/Al_2O_3 and unsupported Ni-Co and Ni-Mo alloys. A summary of the

five test procedures and corresponding experimental conditions is listed in Table 1. The temperature conversion tests were completed during the previous contract period (3).

Task 3: Kinetic Studies

In order to carry out extensive kinetic studies of selected catalysts a new mixed flow reactor system will be constructed. This system will be capable of operation to 7500 kPa and 775 K and over a range of reactant compositions. The reactor for this sytem will be a "Berty" type constant volume mixed flow Autoclave reactor.

Intrinsic rate data will be obtained for alumina-supported Ni and Ru catalysts over a range of pressures and feed compositions in order to obtain detailed rate expressions at low and high pressures. To insure gradientless operation in the reaction-limited regime the rates will be measured at low conversions (0-5%) and low temperatures (525-700 K) for samples which have been crushed to obtain small particles.

Task 4: Degradation Studies

H_2S poisoning rates and thermal deactivation rates of Ni at low pressure will be studied using a new quartz reactor system. Quartz was selected as the material for the reactor because it must operate at high temperatures (750-1000 K) and in a corrosive (H_2S) environment. This reactor is also a constant volume mixed flow type reactor according to the design of Katzer (4). The quartz reactor system will be constructed during the early part of the contract period. Thermal deactivation at high pressures will be studied using a tubular stainless steel reactor previously discussed (3).

Operating temperature limits (and specific reaction rates within this range) and thermal deactivation rates near the upper use temperature (in the presence and absence of steam) will be determined for Ni, Ni-Co, Ni-MoO_3, Ni-Pt, Ni-Ru, and Ru catalysts. H_2S poisoning rates (at 525 K in the presence of 1 and 10 ppm H_2S in H_2) will be measured over a range of temperatures for nickel catalysts. The extent of carbon-carbide deposited in the thermal deactivation runs will be determined by chemical analysis and x-ray diffraction.

Task 5: Technical Interaction and Technology Transfer

The principal investigator will continue to communicate closely with other workers in methanation catalysis, continue distribution of quarterly reports to selected laboratories to stimulate interest and feedback, attend important coal and catalysis meetings, and visit other methanation laboratories.

Table 1

Description of Reactor Tests for Task 2

Test Procedures	Experimental Conditions
1. Temperature-Conversion Test: Measure CO conversion and methane production as a function of temperature, with and without 1% (by vol.) of steam present in the reactant mixtures.	475-675 K 140 kPa 30,000 hr^{-1} 1% CO, 4% H_2, 95% N_2 (dry basis)
2. Temperature-Conversion Test (high pressure): Measure CO conversion and methane production as a function of temperature at 2500 kPa.	475-675 K 2500 kPa 30,000 hr^{-1} 1% CO, 4% H_2, 95% N_2
3. Steady State (24 Hr.) Carbon Deposition Test: Measure CO conversion and methane production at 500 and 525 K (250,000 hr^{-1}) before and after an exposure of 24 hours at 675 K.	675 K (24 hrs.) 140 kPa 200,000-250,000 hr^{-1} 25% CO, 50% H_2, 25% N_2
4. In situ H_2S Tolerance Test: Measure intermittently the production of methane and hydrocarbons (by FID) during 24 hours exposure to feed containing 1 or 10 ppm H_2S using a glass reactor.	525 K 140 kPa 30,000 hr^{-1} 1% CO, 4% H_2, 95% N_2 1 or 10 ppm H_2S
5. Support Geometry Tests: Measure CO conversion and methane production as a function of temperature for the same Ni/Al_2O_3 catalyst supported on monoliths and pellets of varying geometries.	575-675 K 140 kPa 30,000 hr^{-1} 1% CO, 4% H_2, 95% N_2

He will also interact closely with Mr. A. L. Lee at the Institute of Gas Technology, with personnel at the Pittsburgh Energy Technology Center and with other coal gasification representatives to promote large scale testing and development of the two or three best catalysts from this study.

II. EXECUTIVE SUMMARY

Accomplishments and results are best summarized according to task:

Task 1. During the contract period several new catalysts were prepared: 12 pelleted, 62 cordierite monolithic, 9 alumina monolithic, and 16 Torvex monolithic catalysts with active metal combinations of Ni, Ni-Co, Ni-MoO_3, Ni-Pt, and Ni-Ru. Catalysts prepared during the previous contract period (3) were also further characterized as part of this task. Hydrogen chemisorption uptake, an indication of active metal surface area, was measured before and after reactor tests for all catalysts. Several catalysts were further characterized by chemical analysis, x-ray diffraction and electron microscopy, selected measurements of CO chemisorption on nickel catalysts as a function of temperature and before and after exposure to dilute H_2S were also performed.

The determination of nickel crystallite size and crystallite size distribution in Ni/Al_2O_3, Ni/SiO_2 and Ni/TiO_2 catalysts by means of hydrogen adsorption, transmission electron microscopy (TEM) and x-ray diffraction (XRD) was investigated. The results suggest that hydrogen adsorption is the most accurate, convenient, and inexpensive technique for measuring average crystallite diameter of Ni/Al_2O_3 and Ni/SiO_2 catalysts. TEM and XRD are the most reliable techniques for measuring nickel crystallite size in Ni/TiO_2, since nickel-support interactions appear to suppress H_2 adsorption. TEM micrographs of Ni/TiO_2 provide evidence of thin, raft-like nickel particles, suggesting an intimate metal/support contact. The adsorption stoichiometry of CO, formation of $Ni(CO)_4$ and effects of preadsorbed sulfur on the adsorptions of H_2 and CO on Ni/Al_2O_3 were also studied. Adsorption of H_2 is decreased in proportion to the fraction of nickel surface covered by sulfur while CO adsorption is <u>increased</u> presumably due to formation of $Ni(CO)_4$.

Task 2. An investigation of carbon formation on nickel and nickel bimetallic catalysts during methanation and its effects on catalyst activity showed that Ni/Al_2O_3 loses 20-60% of its activity within 10-15 hours at 675-700 K, H_2/CO = 2 and high space velocities. Ni-Pt and Ni-Co are significantly more resistant to deactivation by carbon under these conditions. Ni-Mo, however, is highly susceptible to deactivation, losing essentially all activity within 10-15 hours of treatment.

The effects on methanation activity of poisoning the same catalysts with 10 ppm H_2S during reaction were also investigated. All of the catalysts were compleletely deactivated within 2-3 days. Nevertheless all of the catalysts remained active longer than expected on the basis of breakthrough calculations, suggesting that a significant portion of the gas phase H_2S was not adsorbed possibly due to competitive adsorption of reactants.[2] Ni-Mo was found to be significantly more sulfur

resistant than nickel and other nickel bimetallic catalysts. Attempts to regenerate with H_2 and O_2 were not successful.

Support geometry studies were performed on nickel catalysts to compare pellets with various monolith configurations. In these tests at high through-put conditions, monolithic catalysts were significantly more active for methanation than the catalyst pellets. The significantly better performance of monolith catalysts is probably a result of its superior effectiveness for pore diffusion and external mass transport by diffusion. The substantially lower pressure drop through the monolithic catalyst enables it to be operated at much higher space velocities. Accordingly, a reactor containing monolithic catalysts would be significantly smaller than a corresponding pellet reactor, resulting in a substantial savings in capital investment. The low pressure drop could be translated into a significant savings in operating cost.

Task 3. A novel catalyst-reactor combination was developed for transport-free kinetic studies and was subsequently applied to the study of CO methanation kinetics on nickel over a wide range of experimental conditions. A Berty internal recycle reactor system complete with mass flow metering devices and chromatographic analysis was designed and constructed. The Berty internal recycle reactor was chosen to minimize interphase transport while thinly coated monolithic catalysts were chosen to reduce pore diffusional resistance.. The results of the kinetic study reveal significant changes in CO and H_2 concentration dependencies and activation energy with temperature, suggesting the need for a complex rate expression. A complex "shifting order" rate expression derived from a sequence of steps involving CO dissociation and hydrogenation of carbon was found to be consistent with the kinetic data from this study and was also found to successfully correlate kinetic data reported in previous studies.

A one-dimensional mathematical model describing the methanation reaction on monolithic nickel catalysts was also developed. The model successfully predicts conversion-temperature behavior in good agreement with experimental data. It can be used to predict temperature and concentration gradients through a monolithic catalyst bed and the effects of catalyst surface area on the conversion-temperature behavior.

Task 4. Thermal degradation studies were conducted on nickel and nickel bimetallic methanation catalysts under conditions representative of high temperature methanation. All catalysts were observed to lose activity above 723 K as a result of sintering and/or carbon deposition. Ni/Al_2O_4 and $Ni\text{-}MoO_3/Al_2O_3$ were the most thermally stable, even in comparison to commercial catalysts. In a long term test of Ni/Al_2O_3 at 773 K under carbon depositing conditions, the accumulated carbon plugged the reactor, causing catastrophic failure after only 17 hours. Addition of steam prevented this problem but resulted in increased production of CO_2 and decreased production of CH_4.

The kinetics of deactivation of Ni and Ru by carbon during methanation were also investigated using the same recycle reactor system. Rates of deactivation were found to be rapid above 550 K in both catalyst systems; the dependence of the rate on CO concentration was found to be approximately first order and on H_2 concentration -0.3 to -0.5 order in the case of nickel. The activation energy for deactivation was found to be close to that observed for conversion of atomic to polymeric, filamentous carbon.

The effects of H_2S concentration, temperature and other experimental variables on the rates of poisoning of nickel by H_2S during methanation were investigated using quartz and Pyrex glass reactor systems and a flame photometric detector. The results indicate a complex relationship among the rates of poisoning and experimental variables such as concentration and temperature. Since the stoichiometry of deactivation changes with temperature and H_2S concentration the modeling of the deactivation process and prediction of catalyst life is a difficult problem, but is nevertheless possible under limited conditions.

Task 5. During the contract period a significant effort was made to communicate with other laboratories doing similar work and to publish or present the results of our work. For example, the principal investigator visited 14 other laboratories and hosted 22 visitors. Thirteen papers were presented at regional and national meetings while four seminars were presented at other universities and companies. Six journal articles were published or accepted for publication, one was submitted for publication and six more are in preparation. Catalyst samples were submitted to three companies for bench scale evaluation in methanation processes.

Ten chemical engineering students were supported, trained, and educated as part of the contract work. Two received Ph.D. degrees and three M.S. degrees.

III. DETAILED DESCRIPTION OF TECHNICAL PROGRESS

Task 1: Catalyst Characterization

1. Catalyst Preparation

Compositions and codes for catalyst prepared in this study are listed in Table 2; they were prepared using impregnation techniques similar to those previously reported (3). Typically this involved impregnation to incipient wetness of the support (precalcined at 873 K) followed by drying at 373 K and direct reduction in flowing H_2 at 450°C for 12-16 hours according to a previously described temperature schedule (3). However, in the case of those catalysts to be tested at high temperatures (see Task 4), the Kaiser SAS 5x8 mesh alumina pellets were calcined 3 hours at 1075 K before impregnating with aqueous solutions of the nitrate salts.

Since chloride ions act to poison the methanation reaction, Ni-Ru and Ni-Pt pellet catalysts were prepared from chloride-free salts. The Ni-Ru catalyst preparation and the preparation of the impregnating solution for Ni-Pt were described earlier (7). The Ni-Pt catalyst was calcined in air for three days at 423 K and one day at 473 K. During reduction, a very slow temperature ramp was used where the catalyst remained below 473 K for ten hours. The temperature was then slowly raised to 673 K and held there for ten hours.

Ni/Al_2O_3 washcoated monolithic (cordierite) catalysts were prepared according to procedures described earlier (3). Pure alumina monoliths were obtained from Corning Glass Works and prepared similarly to cordierite monoliths (5). Several Torvex Ceramic Honeycombs (DuPont Co.) were also prepared in similar fashion. Some of these had an activated alumina washcoat applied by the manufacturer; alumina washcoat was applied to the rest (6,7). Instabilities of the washcoats at high metal loadings were noted in our second quarterly report (6). To avoid this problem, monolithic catalysts containing low nickel loadings and Al_2O_3 washcoatings of 10 wt.% or less were prepared and used in subsequent studies.

2. Chemisorption

Hydrogen chemisorption measurements are summarized in Table 3. Catalyst samples used in high temperature reactor tests (upper operating temperature tests) generally had lower uptakes than fresh samples (see Table 3). This loss of adsorption capacity is due to both fouling by carbon and loss of metal area by sintering. In the tests involving steam the loss of adsorption capacity is probably mainly due to sintering. In tests in the absence of steam described under Task 4 some of the monolith and pellet samples disintegrated because of massive carbon deposition. Hydrogen chemisorption uptakes for these samples increased. This may be explained by surface restructuring and crystallite fracture during the carbon deposition process.

Table 2

Catalyst Codes and Compositions

Catalysts	Code	Composition	Comments
Ni/Al_2O_3	Ni-A-120	3% Ni	Pellets
Ni/Al_2O_3	Ni-A-121	6% Ni	Pellets
Ni/Al_2O_3	Ni-A-122	20% Ni	Pellets
$Ni\text{-}Co/Al_2O_3$	Ni-Co-A-102	3% Ni, 3% Co	Pellets
$Ni\text{-}Co/Al_2O_3$	Ni-Co-A-103	10% Ni, 10% Co	Pellets
$Ni\text{-}MoO_3/Al_2O_3$	$Ni\text{-}MoO_3$-A-105	10% Ni, 10% MoO_3	Pellets
$Ni\text{-}Ru/Al_2O_3$	Ni-Ru-A-108	2.5% Ni, 0.5% Ru	Pellets, Chloride free
$Ni\text{-}Pt/Al_2O_3$	Ni-Pt-A-101	15.7% Ni, 0.5% Pt	Pellets, Chloride free
$Ni\text{-}Pt/Al_2O_3$	Ni-Pt-A-102	2.5% Ni, 0.5% Pt	Pellets, Chloride free
$Ni/NiAl_2O_4$	Ni-NAL-100	15% Ni	Extrudates, nickel aluminate support
Ni/Al_2O_3	Ni-M-156-159	3% Ni, 10% Al_2O_3	Cordierite monolith with Al_2O_2 washcoat
Ni/Al_2O_3	Ni-M-160- to 167	~20% Ni	Cordierite monolith with alumina wash coat
Ni/Al_2O_3	Ni-M-169 to 174	~22% Ni	Cordierite monolith with alumina wash coat
Ni/Al_2O_3	Ni-M-175 to 181	~17% Ni	Cordierite monolith with alumina wash coat
Ni/Al_2O_3	Ni-AM-101 to 105	~29% Ni	Alumina monoliths 31 squares/cm^2
Ni/Al_2O_3	Ni-AM-201 to 204	~26% Ni	Alumina monoliths 36 triangles/cm^2
Ni/Al_2O_3	Ni-TM-110 to 113 150 to 152 310 to 315 350 to 357	~3% Ni	Torvex monoliths with alumina wash coat

Table 2 (Cont.)

Catalyst Composition Data

Catalysts	Code	Composition	Comments
Ni/Al_2O_3	Ni-A-123	4.3% Ni	Pellets
$Ni/NiAl_2O_4$	Ni-NAL-M-100 thru 103	30% Ni, 20% Al_2O_3	Cordierite monolith
$Ni/NiAl_2O_4$	Ni/NAL-101	30% Ni	Catapal extrudates
Ni/Al_2O_3	Ni-M-182 thru 187	3.0% Ni, 10% Al_2O_3	Cordierite monolith with Al_2O_3 washcoat
Ni/Al_2O_3	Ni-M-188 thru 191	0.5% Ni, 10% Al_2O_3	Cordierite monolith with Al_2O_3 washcoat
Ni/Al_2O_3	Ni-M-193	0.1% Ni, 2% Al_2O_3	Cordierite monolith with Al_2O_3 washcoat
Ni/Al_2O_3	Ni-M-194	0.1% Ni, 2% Al_2O_3	Cordierite monolith with Al_2O_3 washcoat
Ni/Al_2O_3	Ni-M-506	0.5% Ni, 10% Al_2O_3	Cordierite monolith with Al_2O_3 washcoat
Ni/Al_2O_3	Ni-M-508	0.5% Ni, 10% Al_2O_3	Cordierite monolith with Al_2O_3 washcoat
Ni/Al_2O_3	Ni-M-513 to 523	0.15% Ni, 2% Al_2O_3	Cordierite monolith with Al_2O_3 washcoat
Ni/Al_2O_3	Ni-M-531	0.5% Ni, 10% Al_2O_3	Cordierite monolith with Al_2O_3 washcoat
Ni/Al_2O_3	Ni-M-532	0.5% Ni, 10% Al_2O_3	Cordierite monolith with Al_2O_3 washcoat
Ni/Al_2O_3	Ni-M-533	0.5% Ni, 10% Al_2O_3	Cordierite monolith with Al_2O_3 washcoat
Ni/Al_2O_3	Ni-M-539	0.5% Ni, 10% Al_2O_3	Cordierite monolith with Al_2O_3 washcoat
Ni/Al_2O_3	Ni-M-552	0.1% Ni, 2% Al_2O_3	Cordierite monolith with Al_2O_3 washcoat

Table 3

Summary of Metal Surface Area Measurements Using H_2 Chemisorption at 25°C

Catalyst	Nominal Composition (wt.%)	Uptake (μmoles/gram)	Maximum Reactor (1) Temperature
Pellet Catalysts:			
Ni-A-114	14% Ni	211.1[a]	
Ni-A-117	15% Ni	151.0	
Ni-A-120	3% Ni	31.0[a]	
Ni-A-121	6% Ni	73.9[a]	
Ni-A-122	20% Ni	212.7[a]	
		209.8[b,h]	763 K
		175.5[b]	721
		172.8[b]	886
		157.0[c]	835
Ni-A-123	4.3% Ni	78.6	
Ni-Co-A-102	3% Ni, 3% Co	37.6[a]	
Ni-Co-A-103	10% Ni, 10% Co	117.4[a]	
		94.0[b]	725
		78.8[c]	825
Ni-MoO_3-A-105	10% Ni, 10% MoO_3	52.8[a]	
		46.6[b]	816
		58.2[c]	820
Ni-Pt-A-101	15.7% Ni, 0.5 Pt	211.4[a]	
		138.4[b]	820
		123.7[c]	825
Ni-NAL-100	15% Ni	29.0[a]	
		209.4[a,f]	
		162.3[b]	803
		184.5[c]	818
G-87P		138[a]	
		118.6[b]	800
		162.8[c]	822

Table 3 (Cont.)

Catalyst	Nominal Composition (wt.%)	Uptake (μmoles/gram)	Maximum Reactor (1) Temperature
Pellet Catalysts:			
MC-100		130.7[a] 178.7[b,h] 81.9[c]	 820 793
Ni-Co-A-100	10% Ni, 10% Co	107[a] 0[d] 4[e] 80[a,f] 134[a,g] 148[i] 70[i,j]	
Ni-Rh-A-100	2.5% Ni 0.5% Rh	19.0[a] 0[d]	
Ni-Pd-A-100	15% Ni 1% Pd	105[a,g] 99[a,g] 112[a,g]	
Ru-A-100	0.5% Ru	1.6	
Monolith Catalysts:			
Ni-AM-101	29.7% Ni	221.7[a]	
Ni-AM-102	27.8% Ni	196.0[a]	
Ni-AM-201	25.5% Ni	201.1[a]	
Ni-AM-203	25.5% Ni	179[a]	
Ni-AM-204	27.5% Ni	204.5[a]	
Ni-M-250	22.2% Ni	154.8[a]	
Ni-M-179	17% Ni	87.3[a]	
Ni-M-180	17% Ni	138.0[a] 84.0[c]	 818
Ni-M-156	3% Ni	46.0[a]	

Table 3 (Cont.)

Catalyst	Nominal Composition (wt.%)	Uptake (μmoles/gram)
Monolith Catalysts:		
Ni-M-157	3% Ni	38.2
Ni-M-158	3% Ni	38.2
Ni-M-159	3% Ni	41.6
Ni-TM-110	3% Ni	36.8[a]
Ni-TM-111	3% Ni	38.5[a]
Ni-TM-310	3% Ni	29.6[a]
Ni-TM-311	3% Ni	31.5[a]
Ni-TM-312	3% Ni	33.9[a]
Ni-TM-112	3% Ni	34.2[a]
Ni-TM-150	3% Ni	46.1[a]
Ni-TM-151	3% Ni	46.8[a]
Ni-TM-152	3% Ni	42.2[a]
Ni-TM-350	3% Ni	45.2[a]
Ni-TM-352	3% Ni	49.0[a]
Ni-TM-356	3% Ni	26.1[a]
Ni-TM-357	3% Ni	31.5
Ni-TM-113	3% Ni	36.9
Ni-TM-314	3% Ni	29.7
Ni-TM-315	3% Ni	30.2
Ni-M-183	3% Ni	39.6
Ni-M-184	3% Ni	39.0
Ni-M-188	0.5% Ni	7.8

Table 3 (Cont.)

Catalyst	Nominal Composition (wt.%)	Uptake (μmoles/gram)
Monolith Catalysts:		
Ni-M-193	0.1% Ni	2.2
Ni-M-194	0.1% Ni	2.0
Ni-M-506	0.5% Ni	8.8
Ni-M-508	0.5% Ni	8.1
Ni-M-513	0.15% Ni	3.7
Ni-M-515	0.15% Ni	4.4
Ni-M-516	0.15% Ni	3.2
Ni-M-531	0.5% Ni	10.1
Ni-M-532	0.5% Ni	12.7
Powders:		
Ni-A-120	3% Ni	24.9
Ni-A-120	3% Ni	29.0
Ni-Co-A-100 before poisoning	10% Ni, 10% Co	148.2[i]
Ni-Co-A-100 after poisoning		67.7[i]

(1) This column shows the maximum temperature in degrees Kelvin achieved during upper operating temperature limit tests.

[a] Bulk reduced
[b] Upper operating temperature limit tested without steam
[c] Upper operating temperature limit tested with steam
[d] Long term H_2S *in situ* poisoning tested
[e] Long Term H_2S *in situ* poisoning tested followed by CO and air regeneration
[f] Reduced an additional 2 to 4 hours
[g] Reduced an additional 10 to 15 hours
[h] Catalyst support disintegrated after reactor test
[i] Differentially reactor tested
[j] Presulfided

The adsorption stoichiometry of CO, the formation of $Ni(CO)_4$ and effects of preadsorbed sulfur on the adsorptions of H_2 and CO on Ni/Al_2O_3 were investigated (the former two effects over the range of temperature from 185 to 298 K). Adsorption of H_2 at 298 K is decreased in proportion to the fraction of the nickel surface covered with sulfur (8,9). Chemisorption of CO at 185-298 K, however, is increased in proportion to the sulfur present on the nickel surface (see Table 4) apparently due to the formation of $Ni(CO)_4$. Formation of $Ni(CO)_4$ is significant at 298 K but can be avoided by adsorbing CO at 273 K (see Table 5). In the presence of sulfur, however, formation of the tetracarbonyl occurs at significant rates even at 185 K. Details of this study were discussed in earlier reports (10-16) and in a paper presented at the 1980 ACS meeting in Houston (17).

3. Transmission Electron Microscopy and Metal Crystallite Size Measurements

Transmission electron microscopy (TEM) measurements of metal particle size in $Ni-MoO_3$-A-103, Ni-A-119, Ni-Co-A-100, Ni-A-121 and the Kaiser SAS alumina support were carried out early in the contract period (10). The average crystallite diameters determined from TEM are shown in Table 6 and compared with estimates from x-ray diffraction (XRD) and H_2 chemisorption measurements at 298 K (assuming $H/Ni_s = 1$). The particle size estimates by the three different techniques are generally in good agreement except in the case of $Ni-MoO_3$-A-103. The absence of an XRD pattern for Ni or Mo compounds suggests that very small metal particles (<3.0 nm) are predominant in the sample consistent with the TEM data. The larger than expected particle size estimate from H_2 adsorption suggests that an interaction of Ni and MoO_2 or the presence of MoO_x species at the surface of nickel crystallites lowers the adsorption of H_2 on some of the nickel sites.

During the latter half of the contract period the application of H_2 chemisorption, XRD line broadening and TEM to the determination of metal crystallite size and size distribution in Ni/SiO_2, Ni/Al_2O_3, and Ni/TiO_2 catalysts having wide ranges of nickel loadings and dispersions was investigated. The compositions and metal dispersions of these catalysts are listed in Table 7. From electron micrographs such as in Figures 1-3, crystallite size distributions such as in Figure 4 were determined. From crystallite size distributions, surface-mean and volume-mean diameters d_s and d_v were determined for comparison with estimates from hydrogen adsorption and XRD. The crystallite size estimates are compared in Tables 8-10. Average crystallite diameters estimated from H_2 chemisorption and TEM were found to be in very good agreement over wide ranges of metal dispersion and loading in the Ni/SiO_2 system and in good agreement for a 23% Ni/Al_2O_3; poor agreement was evident in the Ni/TiO_2 system, the results suggesting that H_2 adsorption was suppressed possibly by a strong interaction between the metal crystallites and the support. In the few samples where it was possible to obtain information from XRD, the estimates of crystallite diameter were generally in good or fair agreement with those from H_2 chemisorption or TEM. Electron micrographs of Ni/TiO_2 (see Figure 3)

Table 4. H_2 and CO Adsorption Uptakes and CO/H Ratios for Alumina-Supported Nickel before and After Presulfiding[a]

Catalyst	H_2 Uptake[b] (μmoles/g)	Temperature (K) of CO Adsorption	CO Uptake[c] (μmoles/g)	CO/H[d]
3% Ni/Al_2O_3				
Fresh	21	190	80	1.9
Presulfided	14	190	374	13
Fresh	31	273	121	2.0
Presulfided	23	273	950	20
Fresh	31	300	109	1.8
Presulfided	23[e]	300	315	6.8
Fresh[f]	41.5	273	3.6	3.8
Presulfided[g]	0	273	563	6.8

[a]Presulfided in 10 or 25 ppm H_2S/H_2 at 725 K at a space velocity of 2000 h^{-1} for 6.12 h.

[b]Total hydrogen uptake at 300 K and 13-53 kPa.

[c]Irreversible CO uptake at temperature shown and 13-53 kPa. Irreversible uptake is the difference between total uptake and that after evacuation at the adsorption temperature for 30 min., also corrected for adsorption on Al_2O_3.

[d]Molecules of CO adsorbed at the temperature indicated per H atom adsorbed at 300 K.

[e]The same sample was tested before and after poisoning at both 273 and 300 K. The value of 23.2 μmoles/g was determined after poisoning but before CO adsorption at either temperature. After CO adsorption measurements of the poisoned catalyst, the H_2 uptake was 8.0; the sample changed from black to grey, suggesting a significant loss of Ni via formation of the tetracarbonyl.

[f]Different catalyst batch than used in first 2 sets of runs.

[g]Catalyst was presulfided to saturation coverage of sulfur. Upon repetition of the CO adsorption measurement on the presulfided catalyst the uptake was only 35 μmoles/g; the catalyst color changed from black to nearly white.

Table 5. Analysis of 3% Ni/Al_2O_3 and Gas Phase After CO Adsorption at 273 K

	Solid Phase		Gas Phase	
Catalyst	Ni	S	Ni	S
Fresh	no loss	---	neg.	neg.
30% sulfided	60% loss	no loss	positive	neg.
Completely sulfided	95% loss	no loss	positive	neg.

Table 6

Comparison of Particle Sizes Calculated
from X-ray Line Broadening
Hydrogen Adsorption, and Electron Microscopy

Catalyst	X-ray plane	d particle (Å) X-ray	d particle (Å) H_2 Adsorption	d particle (Å) Electron microscopy
Ni-A-115	(200)	53.2	65.3	68
(25% Ni/Al_2O_3)	(200)	36.4		
Ni-A-114	(200)	32.3	46.4	53
Ni-Co-A-100	(200)	95.3	99.1	51
	(102)	77.7		
	(225) or (110)	88.8		
Ni-MoO_3-A-103	--	--	89.5	41

Table 7

Composition, Values of H_2 Uptake, Percent Reduction, and Percent Dispersion for Catalysts Studied

Catalyst and Pretreatment	Wt.% Ni	H_2 Uptake[a] (μmol/g)	% Reduction[b]	% Dispersion[c]
Ni/Al_2O_3[d]	15			
Fresh		188	84	17
Sintered				
in H_2 at 1023 K, 72 h		122	--	9.5
in 3% H_2O/H_2 at 1023 K, 13 h		121	--	9.5
Ni/Al_2O_3[d]	23	305	97	16
Ni/SiO_2[d]	2.7			
Fresh		85	71	51
calcined 573 K, 3 h		35	71	16
Ni/SiO_2[e]	3.6			
Fresh		81	71	37
Ni/SiO_2[e]	13.5			
Fresh		442	93	41
Sintered in H_2				
923 K, 50 h		252	--	22
973 K, 50 h		178	--	15
1023 K, 50 h		177	--	15
Ni/SiO_2[d]	15			
Fresh		217	90	19
calcined 773 K, 22 h		61	82	5.8

Table 7 (cont.)

Catalyst and Pretreatment	Wt.% Ni	H_2 Uptake[a] (μmol/g)	% Reduction[b]	% Dispersion[c]
Ni/TiO_2[d]	2.8			
Fresh		20	74	11
Ni/TiO_2[d]	15			
Fresh		49	90	4.3
Sintered 3 h at 1023 K in H_2		1	90	0.1

[a]Total H_2 uptake at 298 K.

[b]Percent reduction of nickel to the metal based on O_2 uptake at 725 K; in the case of Ni/TiO_2 measured by $Ni(CO)_4$ extraction.

[c]Calculated according to Equation 1 with % reduction taken into account.

[d]Prepared by impregnation.

[e]Prepared by controlled pH precipitation.

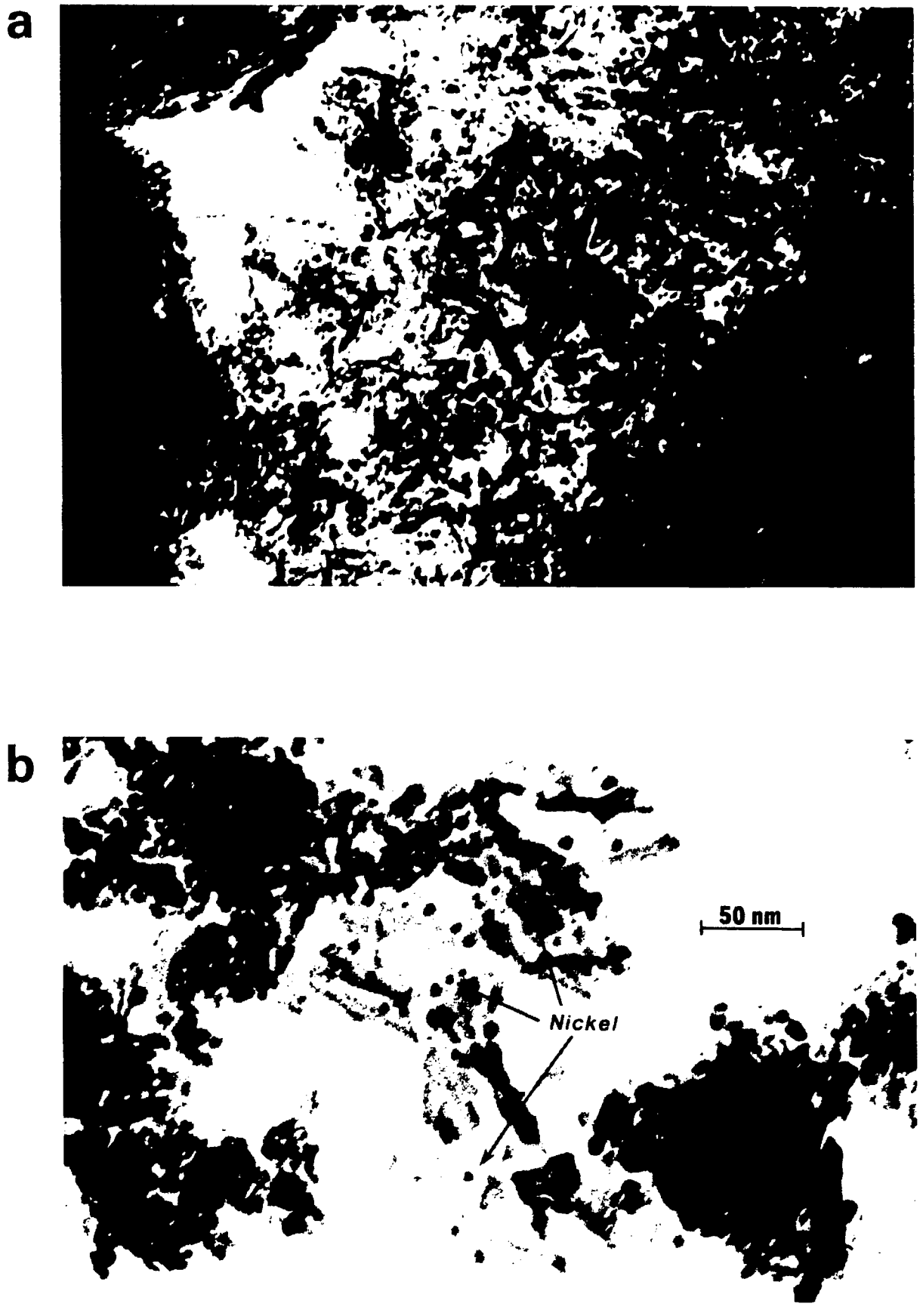

Figure 1. Electron Micrographs of (a) gamma alumina support and (b) 14% Ni/Al_2O_3.

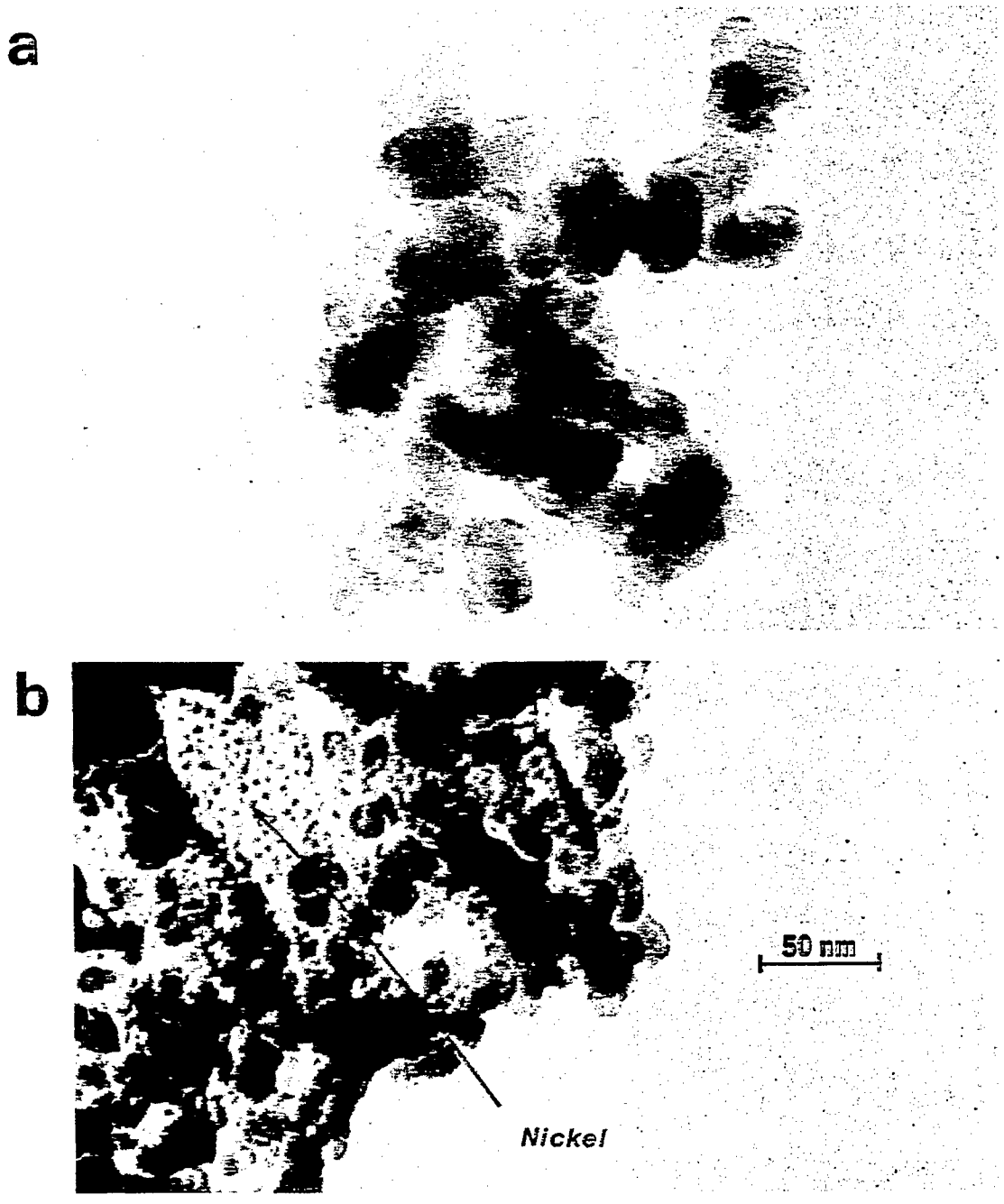

Figure 2. Electron Micrographs of (a) silica support and (b) 3.6% Ni/SiO_2.

Figure 3. Electron Micrograph of 15% Ni/TiO_2 showing Ni rafts.

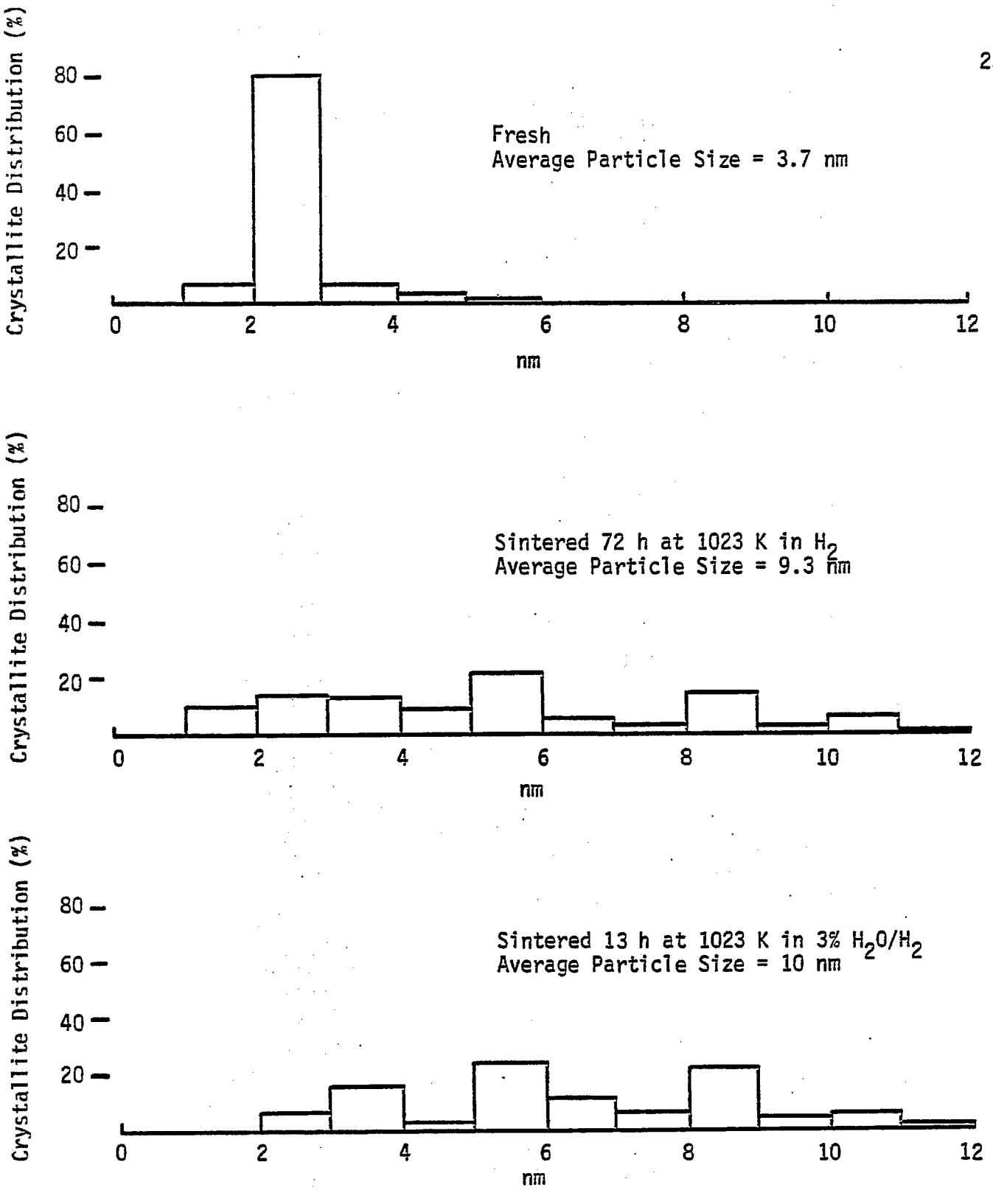

Figure 4. Crystallite Size Histograms of Fresh and Sintered 14% Ni/Al_2O_3.

Table 8

Comparison of Average Crystallite Diameters for Ni/Al_2O_3

Catalyst and Pretreatment	d_s (nm)[a] H_2 Ads.	d_s, d_v (nm)[b] TEM	d_v (nm)[c] XRD
15% Ni/Al_2O_3			
Fresh	5.6	3.7, 4.6	<3
Sintered[d]	10	9.3, 11	4.6
Sintered in H_2O[e]	10	10, 12	4.9
23% Ni/Al_2O_3	6.1	6.0, 6.4	6.8

[a]Surface averaged values calculated from Eqn. 2.

[b]Surface averaged values, volume averaged values from Eqns. 3 and 4.

[c]Volume averaged values from the Scherrer Equation (Ref. 18).

[d]72 h at 1023 K in H_2.

[e]13 h at 1023 K in 3% H_2O/H_2.

Table 9

Comparison of Average Crystallite Diameters for Ni/SiO_2 Catalysts

Catalyst and Pretreatment	d_s (nm)[a] H_2 Ads.	d_s, d_v (nm)[b] TEM	d_v (nm)[c] XRD
2.7% Ni/SiO_2			
Fresh	1.9	2.9	--
Calcined 3 h at 573 K	5.6	11	--
3.6% Ni/SiO_2			
Fresh	2.6	2.7, --	--
13.5% Ni/SiO_2			
Fresh	2.4	2.9, --	<3
Sintered			
923 K, 50 h	4.4	4.1, 4.5	2.8
973 K, 50 h	6.3	6.3, 7.1	5.4
1023 K, 50 h	6.3	6.9, 8.0	4.8
15% Ni/SiO_2			
Fresh	5.1	8.1, 9.4	12
Calcined 22 h at 773 K	17	19, 24	19

[a]Surface averaged values calculated from Eqn. 2.

[b]Surface averaged values, volume averaged values from Eqns. 3 and 4.

[c]Volume averaged values from Scherrer Equation (Ref. 18).

Table 10

Comparison of Average Crystallite Diameters for Ni/TiO_2 Catalysts

Catalyst and Pretreatment	d_s (nm)[a] H_2 Ads.	d_s, d_v (nm)[b] TEM	d_v (nm)[c] XRD
2.8% Ni/TiO_2			
Fresh	8.7	5.5, --	---
15% Ni/TiO_2			
Fresh	23	9.9, 11.5	15, 10
Sintered[d]	1060	32, 35	26, 21

[a]Surface averaged values calculated from Eqn. 2.

[b]Surface averaged and volume averaged values from Eqns. 3 and 4.

[c]Volume averaged values for the (111) and (220) crystal planes respectively calculated from the Scherrer Eqn. (Ref. 18).

[d]3 h at 1023 K in H_2.

provide evidence of electron transparent nickel crystallites having a raft-like structure. The presence of these nickel rafts provides further support for the hypothesis of strong metal-support interactions in Ni/TiO_2.

Further details of the particle size study are available in an M.S. thesis (18), were presented at the 1980 spring meeting of the California Catalysis Society (19) and will be published in the Journal of Catalysis (20).

4. X-Ray Diffraction Scans

Samples of Ni-A-116, Ni-Co-100 and $Ni-MoO_3$-102 were submitted to the University of Kentucky Institute of Mining and Metallurgical Research for automatic slow scan x-ray diffraction analysis. During the fourth quarter, data were obtained for Ni-Co-100 and $Ni-MoO_3$-102. In the case of Ni-Co-100, peaks for γ-Al_2O_3 and the metallic constituents were observed; unfortunately, the metal peaks were sufficiently broad and overlapping to prevent assignment of the peaks to either Ni, Co or Ni-Co. Thus, the data do not confirm nor rule out the possibility of alloy formation. The scan for $Ni-MoO_3$-102 revealed peaks assignable only to γ-Al_2O_3. Hence, the nickel crystallites are apparently masked by the Al_2O_3 and/or are x-ray amorphous as discussed above.

5. ESCA and Surface Analysis

Samples of Ni-Co and $Ni-MoO_3$ catalysts were submitted in 1978 to University Kentucky Institute of Mining and Metallurgical research and to Chevron Research. Because of other priorities the samples have not yet been analyzed. Toward the end of the contract period, the PI and Technical Project Officer agreed informally that the surface analysis work would be deemphasized in favor of emphasis on the kinetic, degradation, and TEM studies.

Task 2: Activity and Support Geometry Tests

1. Steady State Carbon Deposition Tests

The effects of carbon formation on methanation activity of nickel bimetallic catalysts were investigated during the first year of the contract (10). Carbon was deposited on these catalysts at 675-700 K, 1 atm, $H_2/CO = 2$ and space velocities of 80,000 to 200,000 h^{-1} over a period of 6-24 hours. Specific methanation activities were measured before and after carbon depositing treatments at 500-575 K, 1 atm, $H_2/CO = 4$ and space velocities of 100,000 h^{-1} in a fixed bed Pyrex reactor (3). The results (see Figure 5 and Table 11 and 12) show that Ni/Al_2O_3 loses 20-60% of its activity within 10-15 hours of treatment presumably due to encapsulation of metal crystallites (21). Platinum and cobalt promoted nickel are significantly more resistant to deactivation by carbon. However, $Ni-MoO_2$ (reduced $Ni-MoO_3$) is highly susceptible

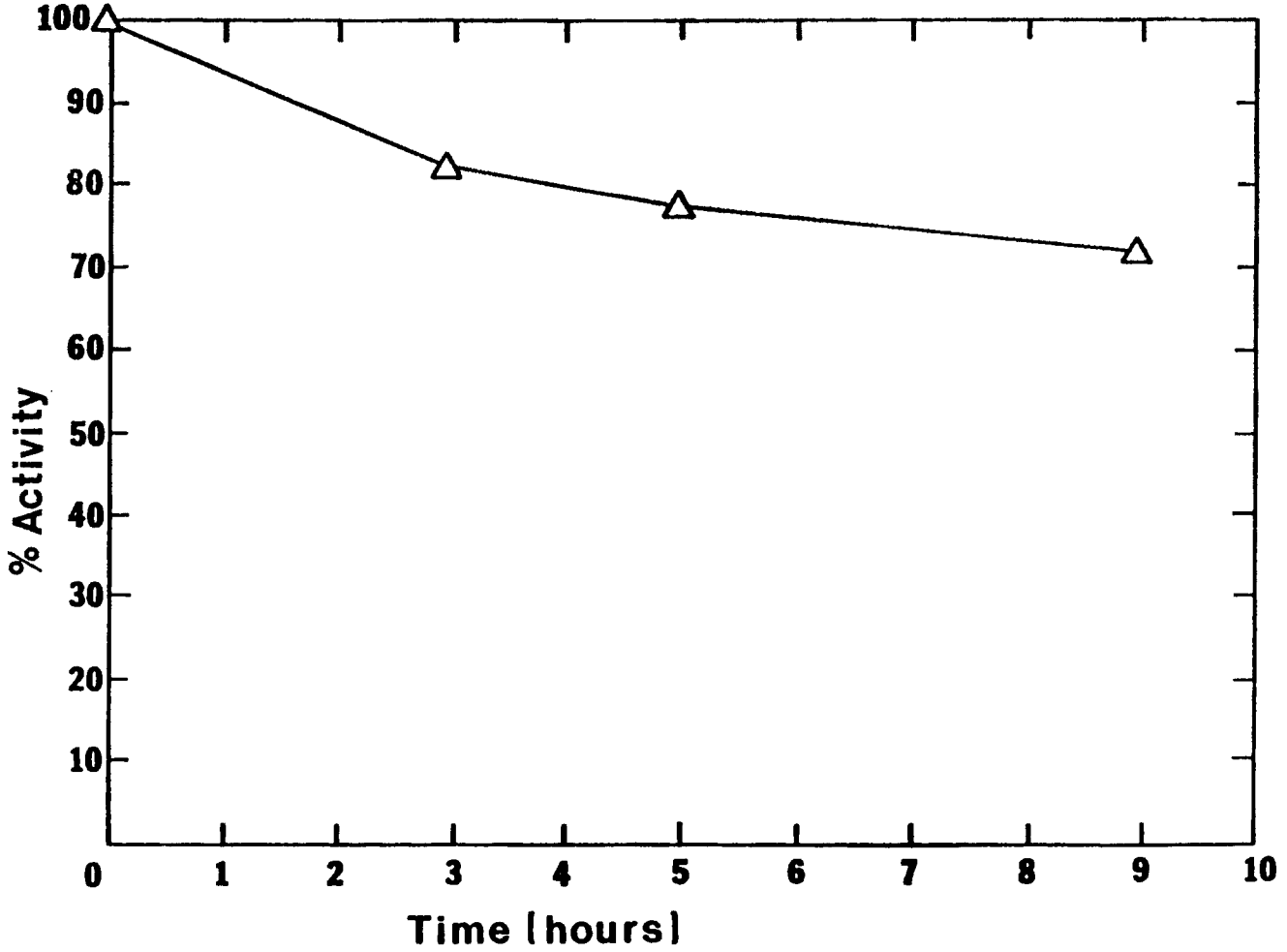

Figure 5. Carbon Deposition Deactivation Curve for 3% Ni/Al_2O_3 Powder. Activity measured at 110 kPa, 575 K, GHSV = 100,000 h^{-1}. Deactivation occurred at 110 kPa, 675 K, and GHSV = 250,000 h^{-1}

Table 11. Effects of Carbon Deposition[a] on Methanation Activity[b] of Alumina-Support Nickel Catalysts in Powder Form

Catalyst[c]	Treatment Time[d] Above 675 K (h)	CH_4 Turnover Number[e] of Fresh Catalyst x 10^3 (s^{-1})		Normalized Activity[f] of Fouled Catalyst	
		550 K	575 K	550 K	575 K
3% Ni[g]	9	21	40	0.63	0.71
	12	16	35	0.85	0.79
2.5% Ni/3% MoO_2	4	30	86	0.00	0.00
2.5% Ni/0.5% Ru	12	9.2	16	0.59	0.81
	12	9.8	20	0.61	0.68
1.5% Ni/1.5% Co	7	20	41	1.10	0.87
3% Ni/0.2% Pt	12	22	46	0.83	0.90

[a]Deposition treatment was carried out at 675-700 K, 100 kPa, $H_2/CO = 2$, GHSV = 165,000 h^{-1} in 25% CO, 50% H_2, 25% N_2 using 0.3 cm^3 samples.

[b]Specific activities (turnover numbers) were measured before and after deposition treatment at 550 and 575 K, 110 kPa, 100,000 h^{-1} in 1% CO, 4% H_2, 95% N_2.

[c]Weight percent metal on γ-Al_2O_3 (Kaiser) carrier.

[d]Time exposed to carburizing conditions (see a)

[e]Molecules methane produced per nickel site (measured by H_2 adsorption at 298 K) per second.

[f]Rate at the treatment time shown divided by the initial rate.

[g]Deposition treatment at 250,000 h^{-1}.

Table 12. Effects of Carbon Deposition[a] on Methanation Activity[b] of Alumina-Supported Nickel Catalysts in Monolithic Form

Catalyst[c]	Treatment Time[d] Above 675 K (h)	CH_4 Turnover Number[e] of Fresh Catalyst at 525 K x 10^3 (s^{-1})	Normalized Activity[f] of Fouled Catalyst at 525 K
6% Ni/20% Al_2O_3	4.5	37	0.37
	16.5		0.40
5% Ni/5% Co/20% Al_2O_3	4.3	18	0.75
	23.0		0.82
4% Ni/4% MoO_2/20% Al_2O_3	12.0	44	0.11
	22.8		0.04
10% Ni/1% Ru/19% Al_2O_3	21.5	2.4	0.57
	24.0		0.74
10% Ni/0.6% Pt/20% Al_2O_3	11.0	11	1.10
	17.0		0.99

[a]Deposition treatment was carried out at 675-700 K, 110 kPa, GHSV = 75,000 h^{-1} in 5% CO, 10% H_2, 85% N_2.

[b]Specific activities (turnover numbers) were measured before and after deposition treatment at 525 K, 110 kPa, GHSV = 80,000 h^{-1} in 1% CO, 4% H_2, 95% N_2.

[c]Weight percent metal and γ-Al_2O_3 (Kaiser) on cordierite monoliths (CELCOR-Corning Glass Works) having 31 square cells per cm^2.

[d]Time exposed to depositing conditions (see a).

[e]Molecules methane produced per nickel site (measured by H_2 adsorption at 298 K) per second.

[f]Rate at treatment time shown divided by initial rate for fresh catalyst.

to deactivation, losing essentially all of its activity within a few hours. The effects of reaction conditions, metal concentration and catalyst composition on the extent of deactivation and the effects of deactivation on catalyst strength were discussed in earlier reports (10) and in a journal publication (21). Apparently the choice of reaction conditions, particularly reactant composition, temperature and space velocity are critical in determining the extent, and rate of deactivation by carbon deposits. Formation of massive deposits of carbon during methanation may result in disintegration of catalyst particles or monoliths, presumably as internal stresses are produced by high concentrations of strong carbon filaments (21).

2. In Situ H_2S Tolerance Tests:

The effects of exposure to dilute H_2S during reaction on the methanation activity of alumina-supported nickel, cobalt and nickel bimetallic catalysts in powder, pellet and monolith form were also investigated during the first year of the contract (10). Early tests were conducted in a fixed bed, Pyrex reactor (3) at 523 K with a GHSV of 30,000 hr^{-1} and a reactant gas mixture of 95% N_2, 4% H_2, 1% CO and 10 ppm H_2S. Later tests were performed with 99% H_2, 1% CO and 10 ppm H_2S as reactants.

Activity (poisoned rate/fresh rate) versus time is plotted in smooth curves in Figures 6 and 7 for each of the catalysts. For the high loading catalysts the order of decreasing sulfur tolerance is apparently Ni, Ni-Co, Ni-Pt. For the 3-5 wt.% catalysts: Ni-MoO_3 > Ni = Ni-Rh > Ni-Ru. All of the catalysts are nearly completely deactivated within a 2-3 day period.

Nevertheless, all of the catalysts tested remained active longer than we had anticipated. For Ni-Rh-A-100 (2.5% Ni, 0.5% Rh) the original H_2 uptake was 19.0 micromoles/gram. Assuming 0.75 sulfur atoms adsorbed per surface Ni atom (22) and a GHSV of 30,000 hr^{-1} with 10 ppm H_2S it should take 1.0 hour to saturate the catalyst if there were no sulfur breakthrough. However, no loss of activity was observed after one hour and after 24 hours the high metal loading catalysts retained 20-30% activity. Analysis of the gas for H_2S downstream of Ni-Rh-A-100 sample revealed a gradual H_2S breakthrough. Apparently, equilibrium adsorption does not occur under these reaction conditions, possibly because of competitive adsorption of reacting species.

Figure 8 shows normalized activity plotted versus time divided by hydrogen uptake for powdered samples of 3% Ni/Al_2O_3, 20% Ni/Al_2O_3, 20% Co/Al_2O_3, 10% Ni/10% Co/Al_2O_3 and 10% Ni/10% MoO_3/Al_2O_3 tested in 99% H_2, 1% CO and 10 ppm H_2S. The results of normalizing time with respect to surface area are very interesting. The deactivation curves for 3 and 20% nickel are very nearly coincidental. The curves for 20% Ni and 20% Co are essentially the same and are represented by a single curve. The curve for Ni-Co shows slightly higher activity for values of the abscissa from 0.1 to 0.5. The activity of 10% Ni/10% MoO_3/Al_2O_3, however, is significantly higher for values of the abscissa

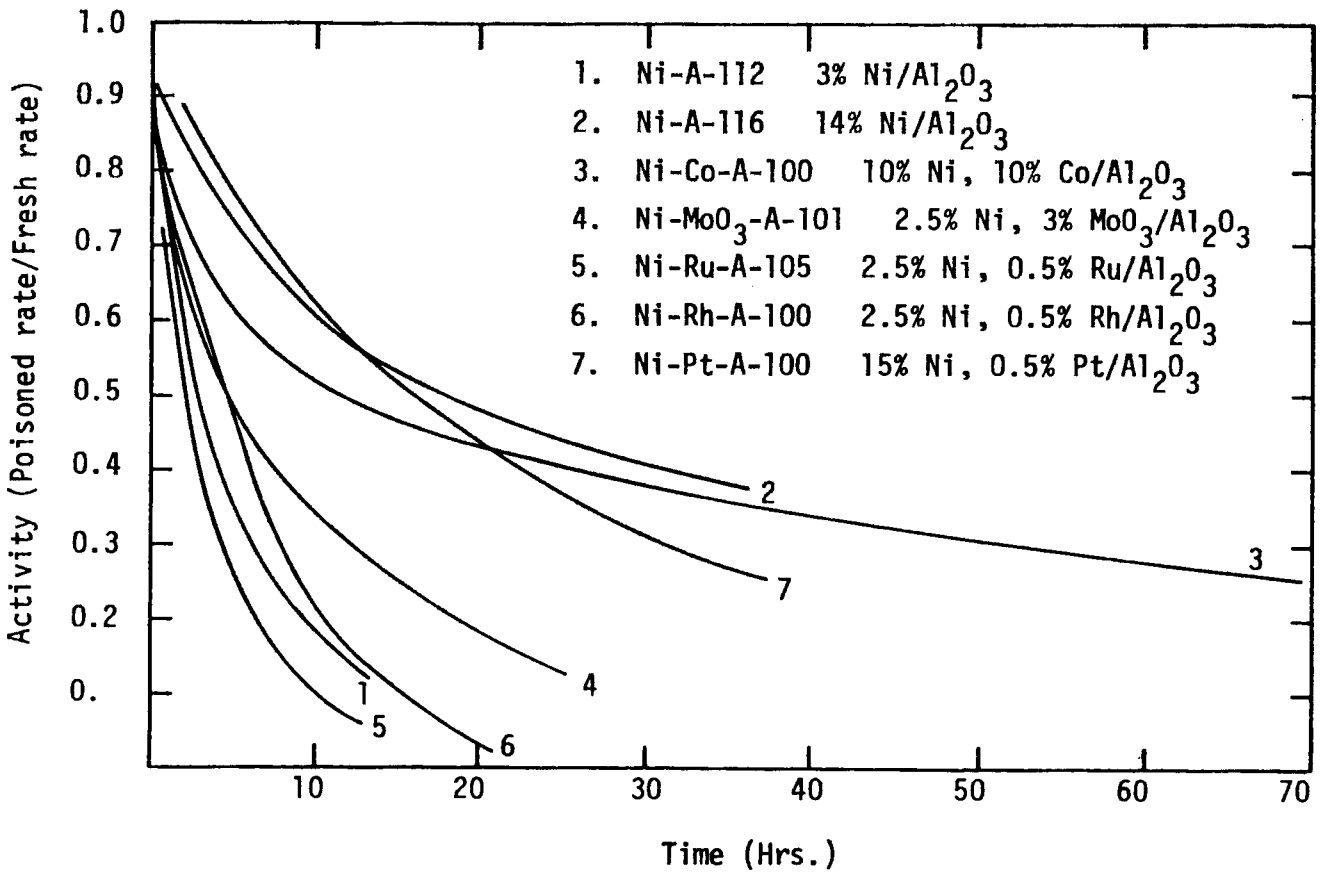

Figure 6. Smoothed Activity-Time Curves for Powdered Alumina-supported Nickel and Nickel Bimetallics during Exposure to 10 ppm H_2S in 1% CO, 4% H_2, and 95% N_2 (GHSV = 30,000 hr^{-1}, 100 kPa).

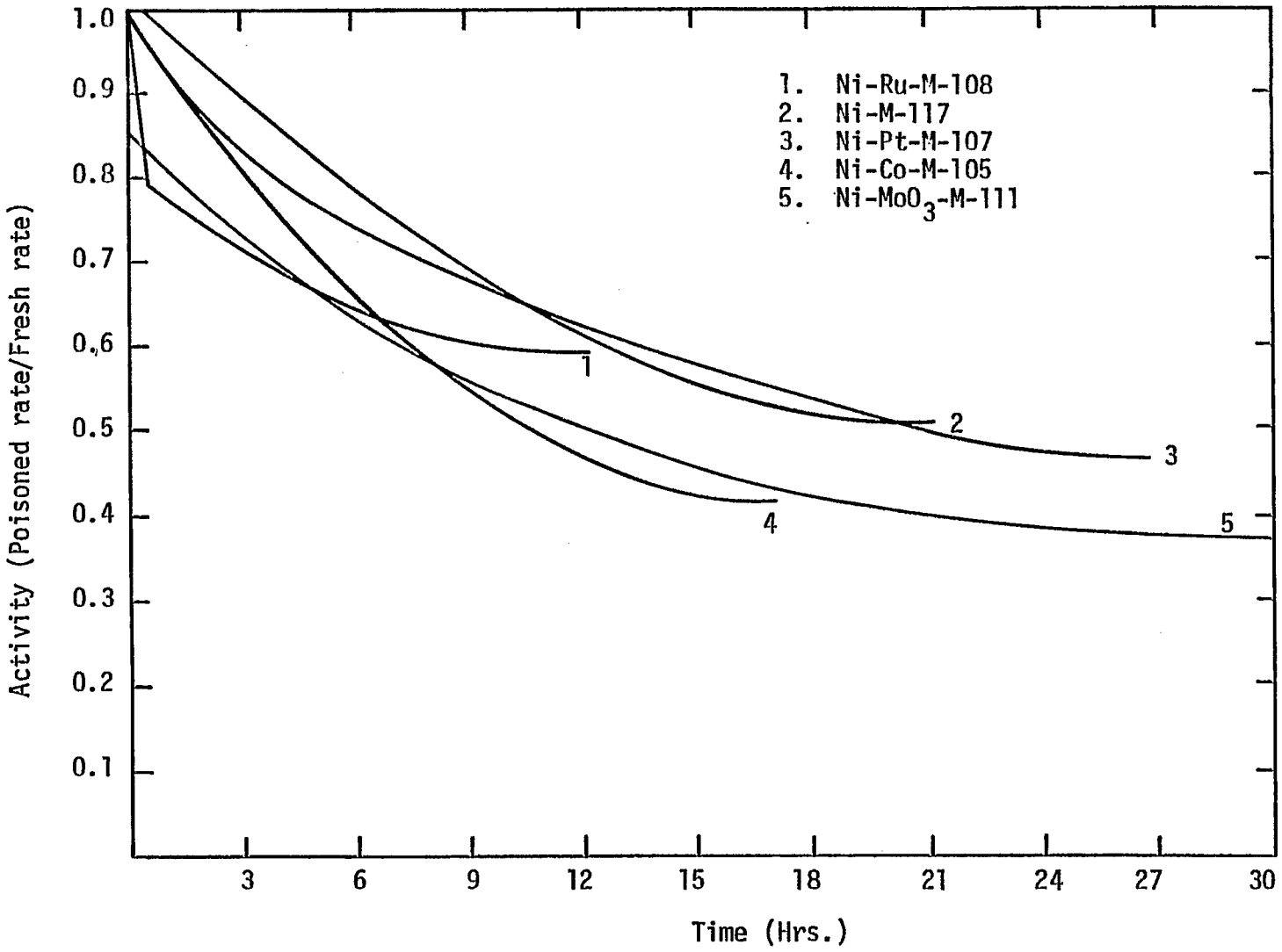

Figure 7. Smoothed Activity-Time curves for Monolithic-Supported Nickel and Nickel$_1$ Bimetallics during Exposure to 10 ppm in 1% CO, 4% H_2, and 95% N_2 (GHSV = 30,000 hr^{-1}, 100 kPa).

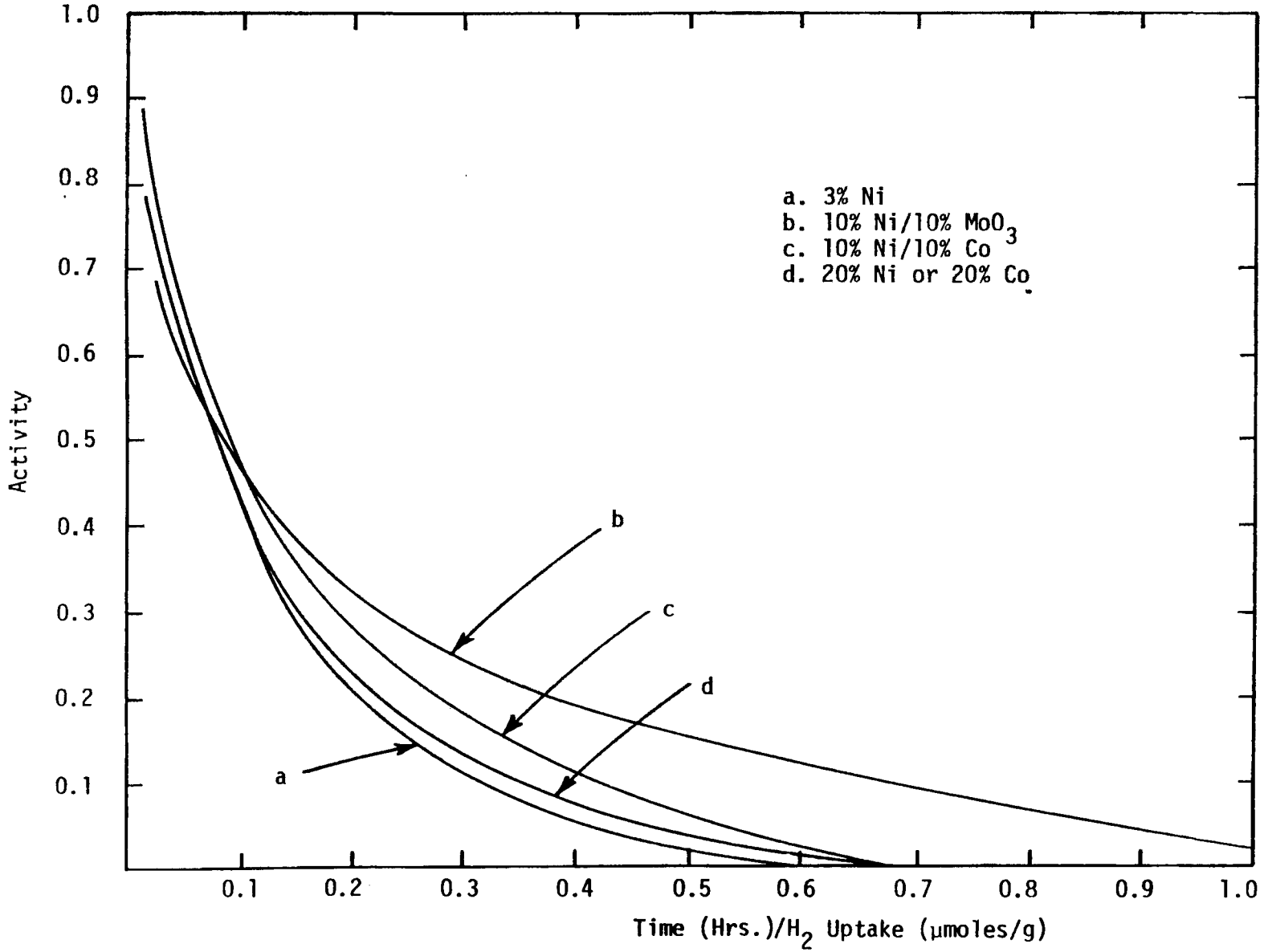

Figure 8. Activity normalized to hydrogen uptake versus time during reaction at 525 K, 110 kPa, and 30,000 hr^{-1}. Reaction mixture = 99% H_2, 1% CO, 10 ppm H_2S.

above 0.2. In other words Ni-MoO_3 is significantly more sulfur resistant than the other catalysts. The data in Table 13 suggest that monolithic catalysts are more sulfur resistant than their catalyst counterparts in powder form. Comparison of the data for 3% Ni in Figures 6 and 8 and Table 14 (two different reactant gas compositions) reveals that the rate of deactivation is higher for the run in the hydrogen rich reactant mixture (99% H_2), although the two curves evidence a similar exponential decay. This effect could be due to a higher rate of carbon gasification in the presence of the hydrogen rich mixture.

Attempts were made to regenerate the poisoned catalysts by heating them in pure H_2, CO, air or H_2/CO mixtures (Table 15). After treating catalysts in H_2 at 723 K for 12-24 hours, it was possible to recover 5-15% of the original H_2 uptake. In no case, however, was any methanation activity recovered. In fact, after treatment at 723 K the activity dropped to zero, even when samples were tested at elevated temperatures. Based upon our previous investigation of sulfur adsorption (22), a surface reconstruction or phase transformation of the adsorbed sulfur to a totally inactive nickel sulfide may be occurring. This change apparently occurs to a greater extent at higher temperatures. Treatment in H_2 at 528 K also resulted in further loss of activity, although samples were active when tested at high temperatures. A Ni-Co powder treated for 3 hours in CO, then 30 minutes in air followed by an 11 hour reduction in H_2 at 525 K showed an increase in activity (measured at 525 K) from 0.20 to 0.37. Unfortunately, further treatment in H_2 at 725 K caused complete loss of activity.

Further details of the in situ poisoning study were reported at the 1978 Meeting of the AIChE (23) and discussed in a Journal of Catalysis publication (24).

3. Activity Measurements of Fresh and Poisoned Catalysts

Both fresh and partially sulfided samples (treated in 10 ppm H_2S/H_2 at 723 K in a fixed bed) of Ni-Co-A-100 (powdered form) were differentially tested at 498, 523 and 548 K at a space velocity of 100,000 hr^{-1}. The results were reported and discussed in our first annual report (10). Because of the nonuniform nature of the sulfur deposition, the results obtained were not considered to be meaningful. A further series of tests was conducted for alumina supported Ni, Ni-Co, and Co catalysts of high metal loading (14-20%) in powder form in which the samples were poisoned in a uniform manner by 24 hour exposure to 10 ppm H_2S/H_2 in a fluidized bed reactor (10). The methane turnover number data obtained before and after poisoning at high space velocities and low conversions are shown in Table 16. Poisoned site activity ratios (PSAR values), ratios of the turnover number of the poisoned to that of the fresh catalyst are also listed. That the PSAR values for the uniformly poisoned catalysts are significantly less than one (on the order of 0.5) suggests that adsorbed H_2S interacts with the nickel surface to deactivate approximately two nickel sites for every adsorbed sulfur atom and/or restructures the surface such that the remaining sites are less active. The larger methane turnover

Table 13. Effects of H_2S Poisoning on Methanation Activity of Nickel and Nickel Bimetallic Catalysts (525 K, 110 kPa, GHSV = 30,000 h^{-1}, in 95% N_2, 4% H_2, 1% CO, 10 ppm H_2S).

Catalyst[a]	H_2 Adsorption[b] (μmoles/g cat.)	% CO Conversion (Fresh Catalyst)	Turnover Number[c] x 10^3 (Fresh Catalyst)	% Activity after 24 hours	% Activity at Time/H_2 Uptake[d] of 0.5 h/μmole H_2
3% Ni/P	35	7.5	5.1	<1	31
14% Ni/P	179	41	6.7	45	37
10% Ni/10% Co/P	107	29	6.5	40	40
2.5% Ni/3% MoO_3/P	19	4.8	10.8	13	54
2.5% Ni/0.5% Ru/P	52	7.8	5.3	<1	9
2.5% Ni/0.5% Rh/P	30	6.6	6.2	<1	34
15% Ni/0.5% Pt/P	130	24	6.2	38	35
12% Ni/M	75	93	23.4	50	50
5.5% Ni/5.5% Co/M	54	88	25.5	35	41
6% Ni/6% MoO_3/M	25	85	41.5	40	62
11% Ni/0.6% Pt/M	73	75	17.7	49	45
6% Ni/1.2% Ru/M	31	37	18.8	--[e]	59

[a] P denotes powdered alumina supported catalyst; M denotes Al_2O_3-coated monolithic support.

[b] Total adsorption measured at 298 K.

[c] Turnover numbers have units of molecules CH_4 per site per second. Conversions were very high for the monolithic catalysts (80-90%); however, effectiveness factors were nearly unity and mass transfer film resistance was negligible under these conditions. Turnover numbers for the fresh catalysts were determined before H_2S was added.

[d] H_2 uptake based on 1 cm^3 of sample and corrected for the appropriate density of each sample. Powder densities ranged from 0.36 to 0.56 g/cm^3; monolithic catalyst densities ranged from 0.6 to 0.8 g/cm^3.

[e] Data were taken over a period of 12 hours at which time 60% of the activity remained.

Table 14. Effects of H_2S Poisoning on Methanation Activity of Nickel and Nickel Bimetallic Catalysts (525 K, 110 kPa, GHSV = 30,000 h^{-1}, in 99% H_2, 1% CO, 10 ppm H_2S).

Catalyst[a]	H_2 Adsorption[b] (μmoles/g cat.)	% CO Conversion (Fresh Catalyst)	Turnover Number[c] x 10^3 (Fresh Catalyst)	% Activity after 24 hours	% Activity at Time/H_2 Uptake[d] of 0.5 h/μmole H_2
3% Ni/P	35	27	31	0	2.5
20% Ni/P	213	90	13	35	4
20% Co/P	76	90	35	12	4
10% Ni/10% Co/P	107	85	26	23	7
10% Ni/10% MoO_3/P	92	60	20	25	16
3% Ni/S	35	22	25	0	4.5

[a] P denotes powdered alumina supported catalyst; S denotes 0.32 cm Al_2O_3 spheres.

[b] Total adsorption measured at 298 K.

[c] Turnover numbers have units of molecules CH_4 per site per second. Conversions were very high (20-90%); however, effectiveness factors were nearly unity and mass transfer film resistance was negligible under these conditions.

[d] H_2 uptake based on 1 cm^3 of sample and corrected for the appropriate density of each sample. Powder densities ranged from 0.36 to 0.56 g/cm^3.

Table 15. Effects of Poisoning and Regneration Treatments on Normalized Activity

Catalyst[a]	Treatment	% Activity[b] after Treatment
14% Ni/P	36 h in reaction mixture[c] containing 10 ppm H_2S at 525 K	39
	2 h in pure H_2 at 725 K	0
20% Ni-Co/P	88 h in reaction mixture[c] containing 10 ppm H_2S at 525 K	20
	3 h in CO; then 30 min in air and 11 h in H_2 all at 525K	37
	1 h in H_2 at 725 K	0
	0.5 h in O_2 and 1 h in H_2 at 525 K	12
	0.5 h in H_2 at 725 K	0
12% Ni/M	27 h in reaction mixture[c] containing 10 ppm H_2S at 525 K	33
	3 1/2 h temperature ramp from 525 to 675 K and 2.5 h at 675 K in reactant mixture[c]	30
	30 h in H_2 at 675 K	22

[a] P denotes dered alumina supported catalysts; M denotes Al_2O_3-coated monolithic support.

[b] Percent of initial activity; i.e. normalized activity

[c] Reactant mixture contained 1% CO, 4% H_2, 95% N_2.

Table 16.

Specific Activity Data[a] Before and After Exposure[b] to 10ppm H_2S of Alumina-Supported Ni, Ni-Co and Co in Powder Form

Catalyst	% CO Conversion	% CH_4 Yield[c]	CH_4 Turnover No. X10^3 (sec^{-1})	Poisoned Site Activity Ratio[d]
At 500 K				
Ni-A-116 (14% Ni)				
fresh	4.04	71.5	2.4	0.42
poisoned	2.69	61.4	1.0	
Ni-Co-A-100 (10% Ni, 10% Co)				
fresh	4.46	61.2	6.0	0.68
poisoned	2.80	81.8	4.1	
Co-A-100 (20% Co)				
fresh	2.6	61.2	3.8	0.53
poisoned	2.2	55.8	2.0	
At 525 K				
Ni-A-116 (14% Ni)				
fresh	9.85	83.6	6.9	0.40
poisoned	6.28	74.2	2.8	
Ni-Co-A-100 (10% Ni, 10% Co)				
fresh	8.60	85.6	16.1	0.83
poisoned	8.44	89.7	13.4	
Co-A-100 (20% Co)				
fresh	5.91[e]	56.9	10.3	0.34
poisoned	3.25[f]	65.2	3.5	

[a]At 140 kPa, a space velocity of about 100,000 hr^{-1} in a gas mixture containing 1% CO, 4% H_2, 95% N_2.

[b]Exposure to 10ppm H_2S in a fluidized bed over a period of several hours sufficient to poison about 50% of the surface.

[c]Methane yeild is the fraction of converted CO which is transformed to methane.

[d]Turnover number for the poisoned divided by that for the fresh catalyst.

[e]Space velocity = 100,000 hr^{-1}

[f]Space velocity = 38,000 hr^{-1}

numbers and PSAR values for Ni-Co compared to Ni and Co, an obvious synergistic effect, provide indirect evidence of an intimate bimetallic interaction or perhaps an alloying effect.

4. Support Geometry Tests:

The catalytic activity and selectivity of pellet and monolithic supported Ni/Al_2O_3 for methanation of carbon monoxide were investigated during the first year of the contract period (10) to determine the role or support geometry in catalyst performance. Turnover numbers, CO conversion versus temperature data, and product distributions were measured at space velocities from 15,000 to 50,000 hr^{-1} and pressures of 140 to 2500 kPa using a fixed bed, stainless-steel reator (3). Figure 9 compares the conversion temperature characteristics of monolithic and pellet catalysts of equivalent nickel loading (vol. basis) under equivalent experimental conditions. The results of rate measurements over a range of conditions for a number of pellet and monolith catalysts are listed in Tables 17-20. These data show that monolithic supported nickel is significantly more active and selective for methane production at both low and high CO conversions compared to nickel catalysts beads and pellets. The higher activities at low conversion for monoliths may be a result of metal-support interactions since the monolith catalysts generally have higher effective nickel concentrations in the catalyst layer. Monolithic-supported methanation catalysts apparently operate with a higher effectiveness and rate of mass transfer at high conversion than do catalyst beads or pellets (see Tables 21 and 22). Because of its superior activity, selectivity and low pressure drop high space velocities, monolithic nickel appears to be the ideal catalyst for use in high throughput recycle methanators.

Additional details regarding the support-geometry investigation were provided in our first annual report (10), presented at the 1979 AIChE Meeting in Houston (25), and published in Chem. Engr. Communications (26).

Task 3: Kinetic Studies

Equipment

Construction and testing of the high pressure mixed flow reactor system was completed by the end of the 6th quarter. A schematic of this system is shown in Figure 10. Gases were stored in high pressure steel cylinders and delivered by means of regulators and mass flow controllers (Tylan). The mixed gases were passed through a heated mole sieve trap to remove iron carbonyl and a ZnO trap to remove sulfur. Steam was delivered by means of a high pressure bubbler described previously (16). The Berty reactor, a standard all stainless steel internal recycle reactor, was obtained from Autoclave Engineers. Gases were analyzed by means of a Perkin-Elmer Sigma I gas chromatograph using an automatic sampling valve to take samples as often as every 5 to 6 minutes. CH_4 concentrations were determined by flame ionization detection while CO_2, H_2, N_2, CO, and CO_2 concentrations were determined

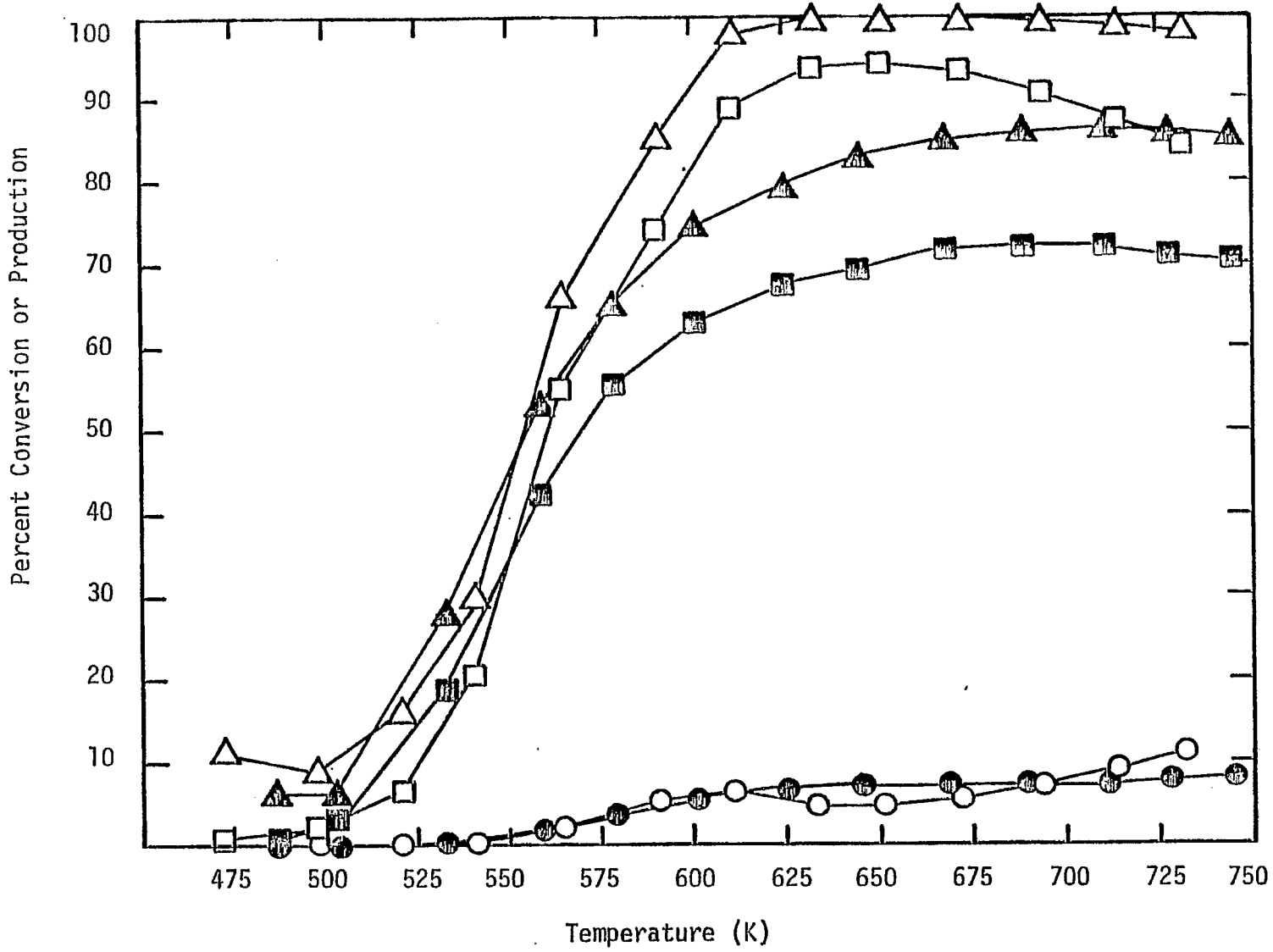

Figure 9. Conversion-temperature curves for 3% Ni/monolith with 46.5 squares/cm^2 (open symbols) and for 6% Ni/Al_2O_3 spheres (closed symbols) at 1000 kPa and GHSV = 50,000 hr^{-1} in 95% N_2, 4% H_2, 1% CO; △ % CO conversion, □ % CH_4 production, ○ CO_2 production.

Table 17. Low Conversion, Differential Reaction Rate Data at 140 kPa, 500 K and 525 K (30,000 hr^{-1} GHSV, 95% N_2, 4% H_2, 1% CO)

Catalyst	H_2 Uptake (μmole/gram)	% CO Conversion at 500 K	CH_4 Turnover Number[a] at 500 K	at 525 K	Apparent Activation Energy (kJ/mole)
a. Tests performed at 140 kPa					
3% Ni/10% Al_2O_3/Monolith[b]	32	6.2	5.2	12.8	82
6% Ni/20% Al_2O_3/Monolith[c]	66	10.6	3.8	11.5	110
11% Ni/19% Al_2O_3/Monolith[c]	105	14.4	2.7	9.2	106
12% Ni/20% Al_2O_3/Monolith[c]	76	13.4	3.7	9.8	106
19% Ni/20% Al_2O_3/Monolith[c]	75	10.9	4.5	12.5	91
20% Ni/20% Al_2O_3/Monolith[c]	65	13.5	4.3	11.7	87
25% Ni/Al_2O_3 Monolith[d]	179	15.4	3.0	7.4	79
3% Ni/Al_2O_3 spheres[e]	38	2.4	1.6	5.7	112
6% Ni/Al_2O_3 spheres	74	4.7	2.5	8.9	112
14% Ni/Al_2O_3 spheres	159	14.6	2.8	6.5	73
~40% Ni/Al_2O_3 (Girdler G-87)	167	14.7	1.8	4.4	77
25% Ni/Al_2O_3 Monolith-crushed	179	12.7	2.5	7.4	95
b. Tests performed at 1000 kPa					
3% Ni/10% Al_2O_3/Monolith[b]	46	15.6	15	47	106
6% Ni/Al_2O_3 spheres[f]	74	6.4	3.1±0.4	12.2±1.8	124±14
c. Tests performed at 2500 kPa					
6% Ni/20% Al_2O_3 Monolith[c]	66	43	9.3	40	131
3% Ni/Al_2O_3 spheres	38	11	6.5	27	105
14% Ni/Al_2O_3 spheres	187	49	4.7	11	90

[a] The units of turnover number are molecules/site sec x 10^3.

[b] 46.5 squares/cm^2.

[c] 31 squares/cm^2.

[d] Pure γ-Al_2O_3 monolith (Corning Glass Works) having 37 triangular channels per cm^2.

[e] All catalyst spheres shown in this table have an average diameter of 0.32 cm.

[f] Data shown are based on the average of 4 different samples. Deviations are expressed as standard deviations--about ± 10% for the turnover numbers.

Table 18. Conversion-Temperature and Activity Data for Methanation of CO over Pellet and Monolithic Nickel Catalysts at Low Pressure (140 kPa) in a reaction mixture containing 95% N_2, 4% H_2, 1% CO.

Catalyst	GSA (cm^2/cm^3)	Temp. for 90% CO Conv.	Yield[c] at 90% CO Conversion		Rate of Methane Production x 10^6 g moles/ cm^3 cat. sec
			CH_4	CO_2	
Tested at GHVS of 15,000 hr^{-1}:					- at 600 K -
19% Ni/19% Al_2O_3 31□/cm^2 monolith		555 K	0.91	0.07	1.8
3% Ni/Al_2O_3 0.32 cm spheres		600	0.78	0.21	1.3
14% Ni/Al_2O_3 0.32 cm spheres		543	0.84	0.11	1.6
~40% Ni/extrudites 1.0 cm x 0.32 cm diam. G-87 (Girdler)		500	0.83	0.14	1.45
Tested at GHVS of 30,000 hr^{-1}:					- at 600 K -
12% Ni/20% Al_2O_3/ monolith, 31 □/cm^2	12.5	584 K	0.87	0.12	2.9
25% Ni/Al_2O_3 monolith	14.9	570	0.80	0.11	2.9
14% Ni/Al_2O_3 0.32 cm spheres	8.7	638	0.82	0.16	2.2
~40% Ni/Al_2O_3 extrudates 1.0 cm x 0.32 cm diam. G-87 (Girdler)	11.3	668	0.77	0.17	2.2
Tested at GHSV of 50,000 hr^{-1}:					- at 700 K -
3% Ni/10% Al_2O_3/ monolith, 46.5 □/cm^2	17.8	625	0.70	0.19	4.0
3% Ni/Al_2O_3 0.32 cm spheres[a]	8.7	698 (58.9)[b]	0.64[b]	0.24[b]	2.3
6% Ni/Al_2O_3 0.32 cm spheres	8.7	685 (80.0)[b]	0.52[b]	0.24[b]	3.0

[a]Data shown for pellets are the average of 4 runs on 4 different samples of the same catalyst; reproducibility was within ±8%. For monolith samples, rates for 2-3 duplicate samples agreed within 5%.

[b]Sample did not reach 90% conversion at any temperature; the temperature at which maximum conversion was reached is listed along with maximum % conversion in parenthesis. The yields were calculated at maximum CO conversion.

[c]Yield is the fraction of converted CO appearing as a given product.

Table 19. Conversion-Temperature and Activity Data for Methanation of CO Over Pellet and Monolithic Catalysts at Intermediate Pressure (1000 kPa; 95% N_2, 4% H_2, 1% CO; GHSV = 50,000 hr^{-1})

Catalyst	GSA (cm^2/cm^3)	Temp for 90% CO Conv.	Yield at 90% CO Conversion		-- Rate of Methane Production at 650 K -- $gmoles/cm^3$ cat.sec. x 10^6
			CH_4	CO_2	
3% Ni/10% Al_2O_3/ Monolith, 31 □/cm^2	15.5[c]	540 K	0.90	0.07	5.8
3% Ni/10% Al_2O_3/ Monolith, 46.5 □/cm^2	17.8[d]	590 K	0.88	0.06	6.0
6% Ni/Al_2O_3 0.32 cm spheres[a]	8.7	719(88)[b]	0.83[b]	0.11[b]	4.4 ± 0.24

[a]Data shown are the average of 4 runs using 4 different samples of the same catalyst; for the rate based on volume the standard deviation was ± 0.24 x 10^{-6} $gmoles/cm^3$ cat.sec. or, in other words, ± 5.5%.

[b]The average CO conversion did not reach 90% at any temperature. The average temperature at which maximum CO conversion occurred and the maximum percent conversion (in parenthesis) are listed. The yields were calculated at maximum CO conversion.

[c]Estimated assuming 18% loss of GSA due to coating.

[d]Measured from enlarged photograph.

Table 20. Conversion-Temperature and Activity Data for Methanation of CO over Pellet and Monolithic Nickel Catalysts at High Pressure (2500 kPa; 95% N_2, 4% H_2, 1% CO)

Catalyst	Temperature for 95% CO Conversion	% Yield at 95% CO Conversion (CH_4)	% Yield at 95% CO Conversion (CO)	Rate of Methane Production at 600 K (gmoles per cm^3 per sec x 10^6)
(The following 3 tests were conducted at 30,000 hr^{-1} GHSV:)				
6% Ni/20% Al_2O_3 Monolith, 31 □/cm^2	518 K	99%	1%	3.6
3% Ni/Al_2O_3 spheres 0.32 cm diameter	615	96	3	2.9
14% Ni/Al_2O_3 spheres 0.32 cm diameter	548	97	1	3.4
(The following test was conducted at 50,000 hr^{-1} GHSV:)				
11% Ni/20% Al_2O_3 Monolith: 31 □/cm^2	588	97	1	5.4

Table 21. Experimental First Order Rate Constants and Theoretical Mass Transfer Coefficients

Catalyst	GSA (cm^2/cm^3)	1 atm and 700 K — Experimental[a] k_s (cm/sec)	1 atm and 700 K — Theoretical[b] k_c (cm/sec)	10 atm and 650 K — Experimental[a] k_s (cm/sec)	10 atm and 650 K — Theoretical[b] k_c (cm/sec)
3% Ni/10% Al_2O_3/ Monolith, 46.5□/cm^2	17.8	5.1	20	1.8-2.0[c]	2.0
3% Ni/Al_2O_3 0.32 cm spheres	8.7	2.7	14	--	--
6% Ni/Al_2O_3 0.32 cm spheres	8.7	5.0	14	0.79	1.2

[a]Calculated assuming first order and log mean concentration.

[b]Calculated from mass transfer correlations for packed beds and monoliths; k_c defined by $J_x = k_c(C_b - C_s)$ where J_x is the molar flux, C_b the bulk concentration and C_s the concentration at the particle surface.

[c]Very approximate estimate since CO conversion was nearly 100%.

Table 22. Values of the Thiele Modulus and Effectiveness Factor for Monolithic and Pellet Catalysts

Catalyst	Thiele Modulus[a] 500 K	525 K	Isothermal Effectiveness Factor 500 K	525 K	600 K[b]
a. Data at 140 kPa:					
3% Ni/10% Al_2O_3/ Monolith (46.5 □/cm^2)	0.064	0.072	1.00	1.00	---
20% Ni/20% Al_2O_3/ Monolith (31 □/cm^2)	0.133	0.22	1.00	0.98	0.88
3% Ni/Al_2O_3 0.32 cm spheres	0.30	0.48	0.95	0.89	---
14% Ni/Al_2O_3 0.32 cm spheres	0.74	1.28	0.77	0.58	0.09
b. Data at 1000 kPa:					
3% Ni/10% Al_2O_3/ Monolith (46.5 □/cm^2)	0.036	0.064	1.00	1.00	0.99
6% Ni/Al_2O_3 0.32 cm spheres	0.19	0.38	0.99	0.92	---

[a] Generalized Thiele Modulus (Ref. 23) based on 1/2 order kinetics of Vannice (Ref. 18).

[b] ΔT particle = 0.2 K; in other words, the particle is essentially isothermal.

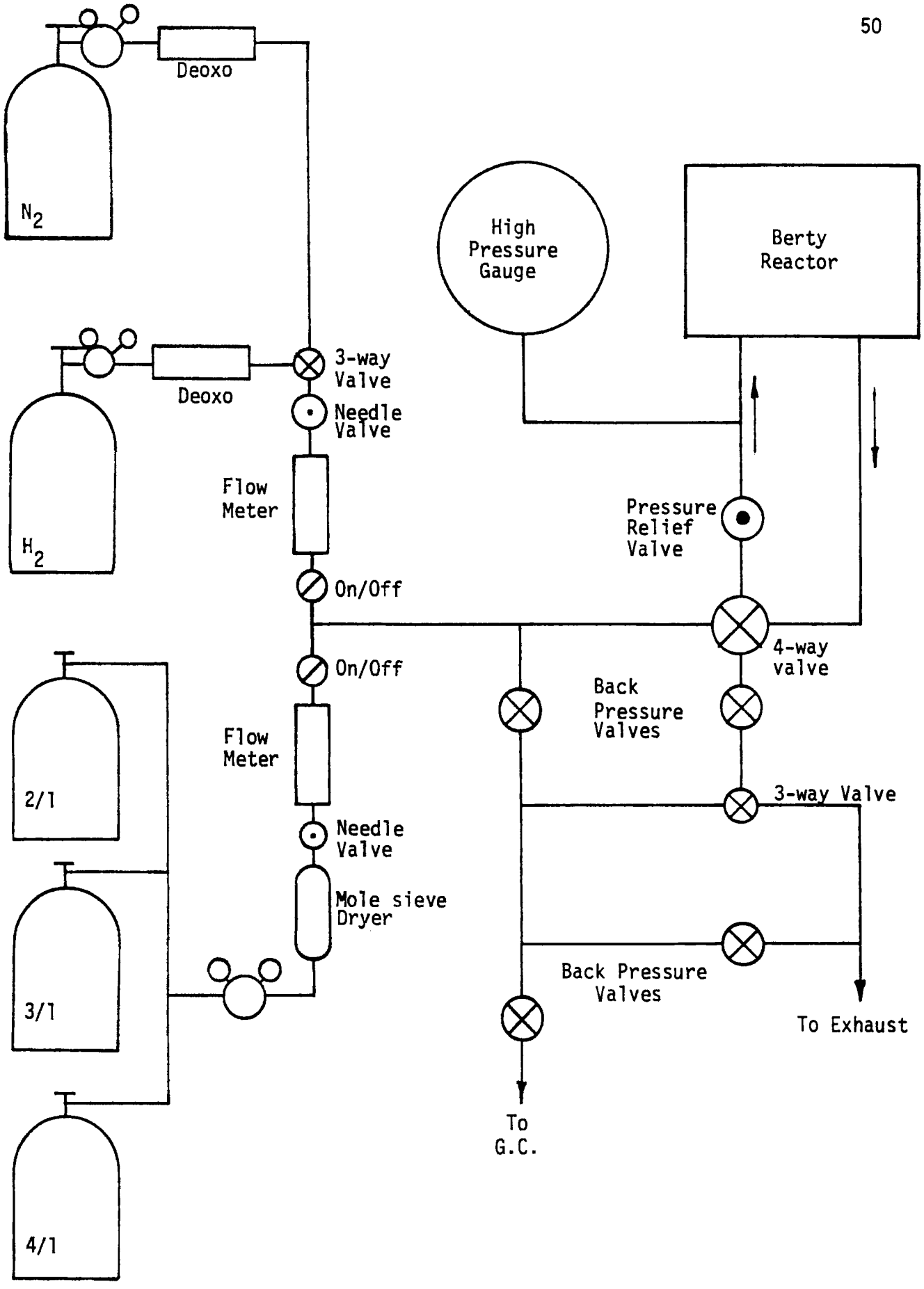

Figure 10. Schematic of Berty Recycle Reactor System.

using thermal conductivity detection. Column packings included porapak and mole sieve 13A; He was used as the carrier gas. Column configurations were described in detail by Erekson (27). Further details regarding the construction, testing and calibration of reactor system have been reported elsewhere (28).

Procedure

Kinetic tests were performed at 690 kPa with N_2 diluent making up between 95 and 97% of the feed gas. Reaction variables included reactant and product partial pressures and temperature. Partial pressures of CO and H_2 were varied from 5 to 12 kPa and 12 to 30 kPa respectively while temperatures were varied in 25 K increments from 473 to 623 K. The H_2/CO ratio was kept near the stoichiometric value ($H_2/CO = 3$) to obtain kinetic data under conditions applicable to industrial use. During these tests, product partial pressures were kept small by maintaining reactor conversions below 15%. Calculation of effectiveness factors and interphase mass transfer coefficients showed pore diffusional and external film resistances to be insignificant.

Catalysts

While some catalyst beads were prepared and used for comparison purposes, monolithic catalysts were used in almost all of the kinetic experiments. Monolithic catalysts (1.25cm x 2.54 cm diam.) were supported on corderite (Celcor, Corning Glass Works), having 36 square channels/cm^2. The corderite supports were coated with a thin layer of 5% Ni/Al_2O_3 as previously described (3,26)

Experimental Results

The Specific Activity of Monolithic Ni. To establish the absence of nonideal flow, geometrical and metal-support effects (26,28) the catalytic activities of monolithic and spherical pelleted catalysts having equivalent Ni loadings in the catalyst ($\sim$ 5 wt.%) were compared under reaction-limiting conditions. Table 23 compares a 4.3% nickel on 0.317 cm alumina spheres with two monolithic catalysts, 0.5% nickel on a 10% alumina coating and 0.097% nickel on 2.0% alumina. The catalyst beads have a much higher hydrogen uptake per gram of catalyst than either monolith catalyst because the fraction of the monolith catalysts actually composed of active material is much smaller than for the pellets (2-10% compared to 100%). If the differences in the overall metal loadings are accounted for by comparing the H_2 uptake per gram of nickel, no significant differences in metal dispersion exist among the three catalysts. The rates of methane production in the form of turnover numbers for the three samples (see Table 23) are the same within 6.0% which is well within experimental error (of $\pm$ 25%). Thus, nickel monolithic catalysts with a coating of 5% Ni/Al_2O_3 have the same catalytic properties as 5.0% Ni/Al_2O_3 beads.

TABLE 23

Metal Surface Areas and Specific Activities
of Monolithic and Pellet Nickel Catalysts

Catalyst	H_2 Uptake[a] (μmoles) /g-catalyst	/g-alumina + Ni	/g-Ni	CH_4 Turnover Number[b] at 523 K (mole/site-sec) x 10^3
Alumina Spheres - 1/8" 4.3% Ni	78.6	78.6	1830	4.7
Corderite Monoliths				
0.5% Ni - 10% Alumina	7.67	93.0	1860	5.0
0.86% Ni - 2% Alumina	1.96	73.0	1825	4.4

[a]Total uptake of H_2 measured at 298 K.

[b]Specific activity in moles methane produced per nickel surface site per second.

Kinetics of CO Methanation on Monolithic Nickel. Reaction rates were calculated directly from conversion versus temperature and concentration data for monolith catalysts and were subsequently fitted to a power law rate model of the form:

$$r_{CH_4} = A \exp(E/RT) H_2^{x} CO^{y} \qquad (1)$$

The reaction orders for CO and H_2 are plotted versus temperature in Figures 11 and 12 respectively and compared with literature data. The data from this laboratory and from the literature agree well over the entire range of temperature. The effect of CO (Figure 12) is to inhibit the methane production rate over the entire range of temperature; however, as the temperature increases from 473 to 573 K, the degree of inhibition decreases and the CO reaction order increases from -0.9 to approximately 0.0. The changes in the H_2 reaction order with temperature for similar H_2/CO ratios (Figure 12) are not as dramatic nor systematic as for CO. The methanation reaction was approximately first order at 573 K.

Apparent activation energies based on the power law model were obtained from plots of the natural logarithm of the reaction rate or turnover number versus the inverse temperature as shown in Figures 13 and 14. Figure 13 shows the results of an early attempt to measure activation energies above 573 K. The line representing a H_2/CO ratio of 20 is straight, with a slope corresponding to an apparent activation energy of 85 kJ, while the line for H_2/CO of 3 is curved, indicating a change in the apparent activation energy with increasing temperature from 85 to 60 kJ. The data points in these experiments were taken by starting at the lower temperatures and then increasing the temperature. Attempts to repeat the data points at the lower temperatures (H_2/CO = 3) were unsuccessful, indicating that the catalyst had deactivated due to carbon deposition. In order to maintain a catalyst surface free of carbon deposits, Sinfelt et al. (29) used a technique of purging the reactor with pure hydrogen between data point measurements. The application of this technique produced the result shown in Figure 14, in which no significant deviations from straight lines are seen for H_2/CO ratios of 3, 5, and 20. However, the slope and thus the apparent activation energy changes with the H_2/CO ratio. Indeed, the apparent activation energy decreases from 104 to 89 kJ as the H_2/CO ratio increases from 3 to 20. This could be explained by the increasing ability of adsorbed hydrogen to compete with more strongly absorbed CO with increasing temperature.

One obvious shortcoming of the apparent activation energies (Figure 14) is that they do not take into account the changes in reaction orders apparent in Figures 11 and 12. This problem can be overcome by plotting the natural logarithm of the reaction constant in place of the reaction rate versus the inverse temperature to obtain the true activation energy. The reaction rate constant can be obtained at each temperature by dividing the reaction rate by the H_2 and CO partial pressures raised to the power of their respective reaction orders. A plot of the logarithm of the reaction constant versus inverse

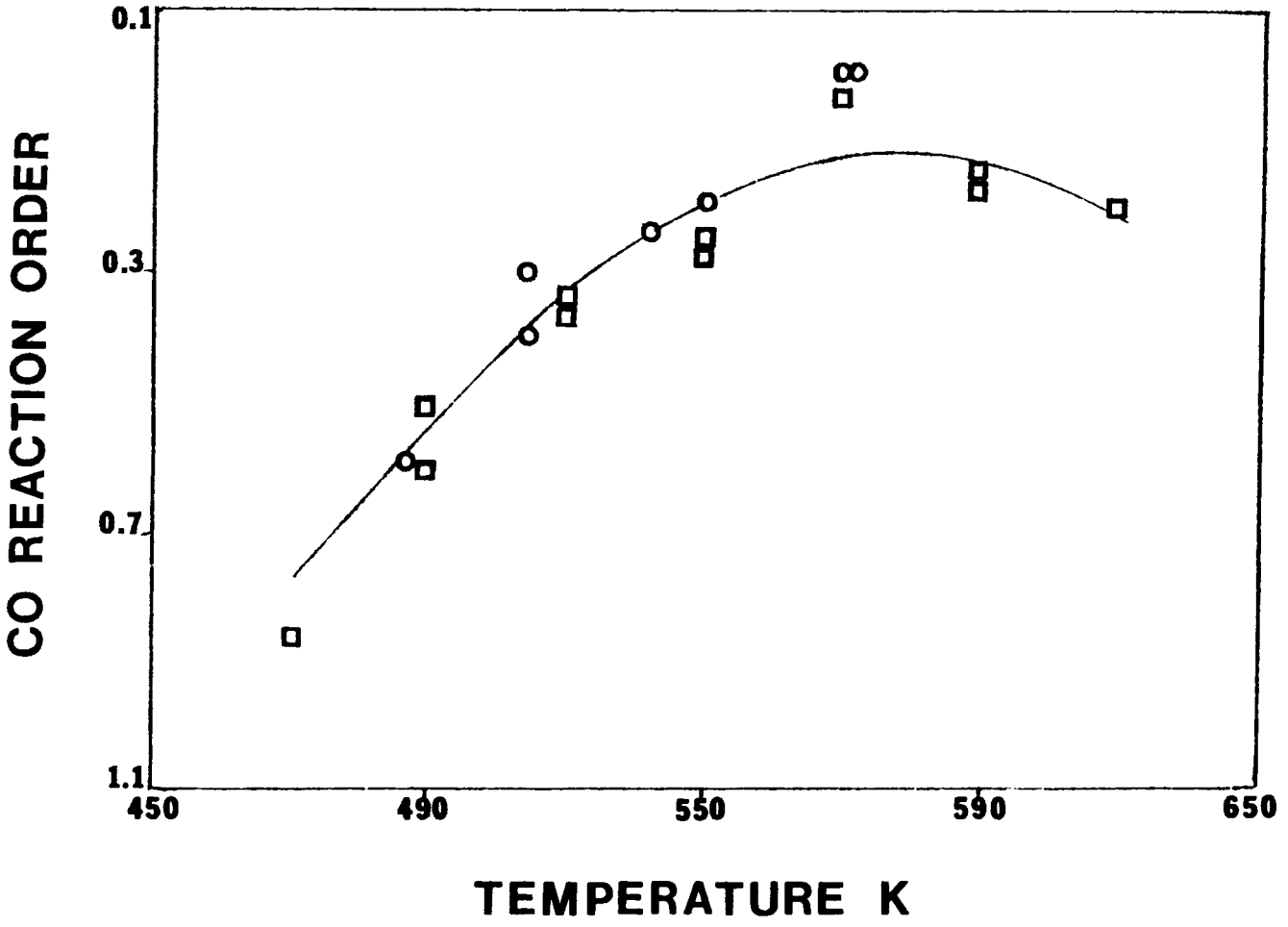

Figure 11. Reaction order of CO versus temperature at P_{H_2} = 20.7 kPa; O literature, □ this study, —— shifting rate model.

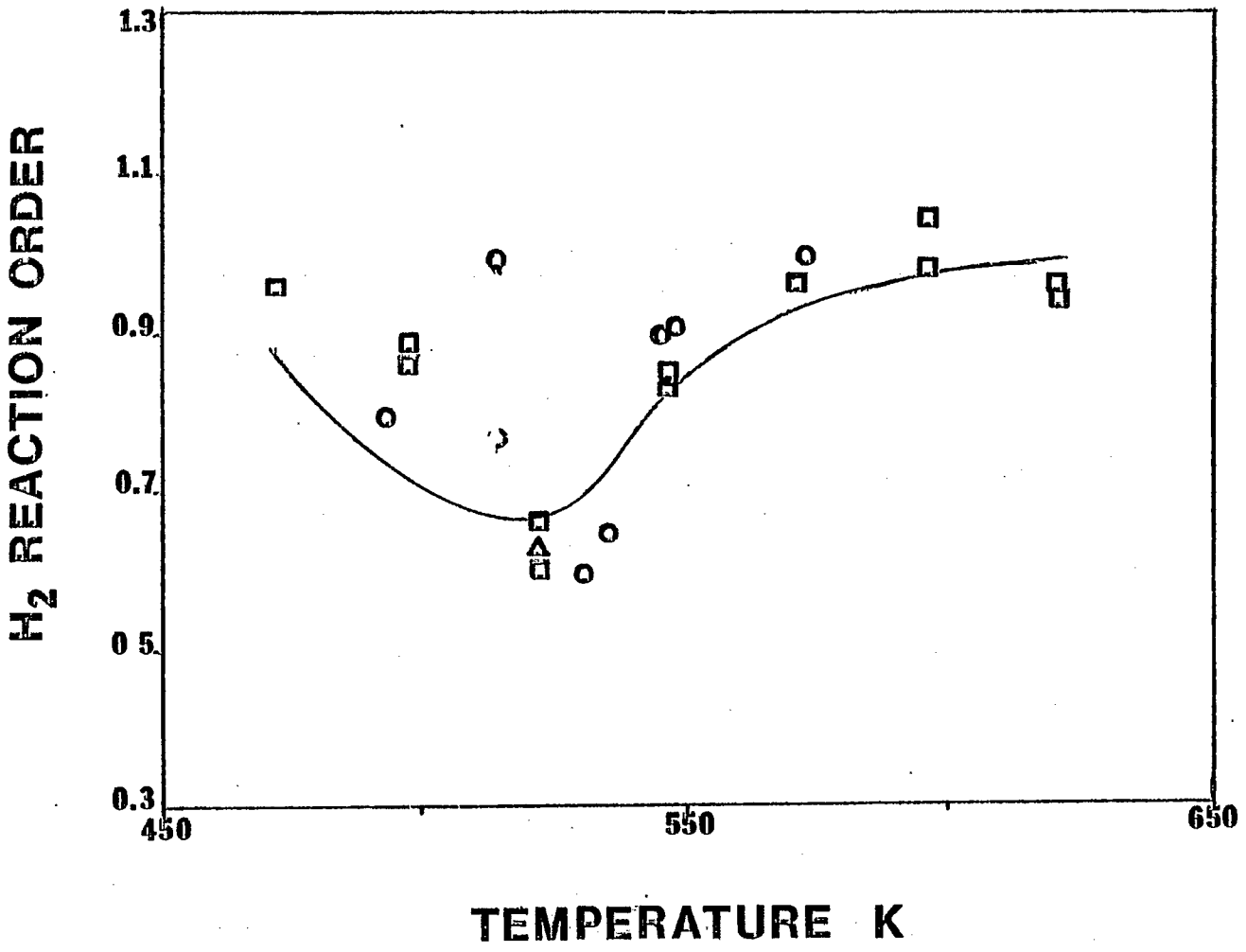

Figure 12. Reaction order of H_2 versus temperature at P_{CO} = 6.9 kPa; O literature, □ this study, Δ carbon gasification (Gardner, 1979), —— shifting rate model.

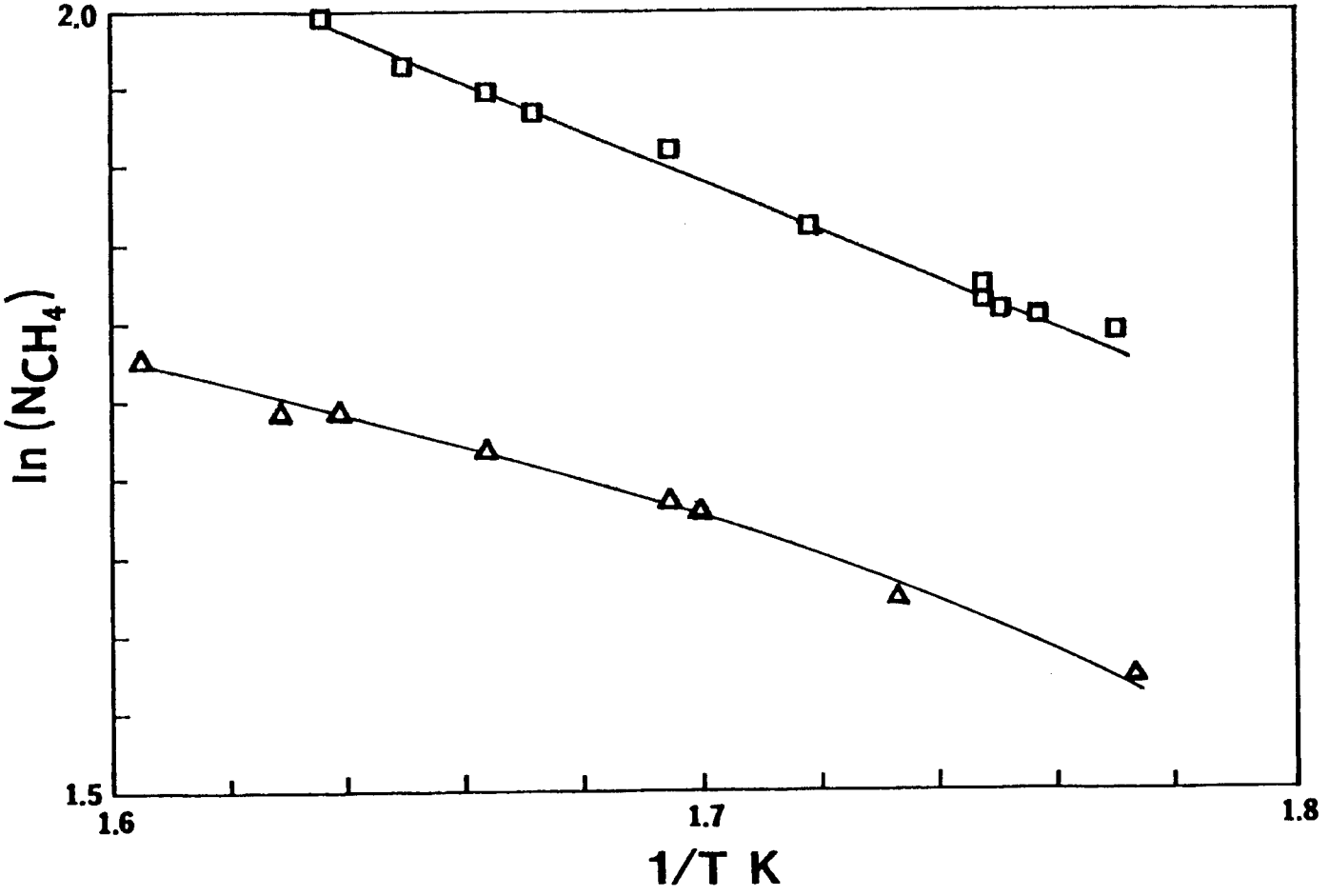

Figure 13. Apparent activation for methanation of CO at P_{CO} = 6.8 kPa (showing effects of deactivation). H_2/CO = □ 20, △ 3.

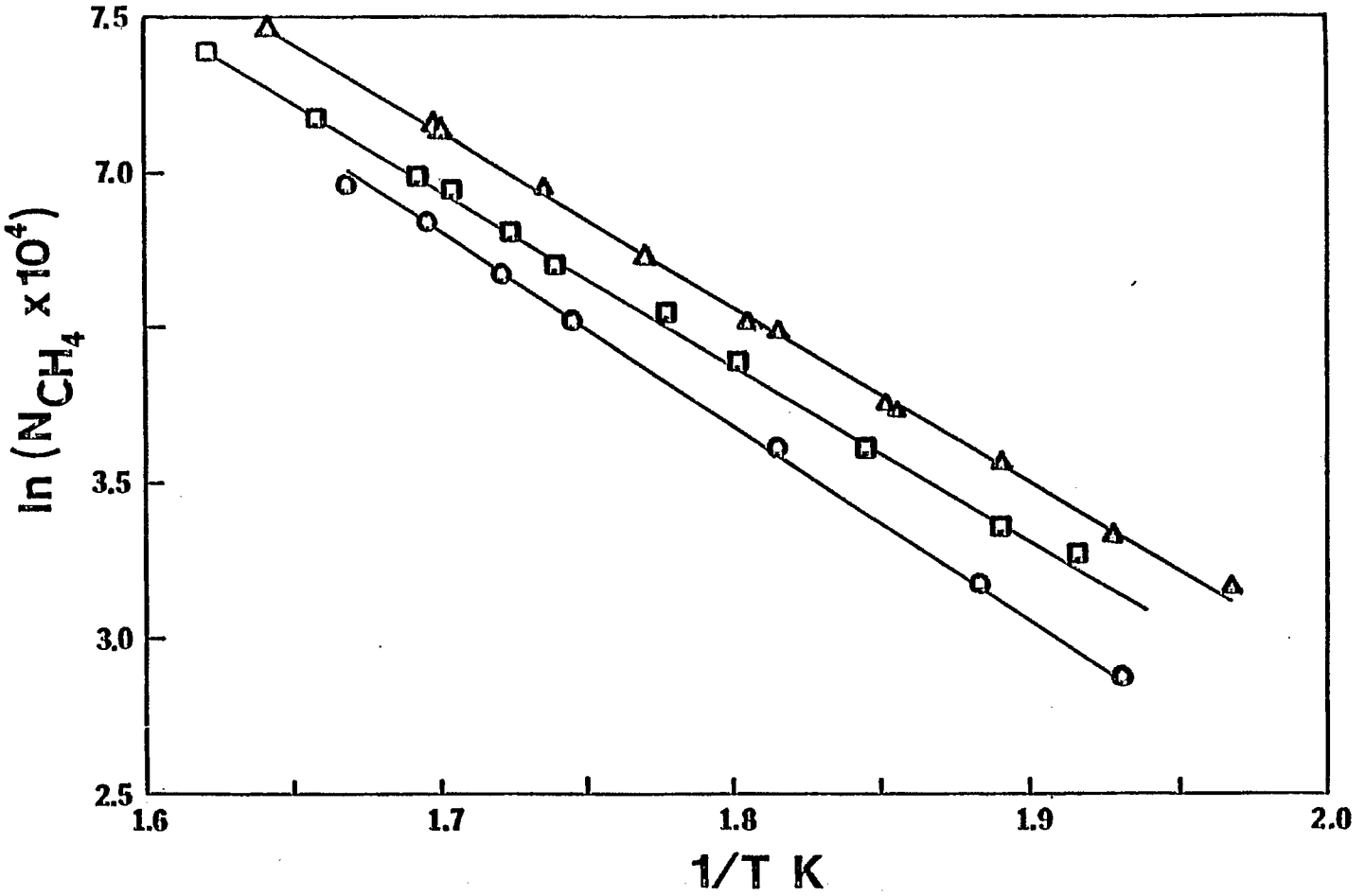

Figure 14. Apparent activation energy for methanation of CO at P_{CO} = 6.8 kPa. H_2/CO - △20; □5; O 3. E_{act} - △89; □93; O102.

temperature is shown in Figure 15. At temperatures below 575 K, the actual activation energy is approximately 135 kJ, which is reasonably close to the activation energy reported for CO disproportionation (30). On the other hand, the actual activation energy for temperatures above 573 K was 70 kJ, which is the same as the activation energy for carbon gasification on nickel (31).

The changes in the reaction orders of H_2 and CO with temperature observed in this study are significant as they indicate that the basic premise of the power law model fails for methanation. This premise is that temperature and concentration parameters of the model are independent of one another. Not only are the reaction orders dependent on temperature, but the Arrhenius constant, A, must also change with the total reaction order in order to maintain unit consistency in the rate equation. The failure of the power law approach to fit the kinetics of methanation is of interest, since the power law model was previously reported to provide an adequate fit of methanation kinetics (32).

There is presently strong evidence in favor of a mechanism with a carbon or carbide intermediate (31,33). The reaction steps for such a mechanism involve adsorption of H_2 and CO, dissociation of CO, hydrogenation of the carbon, and the desorption of the reaction products. Despite the general agreement on the carbidic intermediate, there is still uncertainty concerning the rate determining step and, consequently, the correct kinetic rate equation. In order to adequately fit the available kinetic data, the rate expression must specifically account for:

(i) The increase in CO reaction order from -1.0 to 0.0 over the temperature range from 473 to 623 K.

(ii) The variation in H_2 reaction order from 1.0 to 0.5 and then back to 1.0 for the same temperature range.

(iii) The apparent activation energy of approximately 100 kJ and the shift in the actual activation energy from 130 to 70 kJ with increasing temperature.

A rate expression consistent with these observed facts, the data in this study, and the proposed carbide mechanism is shown in Table 24. The good fit of this model is to the experimental data is illustrated in Figures 11, 12 and 15. Details regarding the assumptions used to derive this model and further detailed discussion of the kinetic data are described elsewhere (28,34).

The Effects of Product Concentrations on Activity of Ni. The effects of CH_4 and H_2O concentrations on the production of CH_4 were also investigated. In the tests involving CH_4, the N_2 diluent was replaced by CH_4, while the H_2 and CO concentrations were held at 3 and 1%, respectively. Concentrations as high as 50% of CH_4 in the reactant gas produced no significant change in CO conversion.

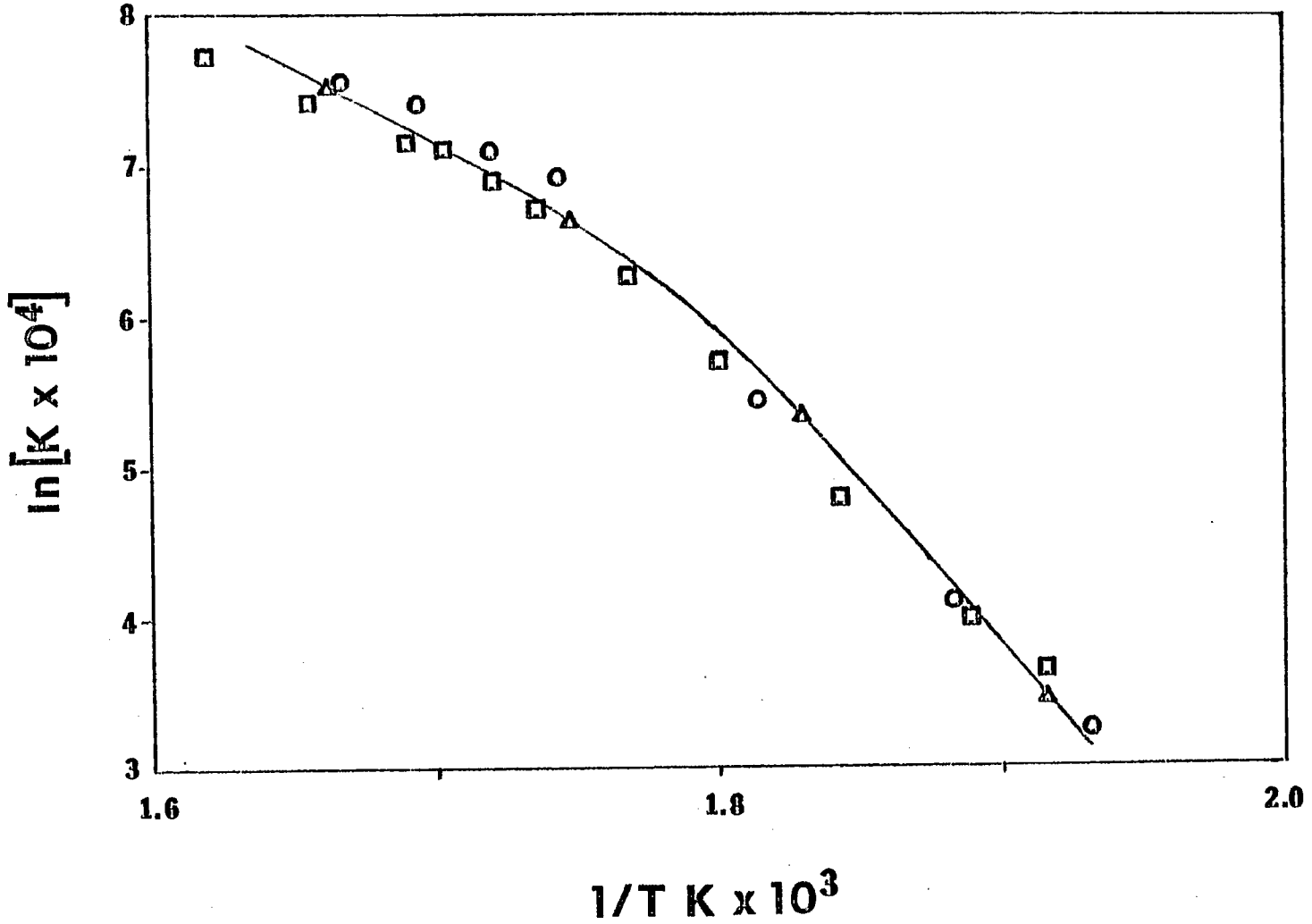

Figure 15. Arrhenius plot of the rate constant versus inverse temperature showing the actual activation energy for methanation of CO at P_{CO} = 6.9 kPa. H_2/CO - O experiment, H_2/CO = 3; □ experiment, H_2/CO = 5; Δ shifting rate model, H_2/CO = 3.

TABLE 24

Shifting Rate Model - Kinetic Rate Expression

$$N_{CH_4}(10^3) = \frac{0.5\ K_1^{\,2} P_{H_2}}{K_1 P_{H_2}^{\,1/2} + K_2 P_{CO} + K_3 P_{CO} P_{H_2}^{\,1/2}} + \frac{K_4 P_{H_2}}{1 + K_5 P_{CO} + K_6 P_{H_2}^{\,1/2}}$$

$$K = Ae\left(\frac{-E}{RT}\right)$$

$A_1 = 7.43 \times 10^{6}$	$E_1 = -61.5$
$A_2 = 4.21 \times 10^{-3}$	$E_2 = -26.7$
$A_3 = 1.16 \times 10^{16}$	$E_3 = -152.9$
$A_4 = 3.36 \times 10^{11}$	$E_4 = -114.8$
$A_5 = 1.54 \times 10^{9}$	$E_5 = -114.8$
$A_6 = 9.77 \times 10^{-20}$	$E_6 = 184.5$

Water significantly inhibits the rate of methanation as is apparent from Figure 16, a plot of the normalized reaction rate versus P_{H_2O}. Increasing inhibition by H_2O with increasing temperature is also evident. That is, the addition of 5% H_2O at 498 K reduced the rate of CH_4 production only about 10%, while at 523 K the addition of only 3% H_2O reduced the level of CH_4 production to 70% of that without H_2O. Finally, at 573 K 3% H_2O resulted in 50% loss of CH_4 production. At both 523 and 498 K the inhibiting effect of H_2O at low concentrations was reversible while the addition of H_2O at 573 K produced a loss in catalyst activity which was only slowly reversible at best. However, the addition of 3% H_2O at 523 K produced irreversible loss of catalyst activity as did the addition of 10% H_2O at 498 K.

Computer Modeling of Methanation Kinetics

A one-dimensional computer model was developed for methanation in a fixed bed of nickel monolith catalyst. The assumptions leading to the development of the differential equations are given in Table 25, while the equations are listed in Table 26. The auxiliary equations for calculation of physical properties and nomenclature are presented in Tables 27 and 28. The differential equations were solved using Adams predictor-numerical methods on a DEC-10 computer.

After initial program debugging and testing, the computer model was used to compare the solutions for several kinetic expressions to actual experimental data. Figure 17 shows the model's predictions using the empirical kinetic expressions for methane production given by Vannice (35). The correlation between the model and experimental values is very good for low conversions. At higher conversion, transport effects and these empirical methanation kinetics alone will not explain the reaction behavior. Product inhibition was next introduced into the kinetic expression. This produced a much better correlation between the model and experimental data for conversion of CO up to 70%; at higher conversions discrepancies still remained.

The effects of introducing a competing reaction, the water-gas shift, into the kinetic expression are shown in Figure 18. The kinetic expression for the water-gas shift reaction kinetics was assumed to involve a Langmuir-Hinshelwood model including inhibition by water. The correlation between experimental and predicted values show that a competing water-gas shift reaction could explain the reaction behavior throughout the conversion range.

The effects of changes in the various physical parameters of the catalyst and reactor were also studied. Figure 19 shows the results of changing H_2 uptake, nickel loading or catalyst activity. It is interesting that the catalyst with lower activity not only reaches a lower maximum conversion but also requires a higher temperature to reach a maximum conversion. The competing reaction becomes more important with temperature. Thus optimization of methane production is not only a function of temperature but of catalyst activity and other reactor variables.

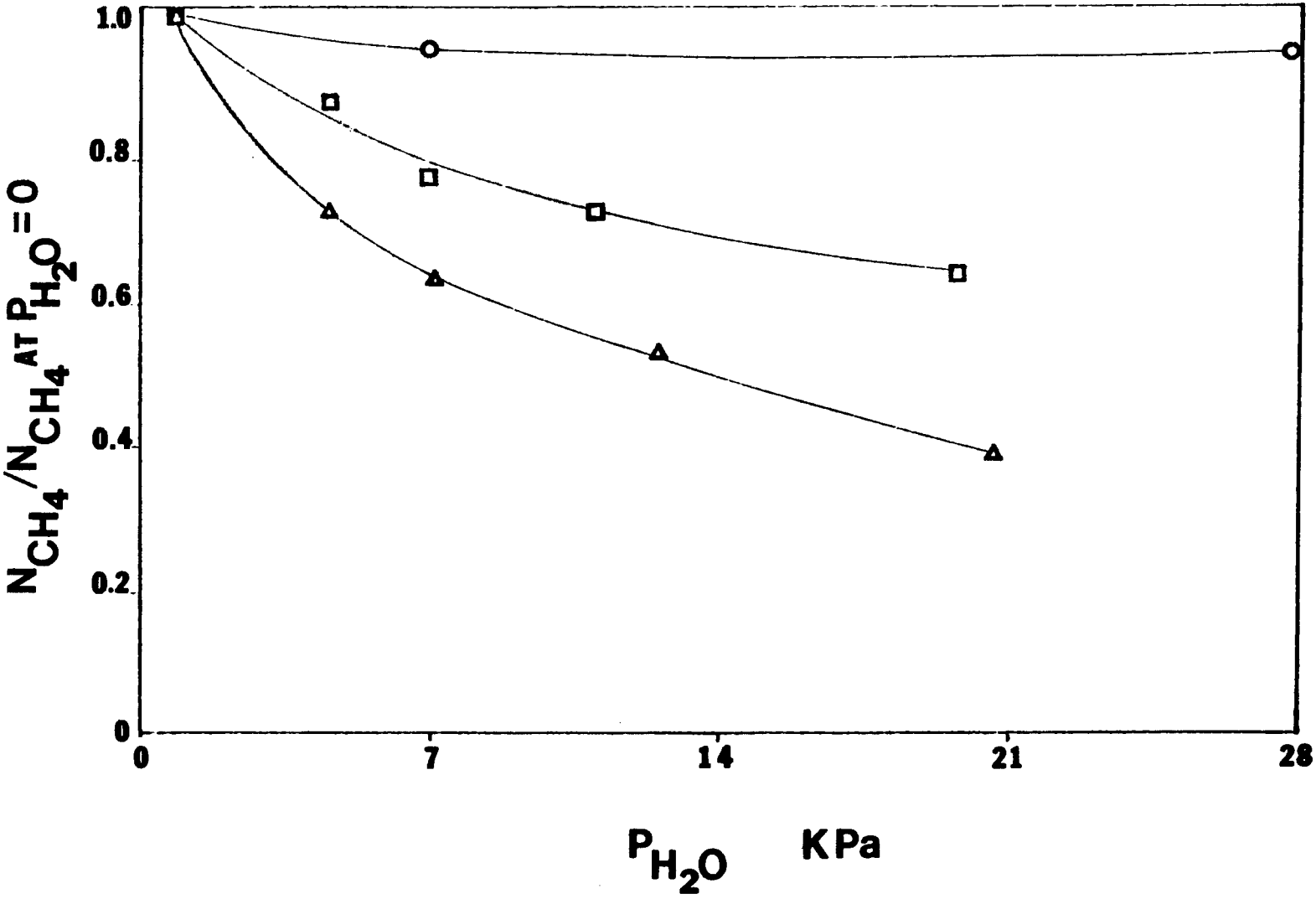

Figure 16. Effects of H_2O on methanation activity at P_{CO} = 6.9 kPa and H_2/CO = 3 (activity is defined as rate with H_2O/rate without H_2O). Temperature (K) - O 498; □ 523; Δ 573.

Table 25

Model Assumptions

1. One channel in the monolith may be chosen as representative of the entire catalyst.

2. The monolith's channels are cylindrical and a cylindrical coordinate system may be used. This is partially true since the corners of the rectangular channels tend to be rounded by the alumina washcoat.

3. The density, thermal conductivity and diffusivity are constant for purposes of deriving the differential equations. However, these are later allowed to vary as function of temperature and composition.

4. The reactor and the catalyst are at steady state.

5. The channel is axially symmetric.

6. The effects of gravity are neglible.

7. All reactions in the reactor take place on the wall of the channel.

8. Axial diffusion and heat conduction are negligible relative to convective transport.

9. Radial velocity is small. No axial heat conduction in the solid.

10. The system can be described in terms of hydrogen and carbon monoxide. Other components may be neglected.

11. The gas phase is in laminar flow and free of developing flow effects.

12. Fourier's and Fick's law can be applied to radial diffusion and heat conduction. This can be later corrected for fluxes and high mass transfer rates.

Table 26

Computer Model - Basic Equations[a]

Equation of Continuity Chemical Species

$$\frac{\partial Y_{H_2}}{\partial Z} = \frac{2\ L\ K_{H_2}}{R\ \langle v \rangle}\ [Y_{H_2} - Y^s_{H_2}]$$

$$\frac{\partial Y_{CO}}{\partial Z} = \frac{2\ L\ K_{CO}}{R\ \langle v \rangle}\ [Y_{CO} - Y^s_{CO}]$$

Equation of Energy

$$\frac{\partial T}{\partial Z} = \frac{2\ L\ H}{C_p\ R \langle v \rangle}\ [T - T^s]$$

Boundary Conditions

At $r = R$

$$Y^s_{H_2} = Y_{H_2} - \frac{3\ RR}{K_{H_2}\ C^i_{H_2}}$$

$$Y^s_{CO} = Y_{CO} - \frac{RR}{K_{CO}\ C^i_{H_2}}$$

$$T^s = T - \frac{HR\ RR}{T^i}$$

At $z = 0$

$$Y_{H_2} = Y_{CO} = T = 1$$

---

[a] Nomenclature listed in Table 28.

Table 27

Auxiliary Equations[a]

Velocity

$$\langle v \rangle = \frac{SV}{3600} \times \frac{CV}{POR} \times \frac{P}{R_G} \times \frac{273}{T}$$

Density

$$\rho = \frac{AMW \times P}{R_G \times T}$$

Heat Capacity

$$C_p = \sum_i z_i C_{pi} \qquad i = H_2, CO, H_2O, CH_4$$

$$C_p = 6.947 - 2.0 \times 10^{-4} T + 4.81 \times 10^{-7} T^2$$

Diffusion Coefficient

$$D_{CO-N_2} = \frac{3.7585 \times 10^{-5} \, T^{1.5}}{P \times \Omega}$$

Mass Transfer Coefficient

$$K_{CO} = D_{CO-N_2} (1.48) \, R \left(1 + \frac{.095 \times 4R^2 \times \langle V \rangle}{D_{CO}}\right)^{.45}$$

K_H, D_H = similar to K_{CO} D_{CO}

Knudsen Diffusion

$$DK_{CO} = 1.010 \times 10^{-3} \, T^{.5}$$

Viscosity

$$U = \frac{1.024 \times 10^{-5} \, T^{.5}}{\Omega}$$

Thermal Conductivity

$$KT = U \times [C_p + 2.484]/28$$

Heat Transfer Coefficient

$$H = \frac{1.48 \, KT}{R}$$

$$HR = 45{,}122.8 + 16.624T - 3.14 \times 10^{-3} T^2 + 1.755 \times 10^{-6} T^3$$

$$RR = A e^{-\frac{E}{RT}} C_{H_2}^{a} \, C_{CO}^{b}$$

[a]Nomenclature listed in Table 28.

Table 28

NOMENCLATURE

AMW	Gas average molecular weight
Cp	Heat capacity
C	Concentration
CV	Catalyst Volume
H	Heat transfer coefficient
HR	Heat of reaction
K	Mass transfer coefficient
KT	Thermal conductivity
L	Channel Length
P	Pressure
POR	Catalyst porosity - % Cross sectional area open to flow
r	Radial direction
R	Channel radius
RR	Kinetic rate expression
T	Dimensionless temperature
V	Viscosity
Y	Dimensionless concentration
x	Mole Fraction
Z	Dimensionless length

SUPERSCRIPT

a,b	reaction orders
i	initial values
s	surface values
H	Hydrogen
CO	Carbon monoxide

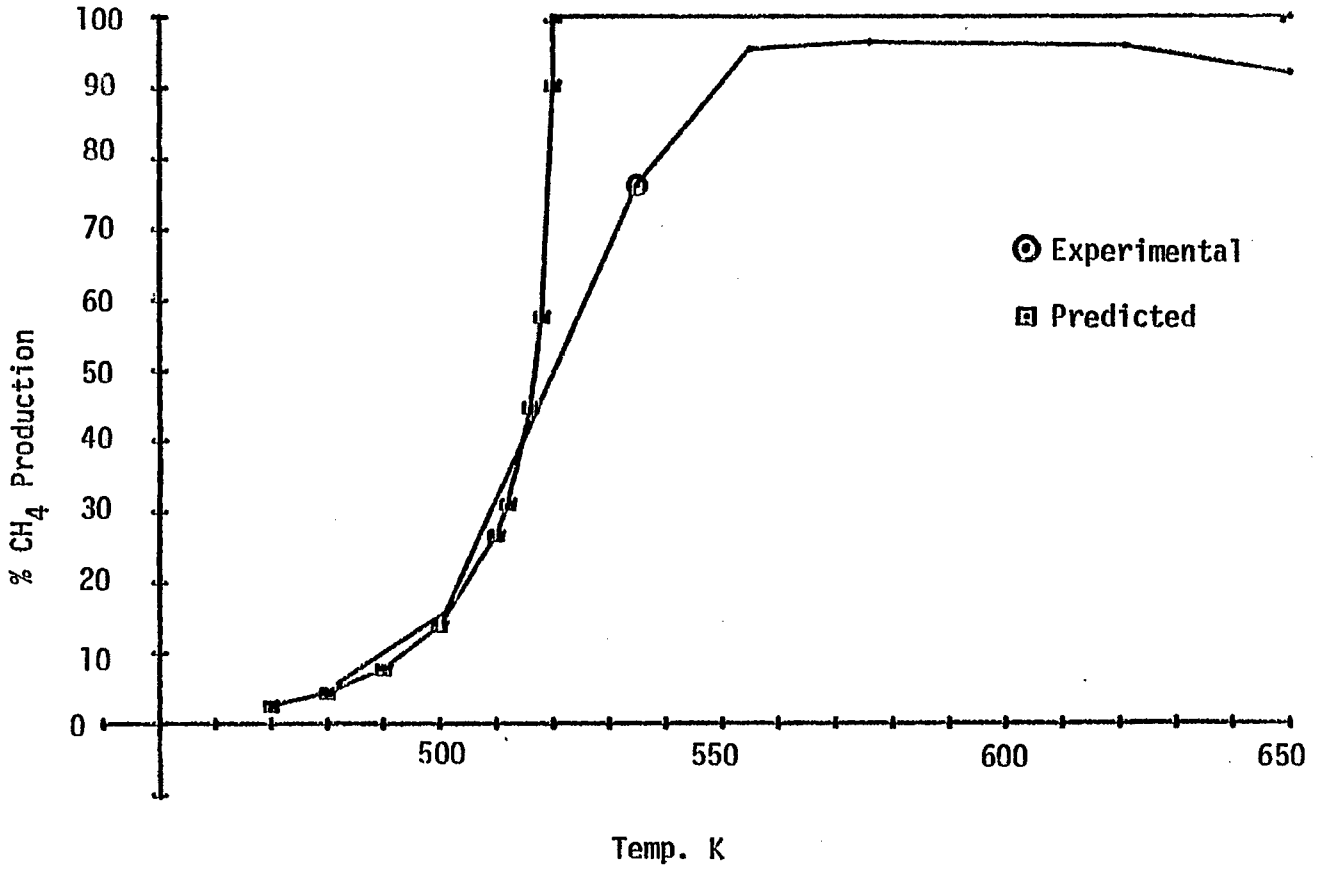

Figure 17. Comparison of Experimental Results with Calculatations from a Power Rate Law Model. Space Velocity = 43,000, P = 1300 kPa, H_2/CO = 4.4/1.

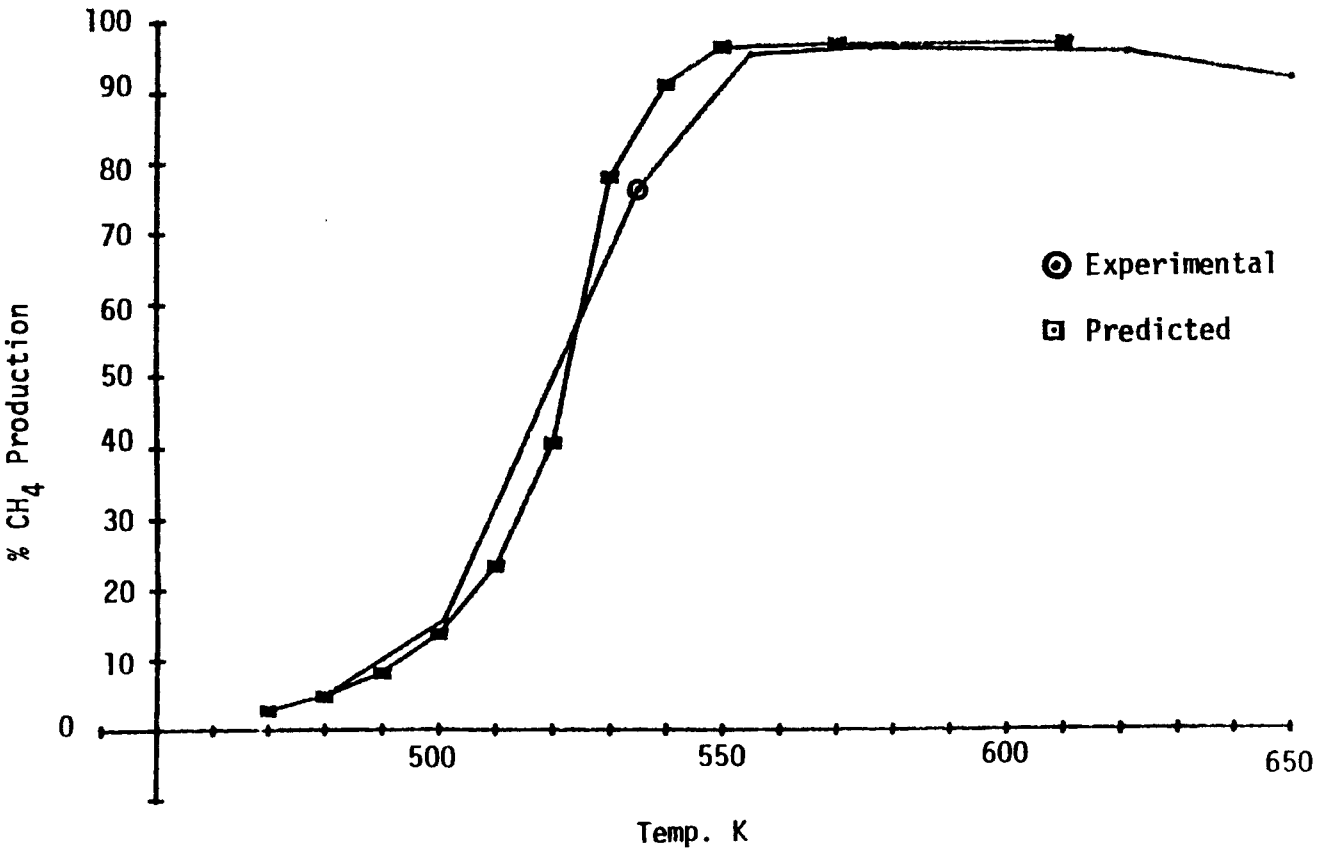

Figure 18. Comparison of Experimental and Calculated Results Based on a Langmuir Hinshelwood Competing Reaction Model.

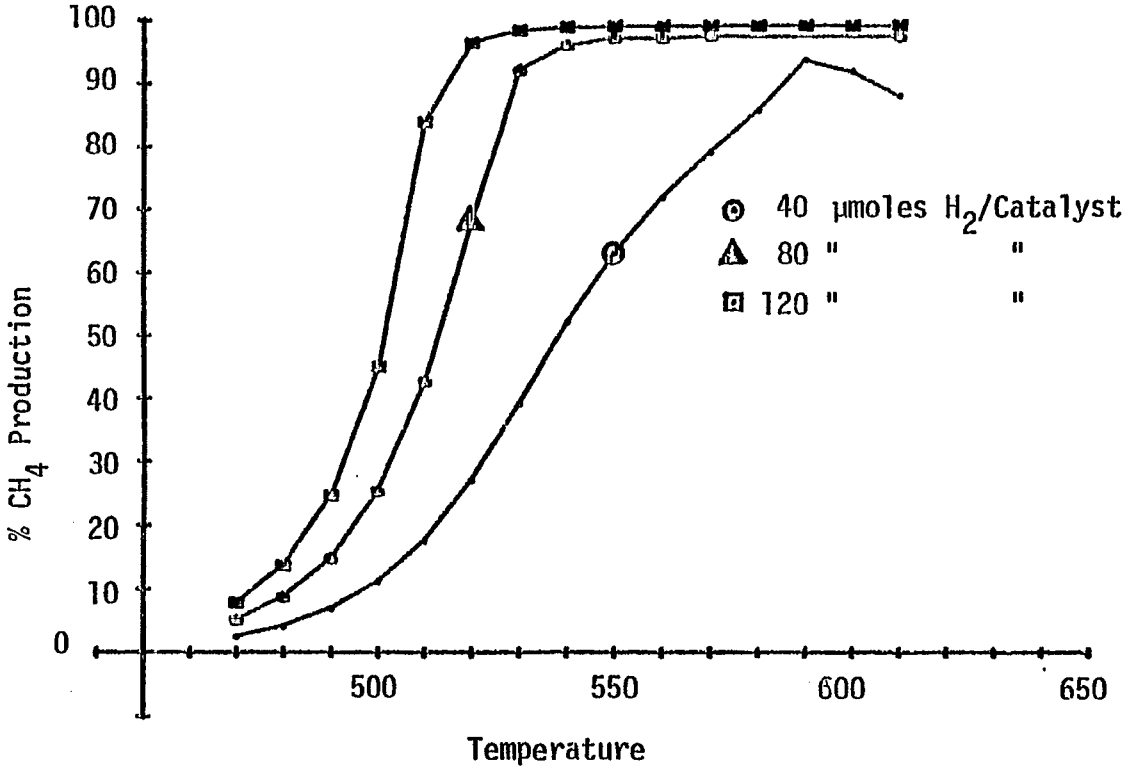

Figure 19. Effects of Increased Ni Surface Area on Catalyst Performance. Space Velocity = 30,000 h^{-1}, H_2/CO = 3/1, P = 1030 kPa.

Tast 4: Degradation Studies

1. Thermal Degradation Studies

The activity of nickel and nickel bimetallic methanation catalysts (including two commercial catalysts) was investigated under conditions representative of an industrial high temperature methanator. Conversion-temperature tests were made in a high pressure, fixed bed, stainless steel reactor (3) over the temperature range of 573 to 873 K at 2500 kPa and a space velocity of 30,000 h^{-1} in a reactant mixture containing either 4% CO, 14% H_2, 2% CO_2, 64% CH_4 and 16% Ar (dry test) or 3% CO, 10% H_2, 2% CO_2, 45% CH_4, 11% Ar, and 29% H_2O (steam test). Catalysts were analyzed for carbon following these tests; metal surface areas were measured by H_2 chemisorption before and after each test. The results of hydrogen adsorption measurements and carbon analyses are summarized in Table 29 and representative conversion-temperature data are plotted in Figures 20-23. The dry test conditions are predicted by thermodynamics to cause massive deposits of carbon; the steam tests should not result in carbon deposition. All catalysts were observed to suffer significant losses in activity above 723 K as a result of sintering and/or carbon deposition (see Figures 20-23). At temperatures exceeding 723 K Ni/Al_2O_3 and $Ni/NiAl_2O_4$ catalysts are the most active while $Ni/NiAl_2O_4$ and $Ni\text{-}MoO_3/Al_2O_3$ catalysts are the most thermally stable, even in comparison to commercially available catalysts. Ni and Ni bimetallic catalysts generally lose 20 to 30% of metal surface area when tested above 800 K (see Table 29). Ni on $NiAl_2O_4$ and commercial G-87P lose 10 to 15% of metal surface area due to carbon deposition (dry test), but not more than 10% due to sintering (steam test). $NiMoO_3/Al_2O_3$ appears to lose little or no surface area under the same conditions. Carbon build-up on a catalyst is a function of temperature and gas composition in the catalyst bed (see Table 29). In a carburizing atmosphere, the extent of carbon deposited increases with increasing temperature (see Table 29). Reactant steam can be used to eliminate carbon deposition; however, it also contributes to thermal deactivation (Figure 22) and at high temperatures shifts product distribution in favor of CO_2 (Figure 23). Catalyst composition also influences the rate and extent of carbon build-up. $Ni\text{-}NiAl_2O_4$, $NiMoO_3$, and Ni-Pt deposit less carbon than Ni (see Table 29). In 24 hour tests involving Ni/Al_2O_3, at 773 K (no steam), accumulated carbon resulted in plugging of the reactor and catastrophic failure after only 17 hours (see Figures 24 and 25). Analysis by transmission electron microscopy of samples run at high temperature shows the presence of carbon filaments terminated by nickel crystallites (see Figure 26).

The results of the thermal degradation study show the importance of optimizing operating conditions at sufficiently high H_2/CO and H_2O/CO ratios to avoid carbon formation while minimizing H_2O/CO so as to maximize selectivity to methane. The data suggest that $Ni/NiAl_2O_4$ and $Ni\text{-}MoO_3$ are promising compositions for high temperature methanation because of their resistance to carbon deposition and sintering relative to nickel. Further details of this study were reported in earlier reports (10-12), at the 4th Rocky Mountain Fuel Symposium in 1979 (36), and in a paper submitted to Fuels Processing Technology (37).

Table 29

Hydrogen Uptakes and Carbon Analyses Before and After Conversion Versus Temperature Tests

Catalyst	Support	Metal Loading (wt.%)	Before Test Hydrogen Uptake (μmoles/g)	After Dry Test Hydrogen Uptake (μmoles/g)	After Dry Test % C	After Dry Test Max. Reactor Temperature	After Steam Test Hydrogen Uptake (μmoles/g)	After Steam Test % C
Ni-A-122	Al_2O_3	20	213	210	18 10.4 2.6	886 763 721	157	0.3
Ni-Co-A-102	Al_2O_3	Ni = 10% Co = 10%	117	94	0.3	725	79	0.1
Ni-Pt-A-101	Al_2O_3	Ni = 15% Pt = 0.5%	211	138	6.3	820	124	0.2
Ni-M-180	Al_2O_3 on monolith	15% Ni	138	---	---	---	84	---
Ni-NAL-100	$NiAl_2O_4$	30% Ni	209	162	1.3	803	185	0.2
Ni-MoO_3-A-105	Al_2O_3	Ni = 10% MoO_3 = 10%	53	47	0.2	816	58	0.2
G-87P	Al_2O_3	Ni = 30-40%	138	119	9.8	800	103	0.8
MC-100	Zeolite	Ni = 20-30%	131	179	15	820	82	0.0

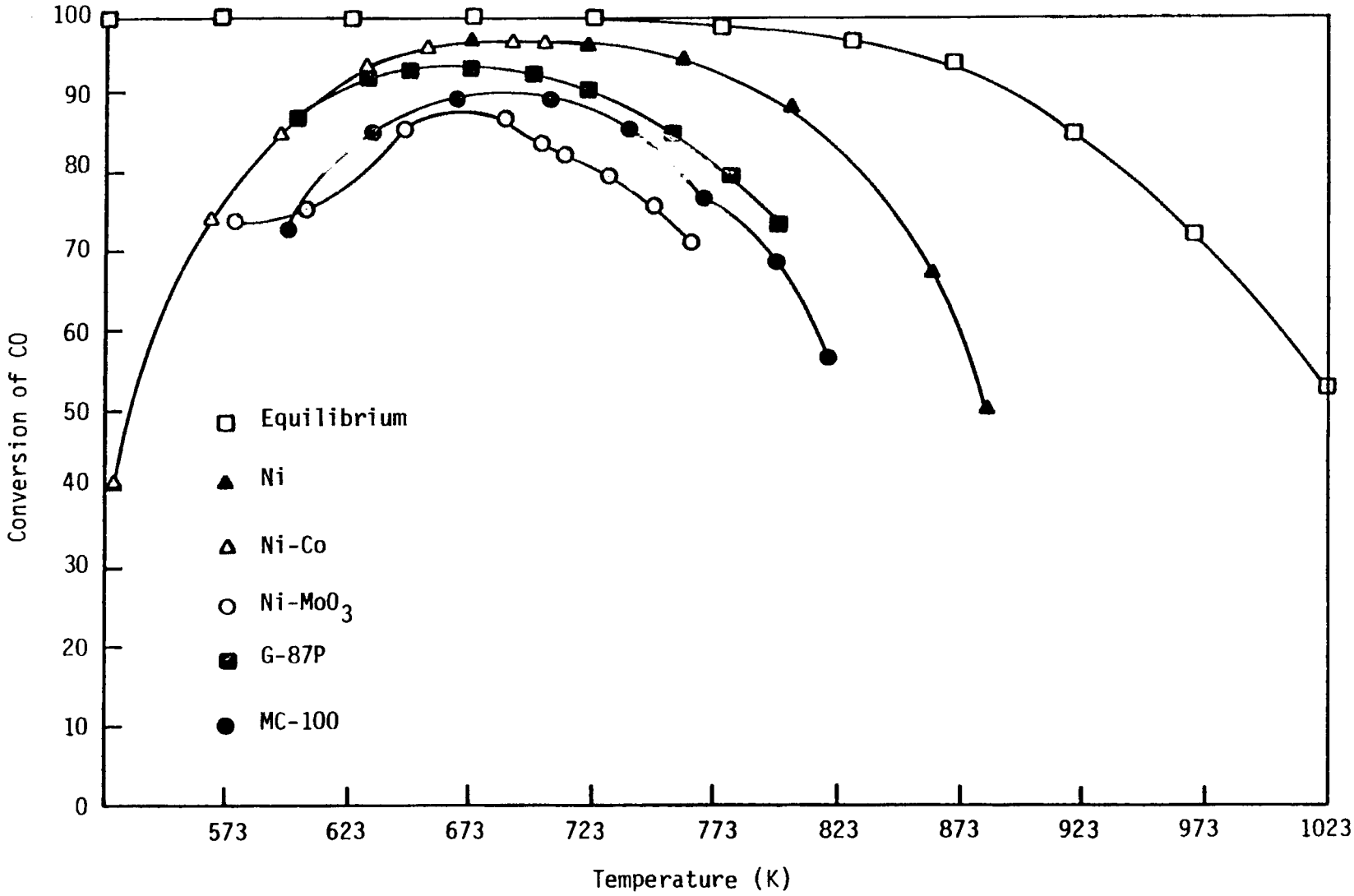

Figure 20. Conversion of Carbon Monoxide versus Temperature for High Loading Catalysts at 2500 kPa, space velocity = 30,000 h^{-1}, and reaction mixture containing 64% CH_4, 16% Ar, 14% H_2, 4% CO, and 2% CO_2 (no steam). □ equilibrium, ▲ Ni, △ Ni-Co, ○ $Ni-MoO_3$, ■ G-87P, ● MC-100.

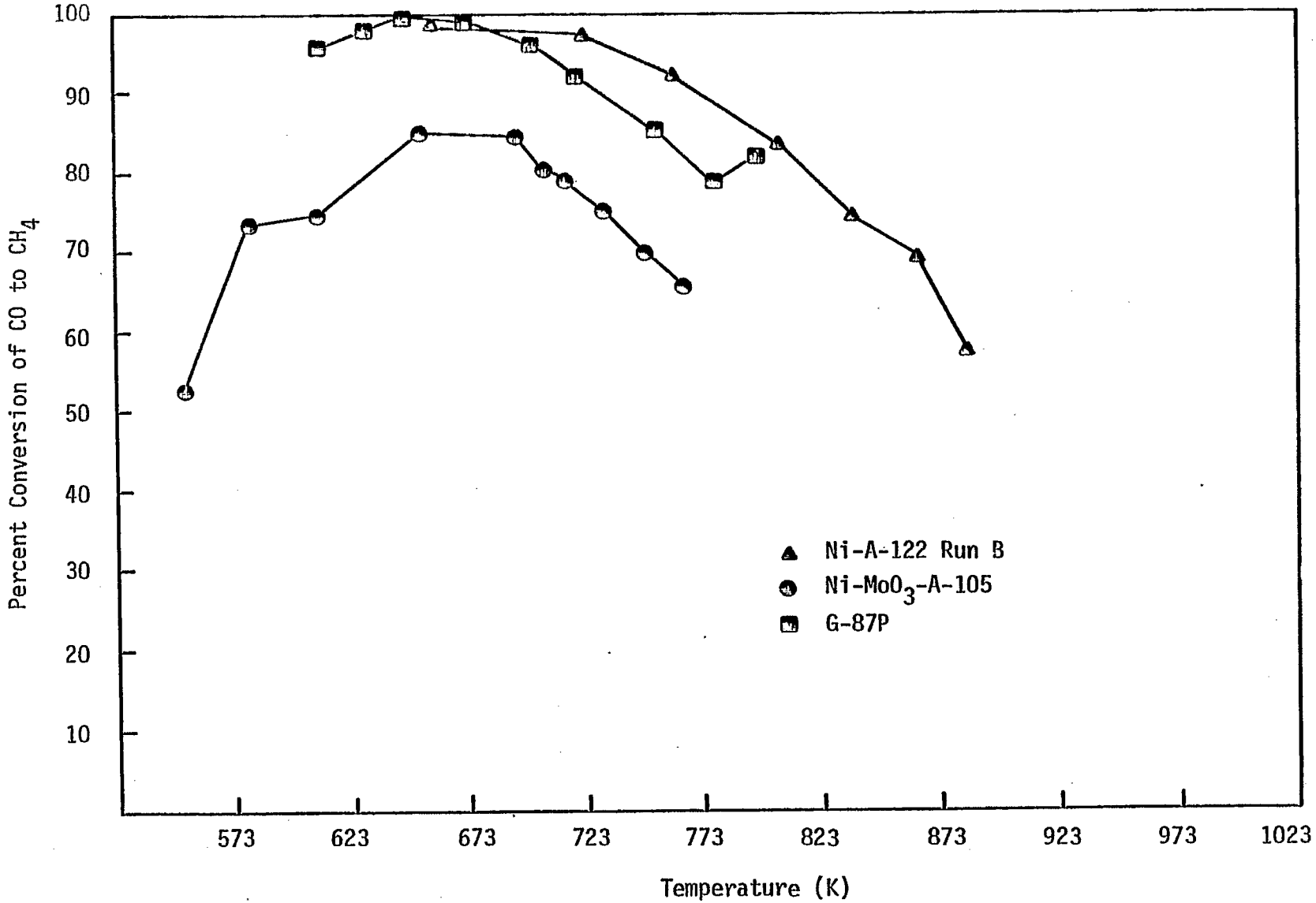

Figure 21. Conversion of CO to CH_4 vs. Temperature for High Loading Catalysts at 2500 kPa, space velocity = 30,000 h^{-1}, and reaction mixture containing 64% CH_4, 16% Ar, 14% H_2, 4% CO, and 2% CO_2. ▲ Ni, ◉ Ni-MoO_3, ■ G-87P.

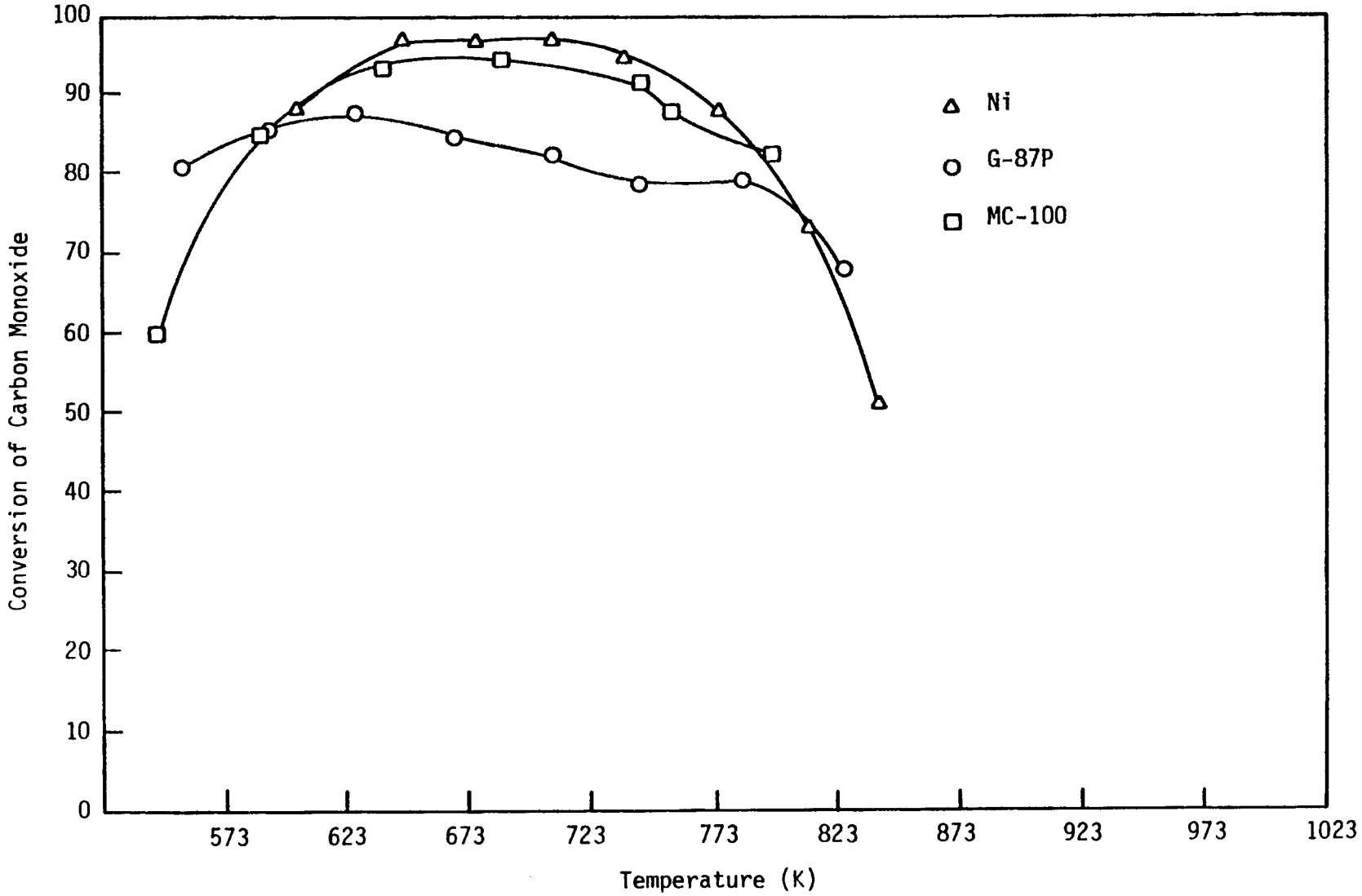

Figure 22. Conversion of Carbon Monoxide versus Temperature for High Loading Catalysts at 2500 kPa, space velocity = 30,000 h^{-1}, and reaction mixture containing 45% CH_4, 11.5% Ar, 10% H_2, 3% CO, 1.5% CO_2 and 29% H_2O. △ Ni, ○ G-87P, □ MC-100.

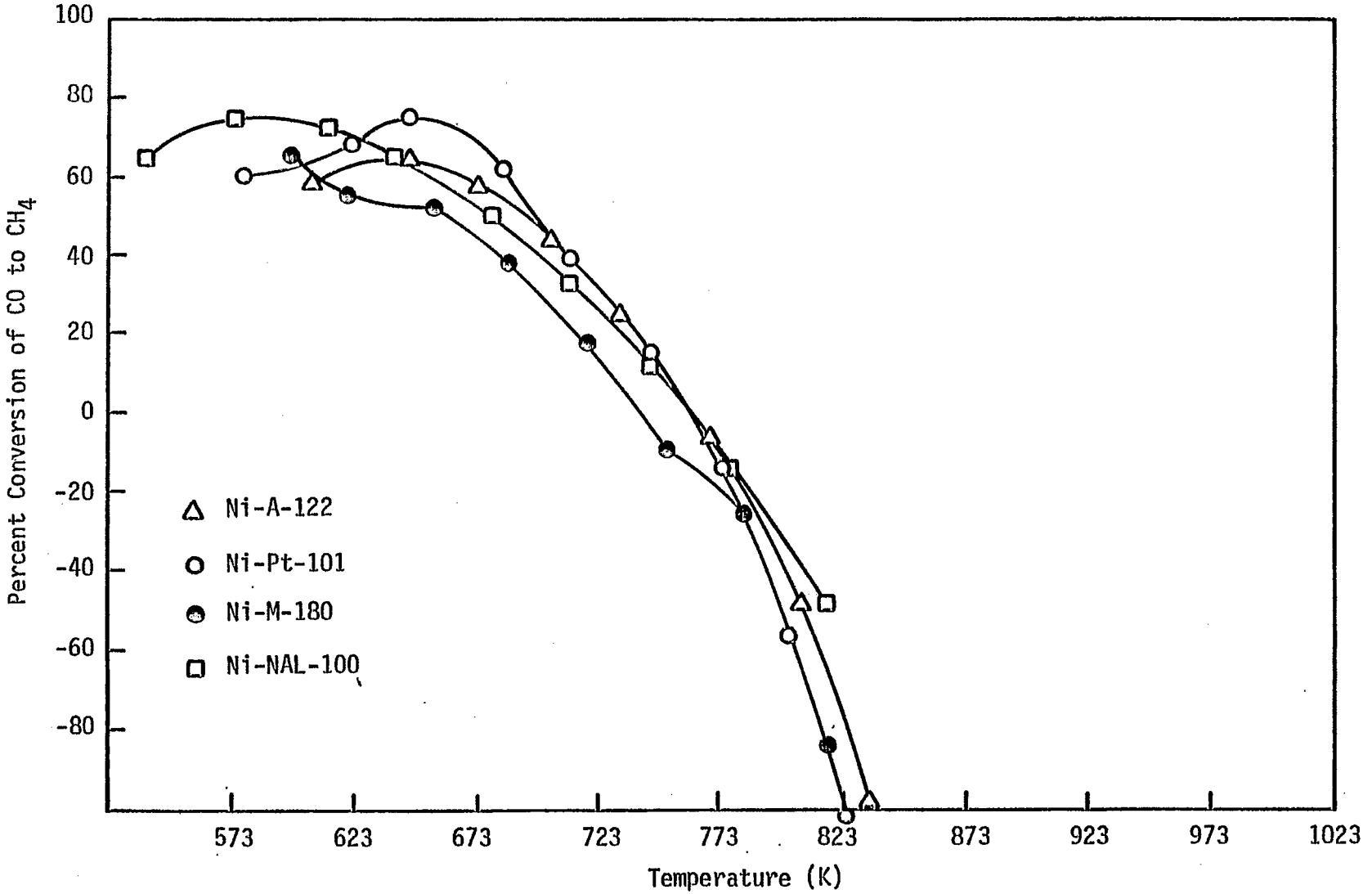

Figure 23. Conversion of CO to CH_4 vs Temperature for High Loading Catalysts at 2500 kPa, space velocity = 30,000 h^{-1}, and reaction mixture containing 45% CH_4, 11.5% Ar, 10% H_2, 3% CO, and 1.5% CO_2. △ Ni, ○ Ni-Pt, ● Ni-M, □ Ni-$NiAl_2O_4$.

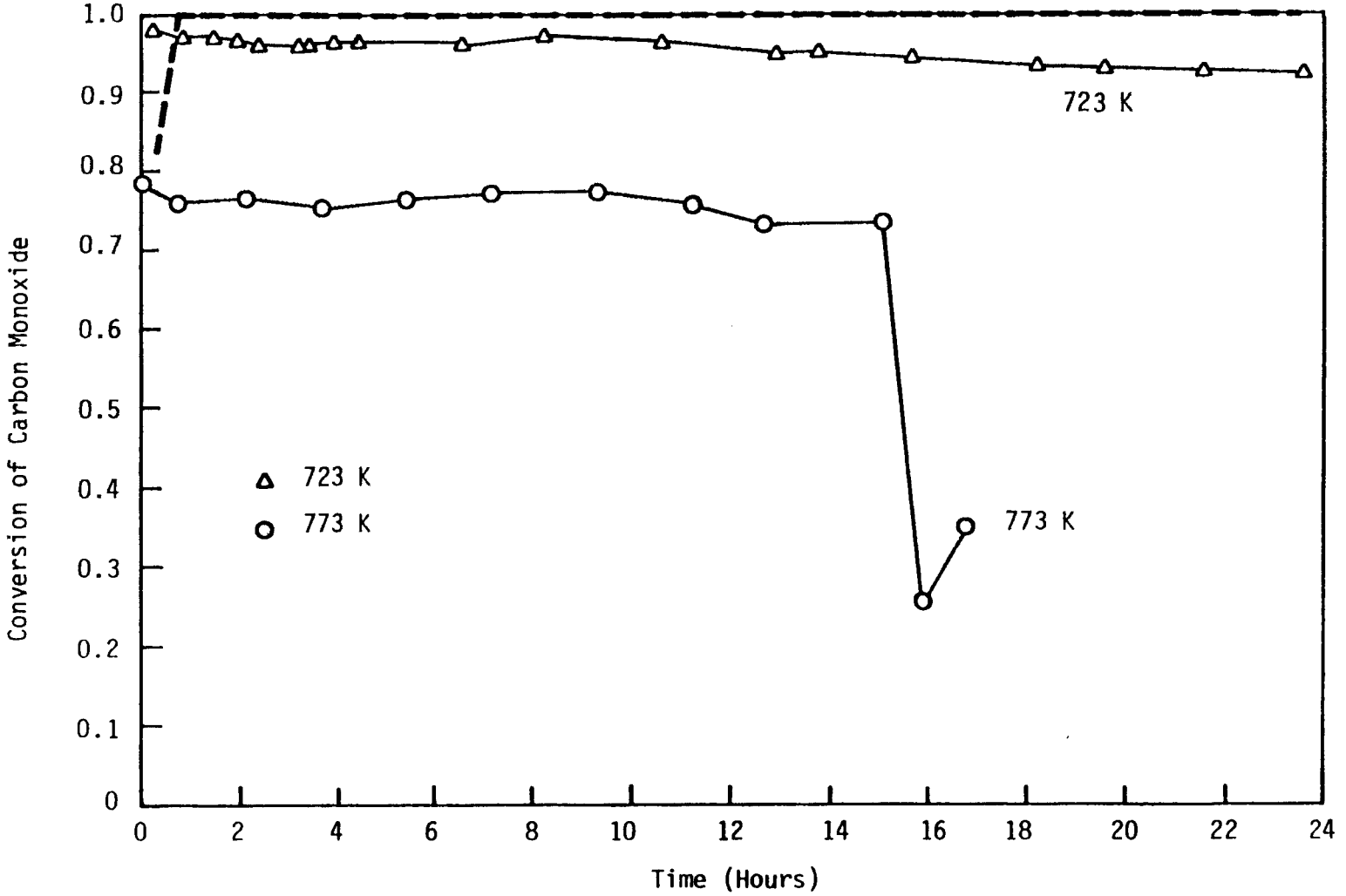

Figure 24. Long Term Deactivation Curves for Tests at 2500 kPa, and space velocity = 30,000 h^{-1} on 20% Ni on Al_2O_3. For the steam test the reaction mixture was 45% CH_4, 11.5% Ar, 10% H_2, 3% CO, 1.5% CO_2 and 29% H_2O. For the dry tests the mixture was 64% CH_4, 16% Ar, 14% H_2, 4% CO, and 2% CO_2. --- Steam test at 773 K; dry tests at Δ 723 K, O 773 K.

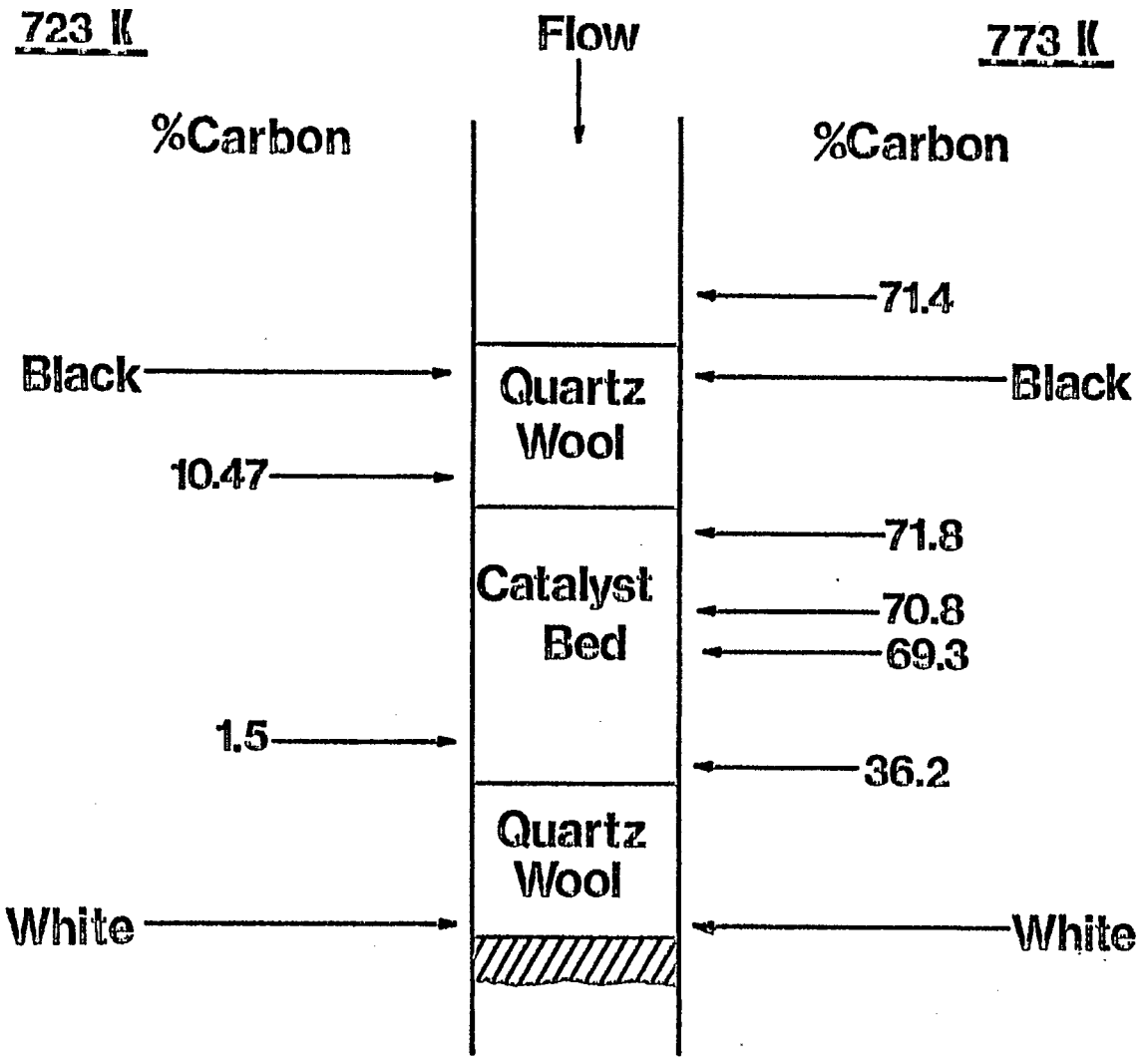

Figure 25. Schematic Diagram of Carbon Deposits after Long Term (24 hour) Tests (no steam).

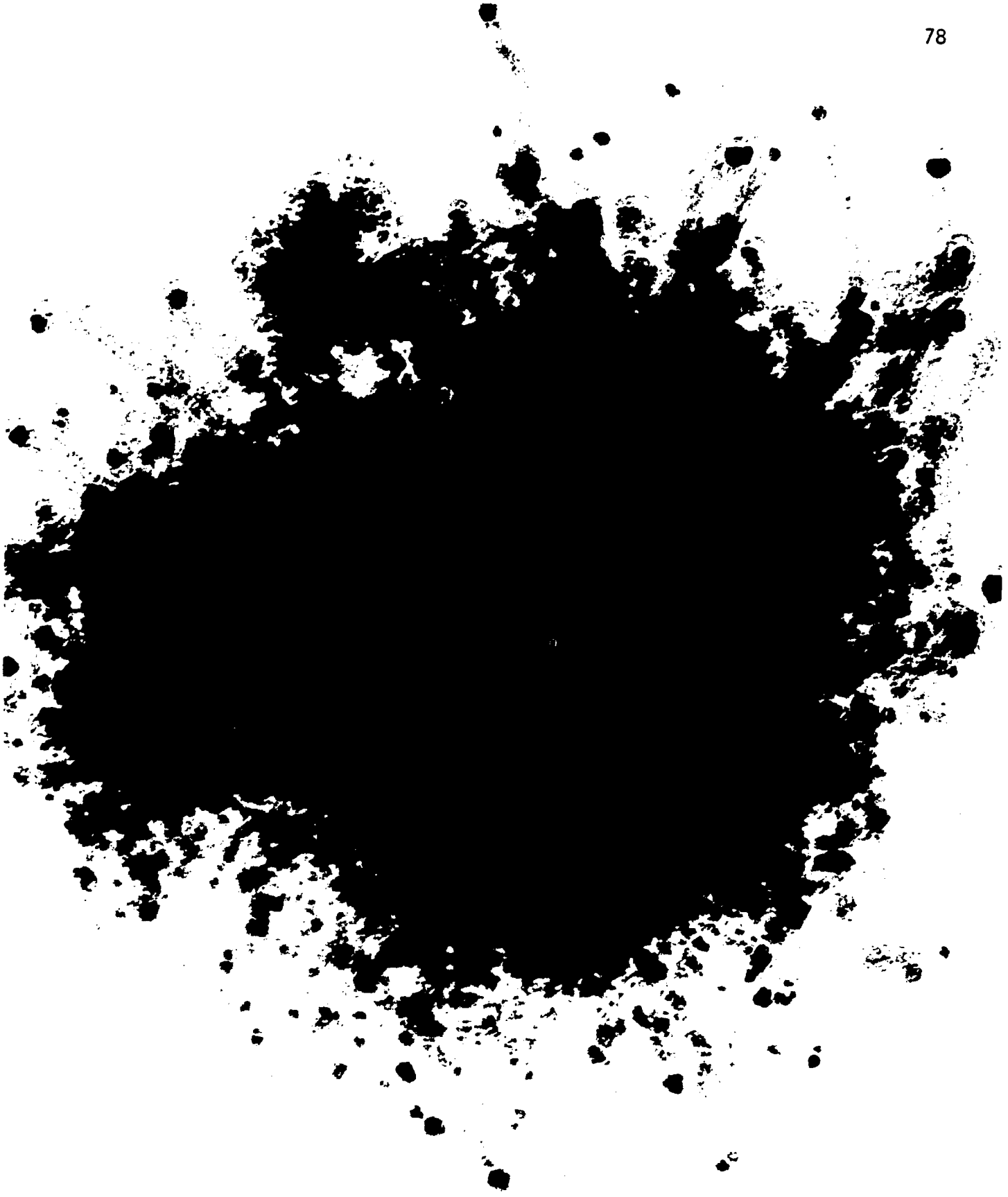

Figure 26. Electron Micrograph of Carbon Formed in the Catalyst Bed during the Long Term Test at 777 K (no steam).

2. Studies of Deactivation of Ni and Ru by Carbon

In the previously discussed investigations of reaction kinetics over nickel catalysts, attempts to measure intrinsic rates at higher reactor pressures were complicated by competing carbon deposition reactions, especially at high reaction temperatures. Similar effects were also observed for ruthenium catalysts (16). During the last three quarters of the contract, experiments were carried out to quantify the effects of deactivation by carbon.

Nickel Catalysts. Rates of deactivation were measured in the Berty recycle reactor at 523 to 623 K and 3450 kPa in a reaction mixture containing 3% H_2, 1% CO and 96% N_2. Conversions were maintained at 10% or below to minimize the effects of product inhibition by water. The use of the recycle reactor enabled kinetic data to be obtained at a constant conversion (i.e. constant CO concentration) and temperature with respect to time and location in the bed.

The results are summarized in Figures 27-31. Normalized rates of CH_4 production are plotted versus time in Figure 27 for temperatures of 548 and 598 K. The catalyst deactivation is more rapid and extensive at 598 than at 548 K. The analysis of several of these deactivation plots indicated a rapid initial loss of activity in the first two hours followed by a slower straight line deactivation rate. The first two hours of the experiments were complicated by unsteady state reactor conditions, which made the data collected during this time inconsistent. Since the data collected after the first two hours were free of such complications and thus more reliable, only these deactivation rates are reported. The rates of deactivation were calculated from the slopes of lines as in Figure 27.

A power law model for deactivation was assumed to have the form:

$$r_d = Ae^{(-E_d/RT)} P_{H_2}{}^a P_{CO}{}^b \qquad (2)$$

The energy of deactivation, E_d, was determined by plotting the natural logarithm of the rates of deactivation versus the inverse temperature (Figure 28). The resulting curve was linear between 523 and 598 K, from which an activation energy of 30 kJ/mole for the rate of deactivation was determined. This value is very close to the activation energy reported by SRI for the conversion of atomic to polymeric carbon (38). Above 598 K, a decrease in the rate of deactivation with increasing temperature was observed. This could be explained by a change in mechanism, i.e. at this point the hydrogenation of carbon may become important.

The effects of H_2 and CO concentration on the rate of deactivation at 598 K are shown in Figures 29 and 30. Decreasing the partial pressure of H_2 from 103.5 to 69 kPa and the H_2/CO ratio from 3 to 2 produced only a small increase in the deactivation rate. On the other hand, increasing the partial pressure of the CO from 38 to 56 kPa and

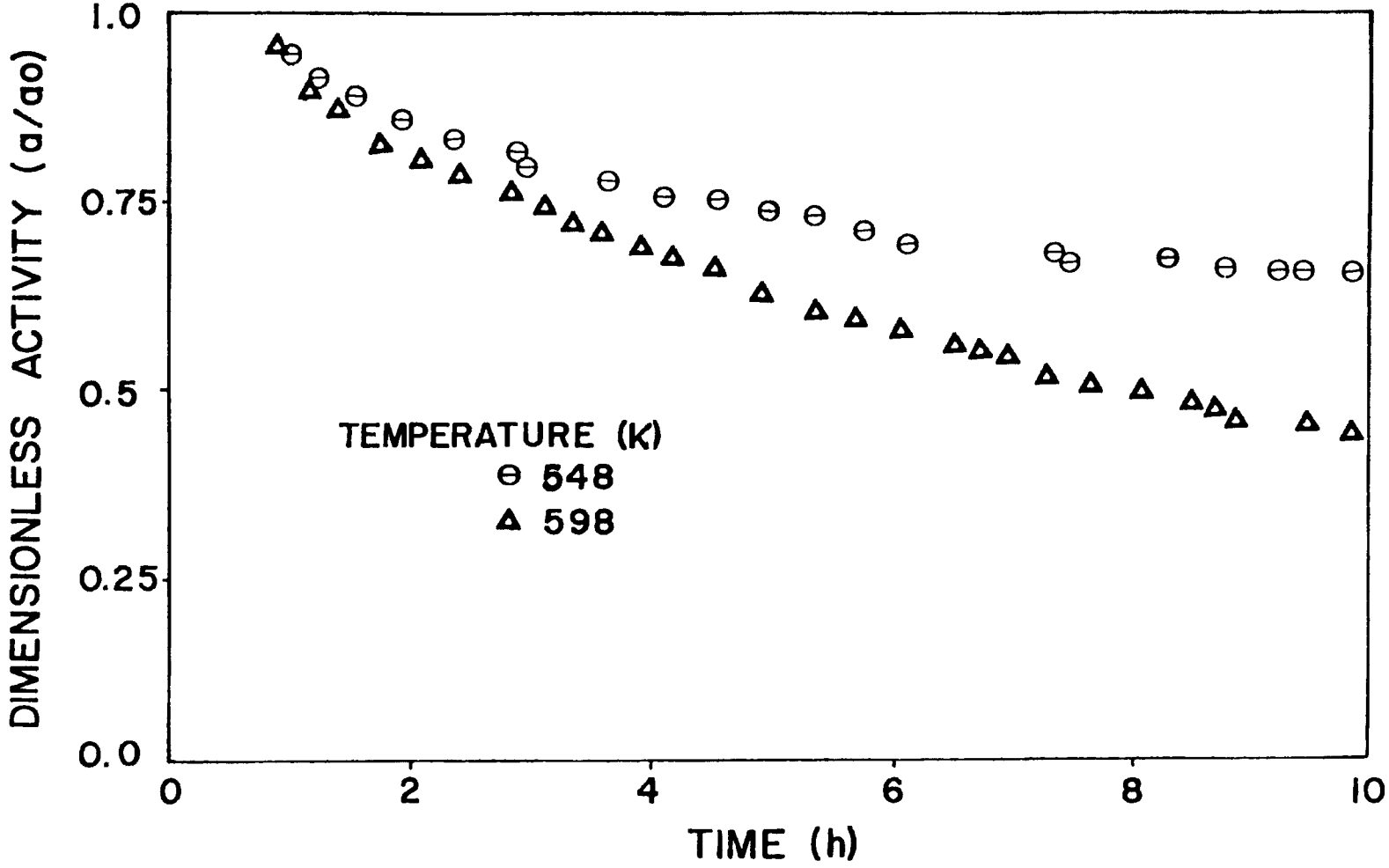

Figure 27. Effect of Time and Temperature on Deactivation of 5% Ni/Al_2O_3/Monolith by Carbon at P_{CO} = 38 KPa and H_2/CO = 3.

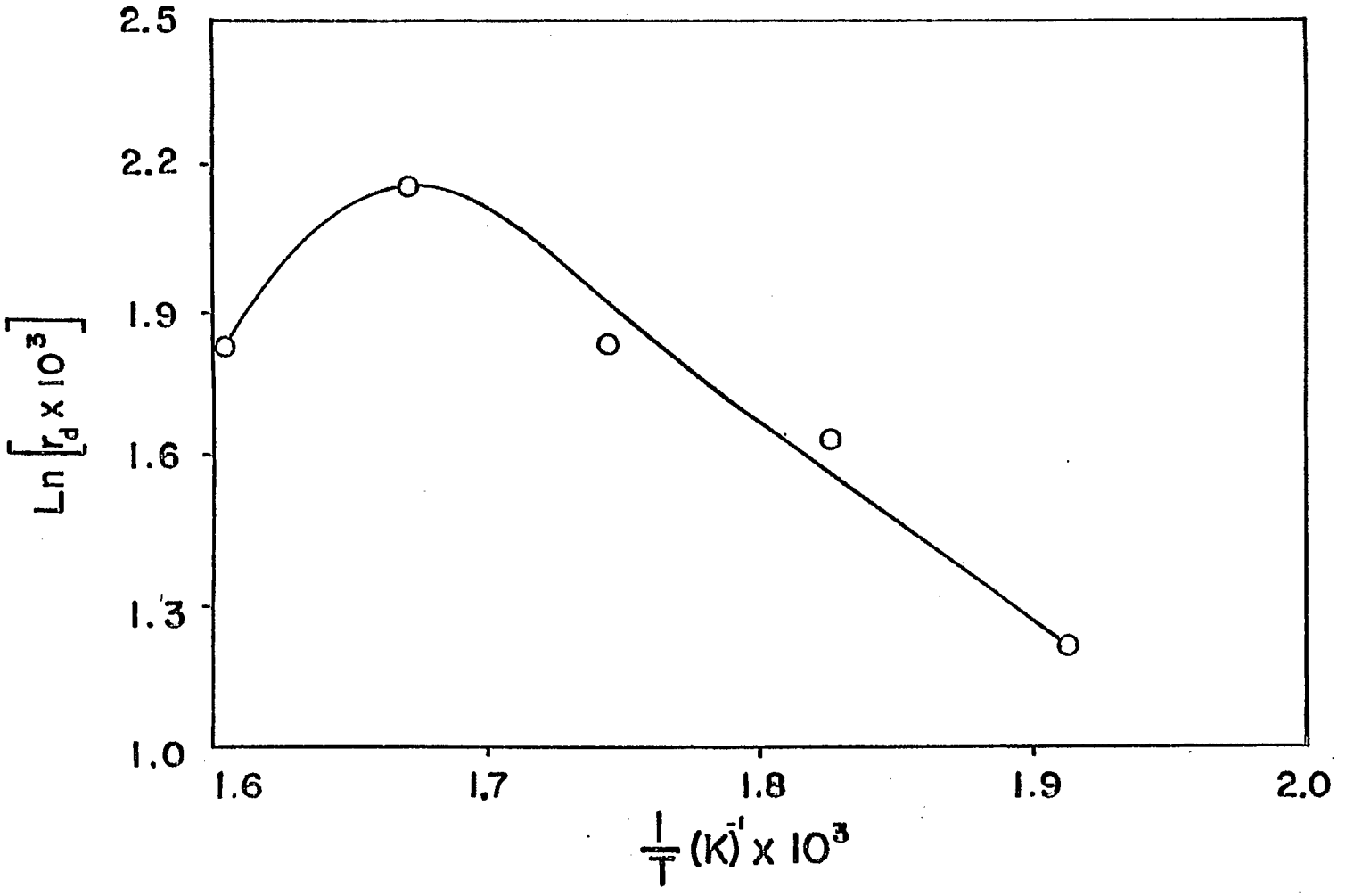

Figure 28. Arrenhius Plot of the Carbon Deactivation Rate [&n Scale] Versus Reciprocal Temperature.

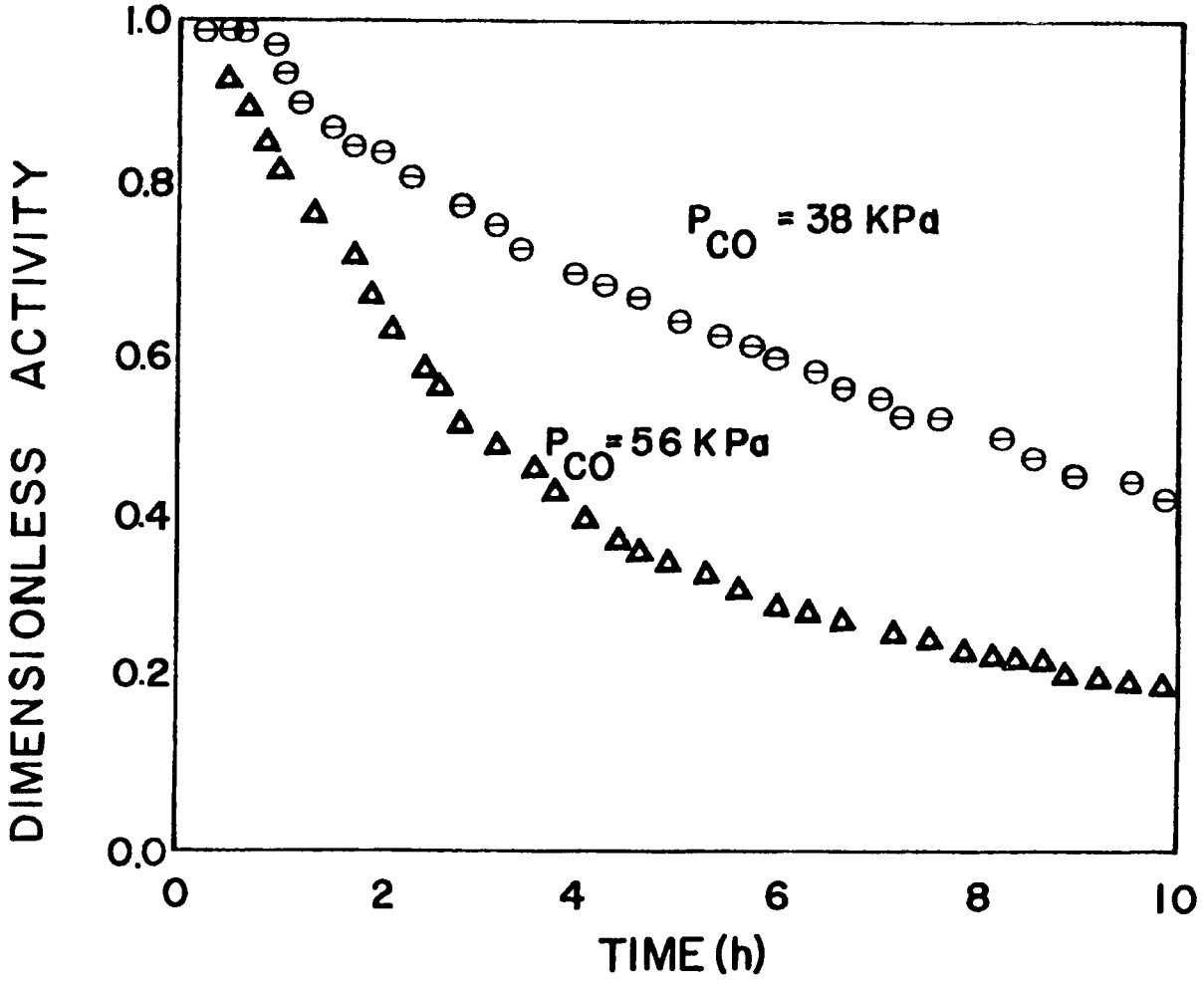

Figure 29. Effects of CO Concentration on Rate of Deactivation by Carbon at 598 K and P_{H_2} = 114 KPa.

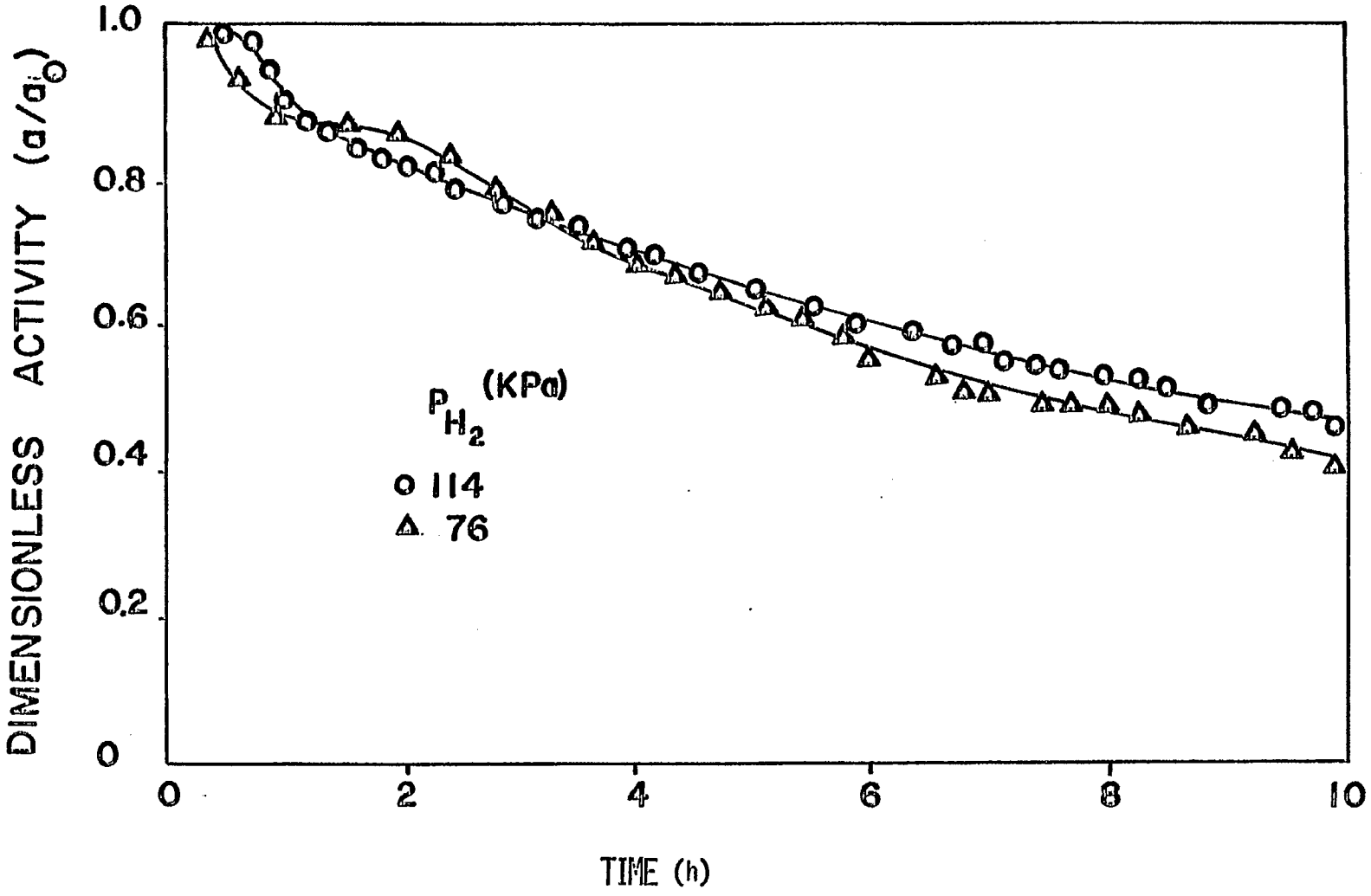

Figure 30. Effect of H_2 Concentration on Rate of Deactivation by Carbon at 598 K and P_{CO} = 38 KPa.

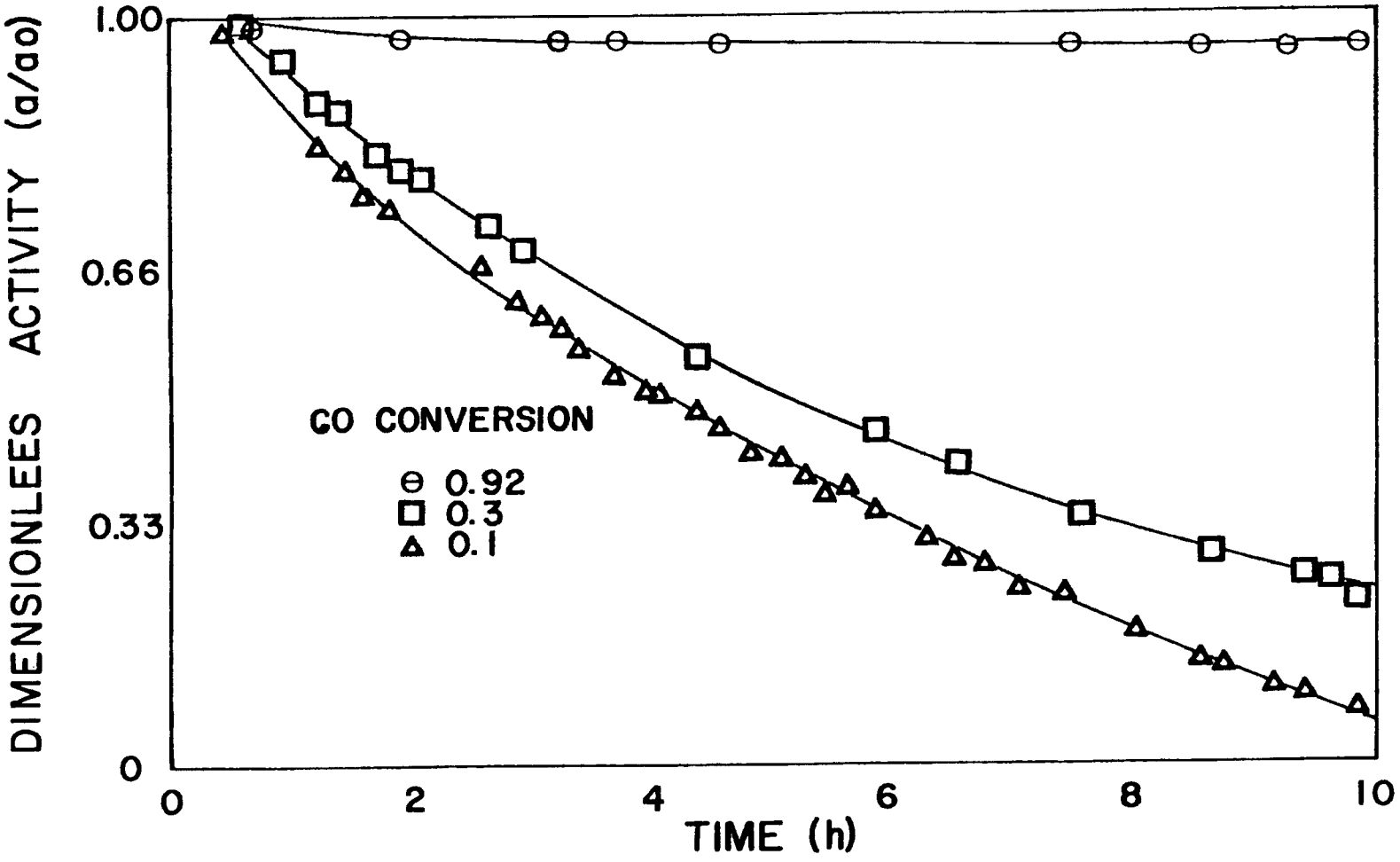

Figure 31. Effects of CO Conversion on Rate of Deactivation by Carbon at 598 K, P_{CO} = 38 KPa (for X_{CO} = 0.1) and H_2/CO = 3.

again decreasing the H_2/CO from 3 to 2 produced a strong increase in the rate of deactivation. The reaction orders for the power law deactivation expression were found to be 1.2 for CO and -0.3 for H_2. A deactivation model of the form

$$da/dt = k_d(P_{CO}/P_{H_2}^{1/2})a \qquad (3)$$

was found to provide an excellent fit to the deactivation data in Figure 27.

It should be emphasized that the data discussed to this point were obtained at low conversions (10% or less). At higher conversions the rates of deactivation were significantly less (see Figure 31). In fact, at 92% conversion the rate of deactivation was barely measureable (again see Figure 31). This fact is not altogether surprising since water, one of the reaction products, has been shown to inhibit the formation of carbon (30).

It should also be mentioned that regeneration of the carbon-deactivated catalysts with H_2 was attempted with limited success. For example, a catalyst (Ni-M-520) which had been tested at 575 K, 3500 kPa and $H_2/CO = 3$ for 10 hours showed a relative activity of 0.45. A portion of the activity (about 10%, i.e. from 0.45 to 0.55) was recovered after treatment in H_2 for 12 hours at 575 K. During the regeneration treatment methane was evolved indicating that hydrogenation of carbon was responsible for the activity recovery.

Further details of this investigation were reported in a Ph.D. dissertation (28) and will be published in a journal article to be submitted (39).

Ru Catalysts. A 0.2% Ru on alumina monolith catalyst was tested for methanation activity in the tenth quarter. Specific rates were obtained using the Berty recycle reactor at temperatures from 515 K to 615 K and 690 kPa (see Figure 32). Conversions were maintained below 10% by increasing space velocities as temperature increased. Methanation activity was found to be highly dependent on temperature over the entire temperature range studied with an apparent activation energy of 113 kJ/mol. Deactivation of the catalyst was temperature dependent with minimal deactivation occurring below 550 K. However, above 575 K extensive deactivation occurred within the first half hour of catalyst use (Figure 33). This shows that the true activation energy behavior is masked if steady state rates are used instead of initial rates. Further details of this study are reported in a note to be submitted (40).

3. Sulfur Poisoning of Nickel Catalysts During Methanation

The effects of H_2S concentration, temperature, and other experimental variables on the rate of sulfur poisoning of nickel during methanation was investigated during the last 1 1/2 years of the contract period.

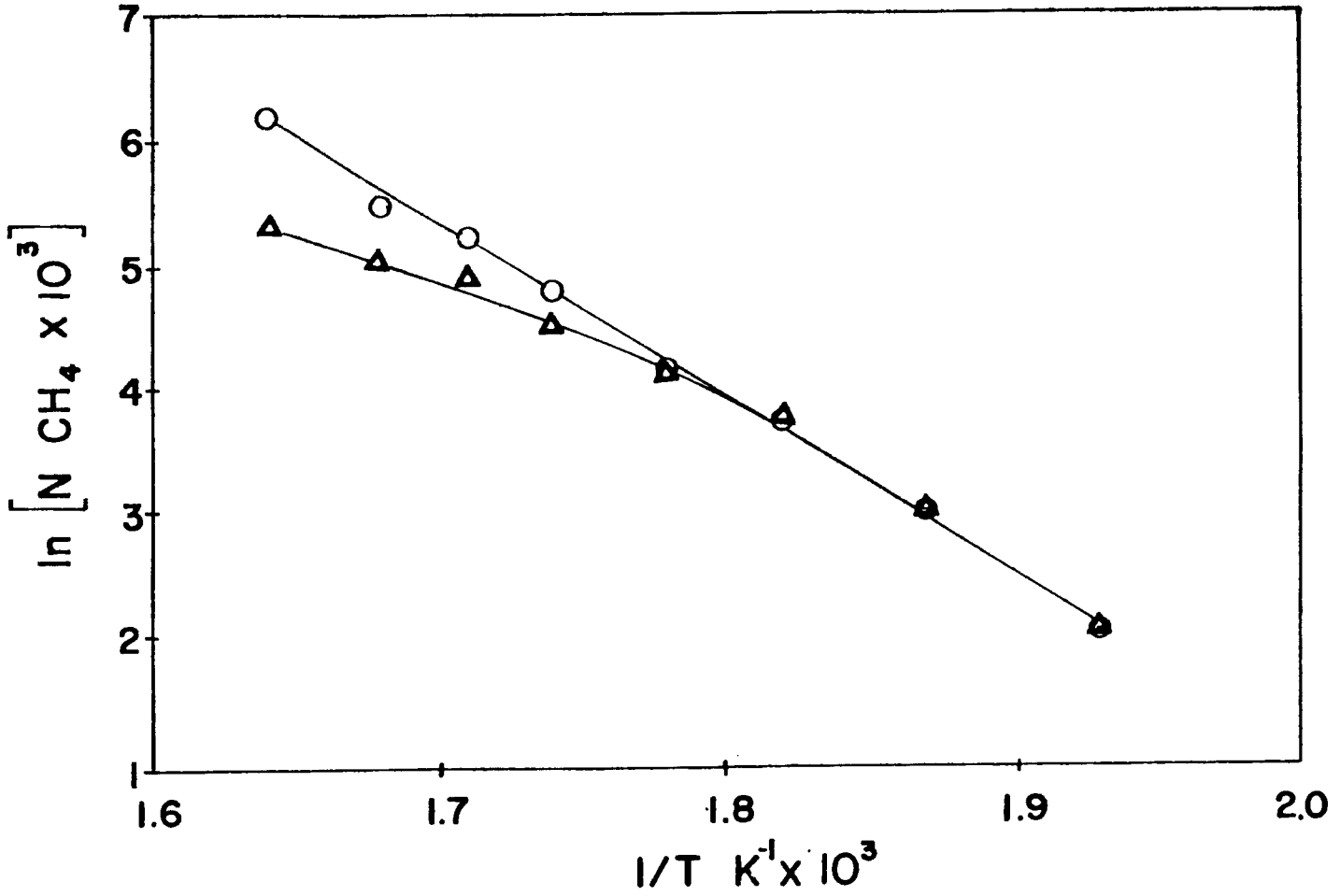

Figure 32. Specific rates of methanation on 0.5% Ru/Al_2O_3 (ℓn scale) versus reciprocal temperature. ○initial activities, △activities after 30 minutes.

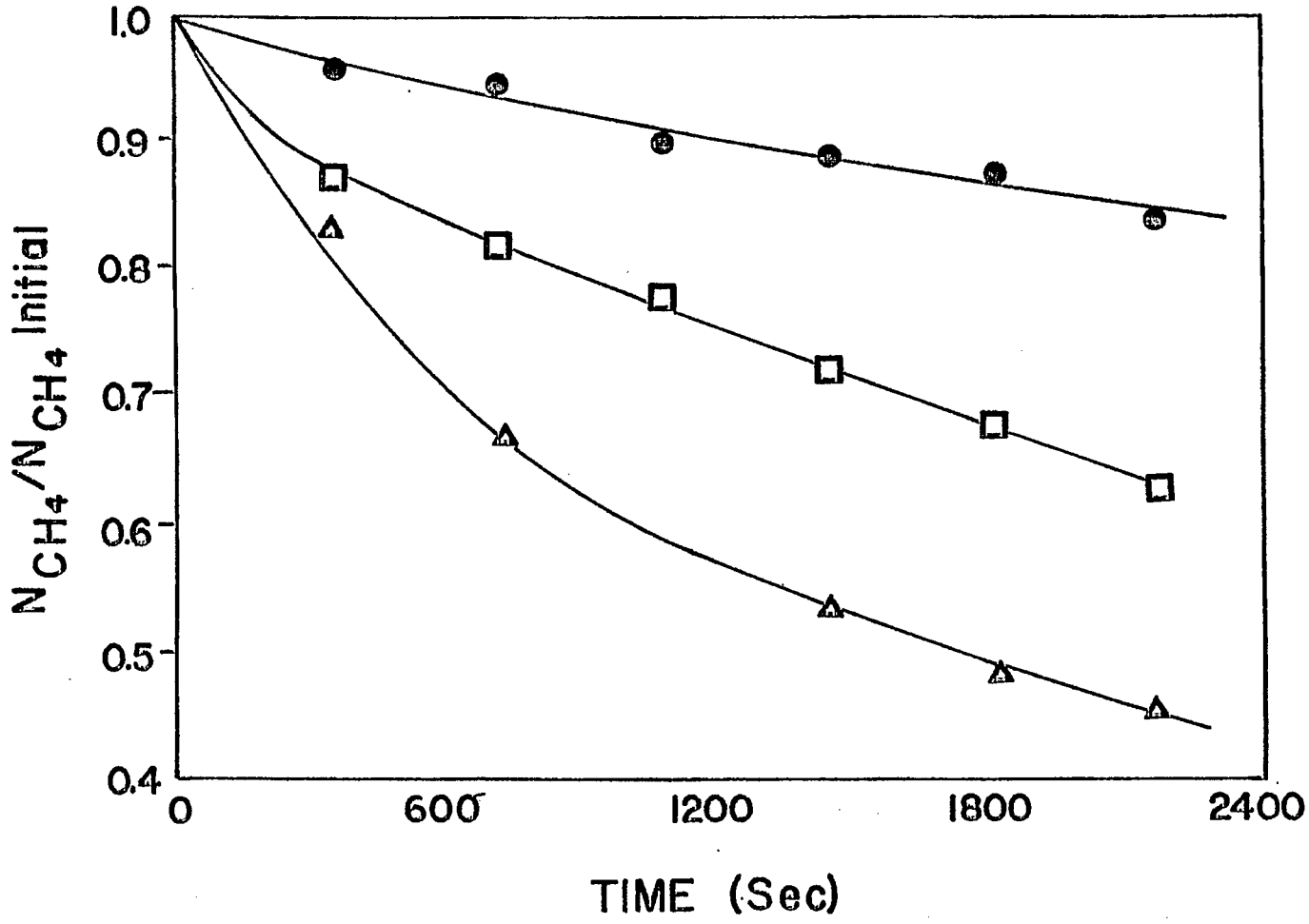

Figure 33. Normalized activity versus time for 0.5% Ru/Al_2O_3. ●561 K, □584 K, △610 K.

a. Catalysts and Equipment

The composition and hydrogen uptakes for the catalysts investigated are shown in Table 30. Unsupported nickel in powder form (INCO No. 287) was used in most of the experiments to avoid the complications of adsorption of H_2S on the support.

A schematic of the reactor system for H_2S poisoning studies is shown in Figure 34. CO/H_2 and H_2 gases were purified with a heated mole sieve and a NiX-0X catalyst followed by a mole sieve trap respectively. CH_4 was analyzed by flame ionization, CO, H_2, CO_2 by thermal conductivity, and H_2S (and other sulfur compounds) by a flame photometric detector. The details of the column configuration are described elsewhere (27). All of the lines, valves and fittings in contact with H_2S were of quartz or teflon. The reactor was generally a fixed bed pyrex or quartz microreactor described previously (3). Selected runs were carried out using a Quartz internal recycle reactor described elsewhere (4,41). Corrections were made for adsorption on each of the reactors.

b. Procedure

A 0.4 to 0.6 g sample of catalyst powder was loaded into the Pyrex or quartz microreactor (or a sample of monolithic catalyst was loaded in the CSTR reactor). The sample was reduced in flowing hydrogen (GHSV = 10,000 h^{-1}) at 573 K for 2 hours. For runs at temperatures above 573 K the reduction temperature was 673 K. The cell was then cooled in flowing hydrogen to the run temperature and the sample was exposed to the reactant mixture, typically 1% CO in H_2 (GHSV = 40,000 h^{-1}) for two hours. H_2S was subsequently added by decreasing the hydrogen flow and replacing it with an H_2S/H_2 mixture. Chromatographic measurements were conducted intermittently every 15-30 min. over a period of 8-24 hours.

c. Results

Effects of Sulfur on Methanation Kinetics. The effects of presulfiding on the kinetics of methanation over Ni/Al_2O_3 were examined during the seventh quarter (13). The results showed that the temperature and concentration dependencies were unaffected by preadsorbed sulfur, a fact suggesting that sulfur poisons by blocking available nickel sites; in other words the activity properties of the unpoisoned sites are unaffected. This observation is in agreement with results reported by Fitzharris (42) and by Pederson and Rostrup-Nielsen (43).

Effects of H_2S Concentration on the Rate of Deactivation. A typical normalized activity versus time plot is shown in Figure 35 and the results of H_2S deactivation runs in the fixed-bed microreactor at several H_2S concentrations are summarized in Table 31. The parameter k_d is the deactivation rate constant based upon the Ablow-Bartholomew deactivation model (27,44) which assumes a deactivation rate $da/dt = k_d(H_2S)(a)$ where a is normalized activity. There is a general trend toward higher k_d values as H_2S concentration is reduced. SR

Table 30

Physical Data for Ni Catalysts

Catalyst	Composition wt% Ni	Hydrogen Uptake μmoles/g	BET Surface Area m^2/g
Inco Powder #287	100	5.1	0.49
Monolith (2% Al_2O_3 on Cordierite)	0.1	3.3	-
Supported Powder	3	25	-

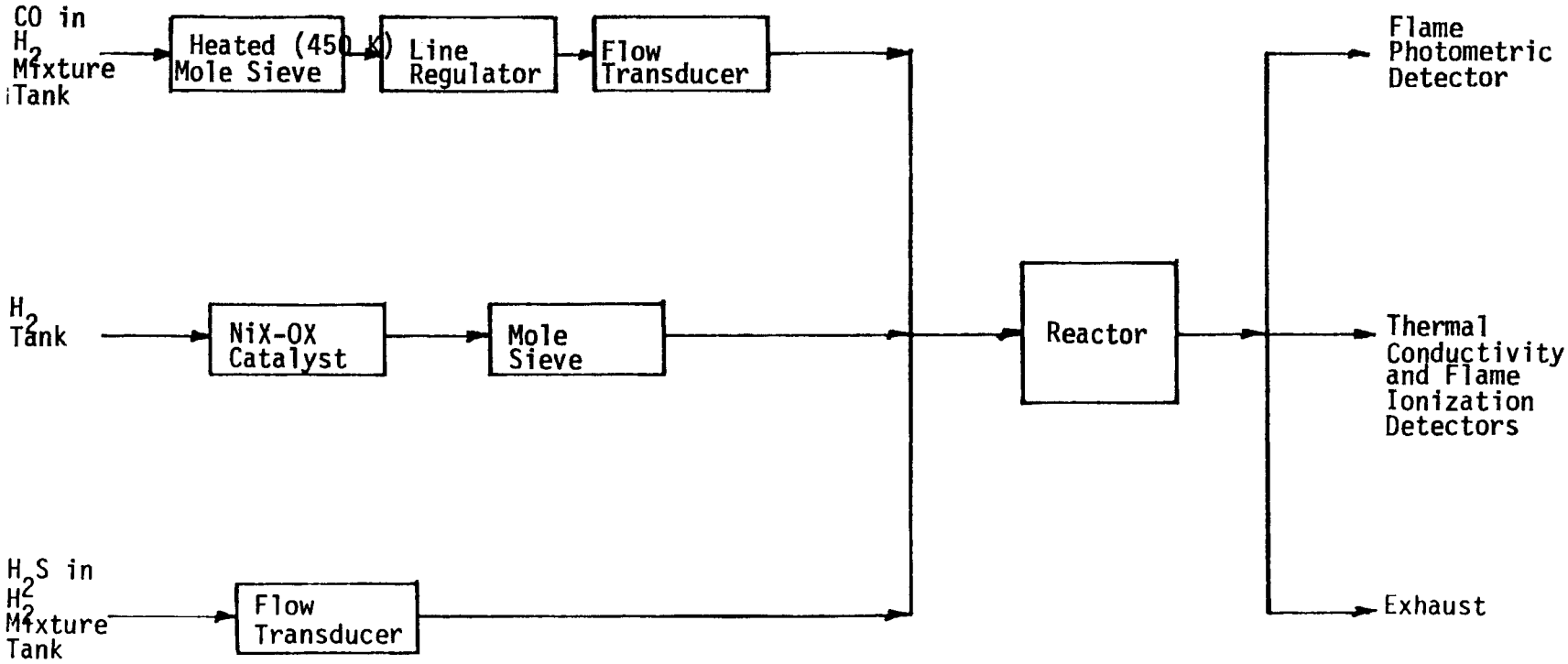

Figure 34. Reactor System for H_2S Poisoning Studies

Table 31

Deactivation Rate Constants For
Several H_2S Concentrations[a]

H_2S Concentration ppm	P_{H_2S}/P_{H_2} x 10^6	k_d[b]	SR[c]
6.6	33	1.3	0.2
1.0	5.0	2.0	0.3
1.0	1.0	2.0	0.3
0.5	0.5	2.3	0.5
0.2	0.2	4.8	0.9

[a]All runs were made on INCO nickel powder at 525 K, 100 kPa, and with large H_2/CO_1 ratios. Space velocity was between 40,000 and 80,000 h^{-1}.

[b]k_d is the deactivation constant from the Ablow-Bartholomew deactivation model (Ref. 41).

[c]SR is the number of nickel sites deactivated per adsorbed H_2S molecule.

is the site ratio corresponding to the number of sites deactivated per adsorbed H_2S molecule. This ratio is calculated from the slope of the deactivation curve shown in Figure 35. For the 1 ppm case, SR is 0.3, i.e. each adsorbed H_2S molecule deactivates only 1/3 of a nickel site. From the plot of the 0.2 ppm H_2S run (Figure 35), the slope of SR is 0.9, corresponding to about 1 site deactivated per adsorbed H_2S molecule. Thus the number of nickel sites deactivated per adsorbed sulfur increases with decreasing H_2S concentration.

Effects of Temperature. Temperature was found to influence the rate of deactivation and SR values only slightly (see Table 32). At 1 ppm H_2S values of k_d and SR increase as temperature is increased from 525 to 625 K. For the runs at 0.2 ppm H_2S, k_d and SR increase only slightly as temperature is increased from 525 to 600 K. At 1 ppm the apparent activation energy for k_d is 18.4 kJ/mol, while the activation energy is 2.4 kJ/mol at 0.2 ppm.

Effects of Carbon Monoxide Concentration. The effects of CO concentration on H_2S deactivation were studied by making four tests with different CO concentrations while holding the H_2S concentration constant. Table 33 lists the k_d and SR values. During these tests H_2S appeared in the exit stream when the CO concentration was 5% or above. In the 20% CO run only 1/4th of the reactant H_2S adsorbed on the catalyst while the remainder exited in the product stream. SR values in Table 33 were calculated according to H_2S adsorbed. For the 20% CO run SR is much greater than any run at 2% CO. It should be emphasized, however, that the actual observed rate of deactivation at $H_2/CO = 5$ is about the same as at $H_2/CO = 20$ because in the latter case only 1/4 of the H_2S adsorbs on the catalyst. It should also be emphasized that these tests were performed at a temperature (525 K) and at CO partial pressures well below those that would result in carbon deactivation (30).

Effects of Water Vapor. Two tests were made with H_2O vapor added to the feed. These tests are compared with a similar dry test in Table 34. With H_2O vapor present k_d increases for the unsupported catalyst. Comparing the supported catalyst to the unsupported Ni, H_2S adsorption capacity was significantly increased in the former since the alumina adsorbed (in addition to Ni) large amounts of H_2S. Thus, k_d is smaller for the supported catalyst as not all the adsorbed H_2S deactivated the metal surface. Nevertheless, SR is the same for both catalysts, as expected if there were no support effect other than adsorption.

Stoichiometry of H_2S Deactivation. H_2S deactivation runs were performed in a quartz mixed-flow reactor in order to determine the stoichiometry of H_2S poisoning of metal over a range of temperature. The approach was similar to that used by Fitzharris (42). Activity of the catalyst was plotted against various functions of the unsulfided surface area of the catalyst. Figure 36 shows such a plot for the deactivation of a nickel monolith at 573 K and 1 ppm. When plotted

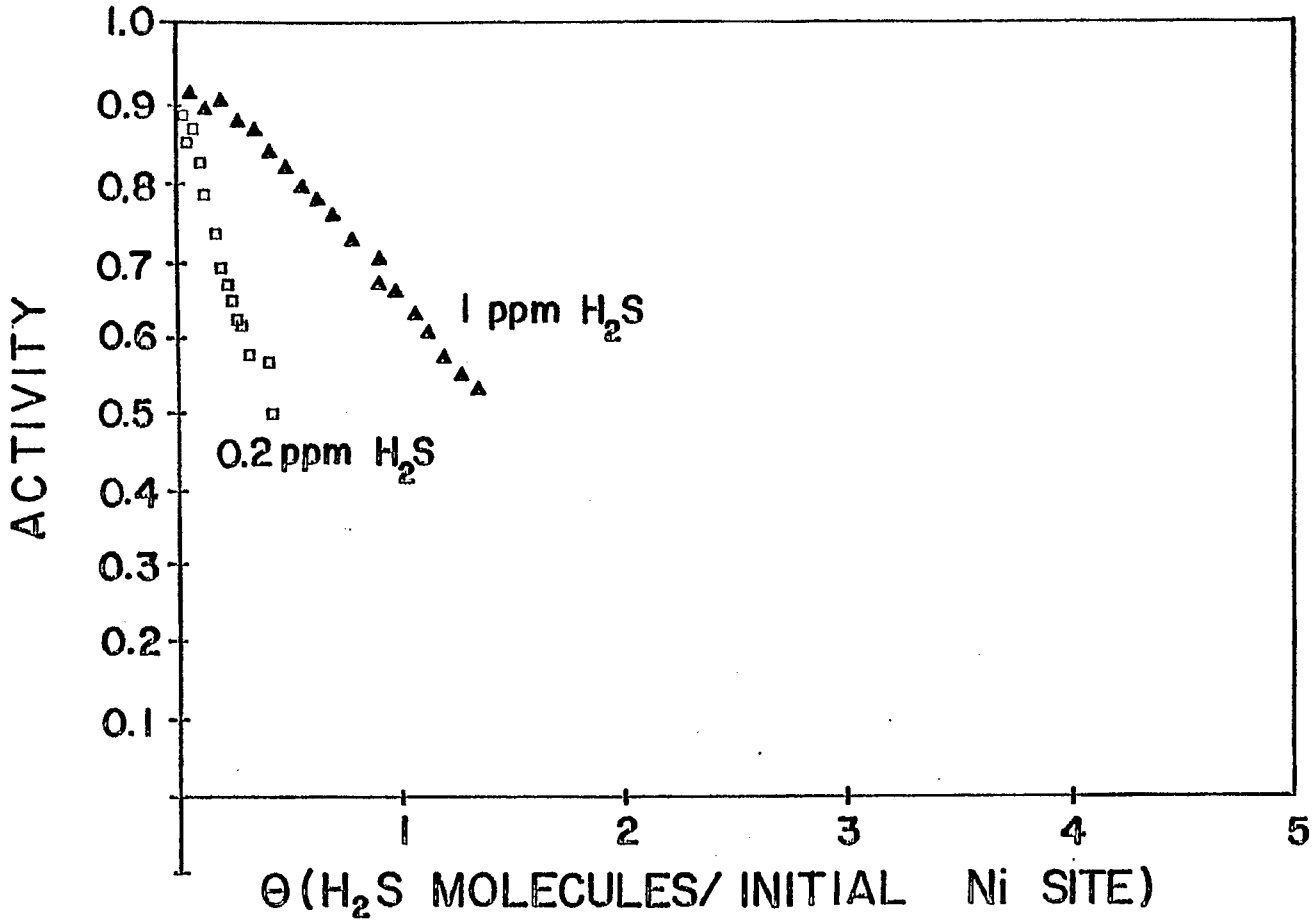

Figure 35. Activity vs. θ (H_2S molecules adsorbed/initial Ni site), Reactor conditions were 525 K, 100 kPa, 3% CO in H_2 and 500 x 10^{-6} m^3/min.

Table 32

Temperature Effects on Deactivation Rate Constants[a]

Temperature (K)	k_d[b]	SR[c]
1 ppm H_2S		
525	2.0	0.3
575	2.3	0.4
625	4.0	0.6
0.2 ppm H_2S		
525	4.8	0.9
575	4.8	1.0
600	5.2	1.0

[a]All runs were performed on INCO nickel powder at 100 kPa and 1 or 2% CO with hydrogen diluent. Thus, the ppm H_2S and the P_{H_2S}/P_{H_2} ratio were the same.

[b]k_d is the deactivation rate constant from the Bartholomew model.

[c]SR is the number of nickel sites deactivated per adsorbed H_2S molecule.

Table 33

Deactivation Rate Constants for a Range of CO Concentrations

Mole % CO	H_2/CO Ratio	P_{H_2S}/P_{H_2} x10^6	k_d [b]	SR [c]
2	50	0.2	4.8	0.9
5	20	0.21	6.3	1.2
10	10	0.22	9.0	1.6
20	5	0.25	22	4.4

[a] All runs were performed on INCO nickel powder at 525 K, 100 kPa, and with a hydrogen diluent. The space velocity was 80,000 h^{-1}, P_{H_2S} = 0.2 ppm.

[b] k_d is the deactivation rate constant from the Bartholomew model.

[c] SR is the number of nickel sites deactivated per adsorbed H_2S molecule.

Table 34

Effects of H_2O Vapor on H_2S
Deactivation Rate Constants

Catalyst	Mole% H_2O	k_d[b]	SR[c]
INCO Powder	0	4.8	0.9
INCO Powder	1	6.7	0.8
3% Ni/Al_2O_3	1	4.4	0.8

[a]All runs were made at 525 K, 100 kPa, 2% CO in Hydrogen and 0.2 ppm H_2S.

[b]k_d is the deactivation rate constant from the Bartholomew model.

[c]SR is the number of nickel sites deactivated per adsorbed H_2S molecule.

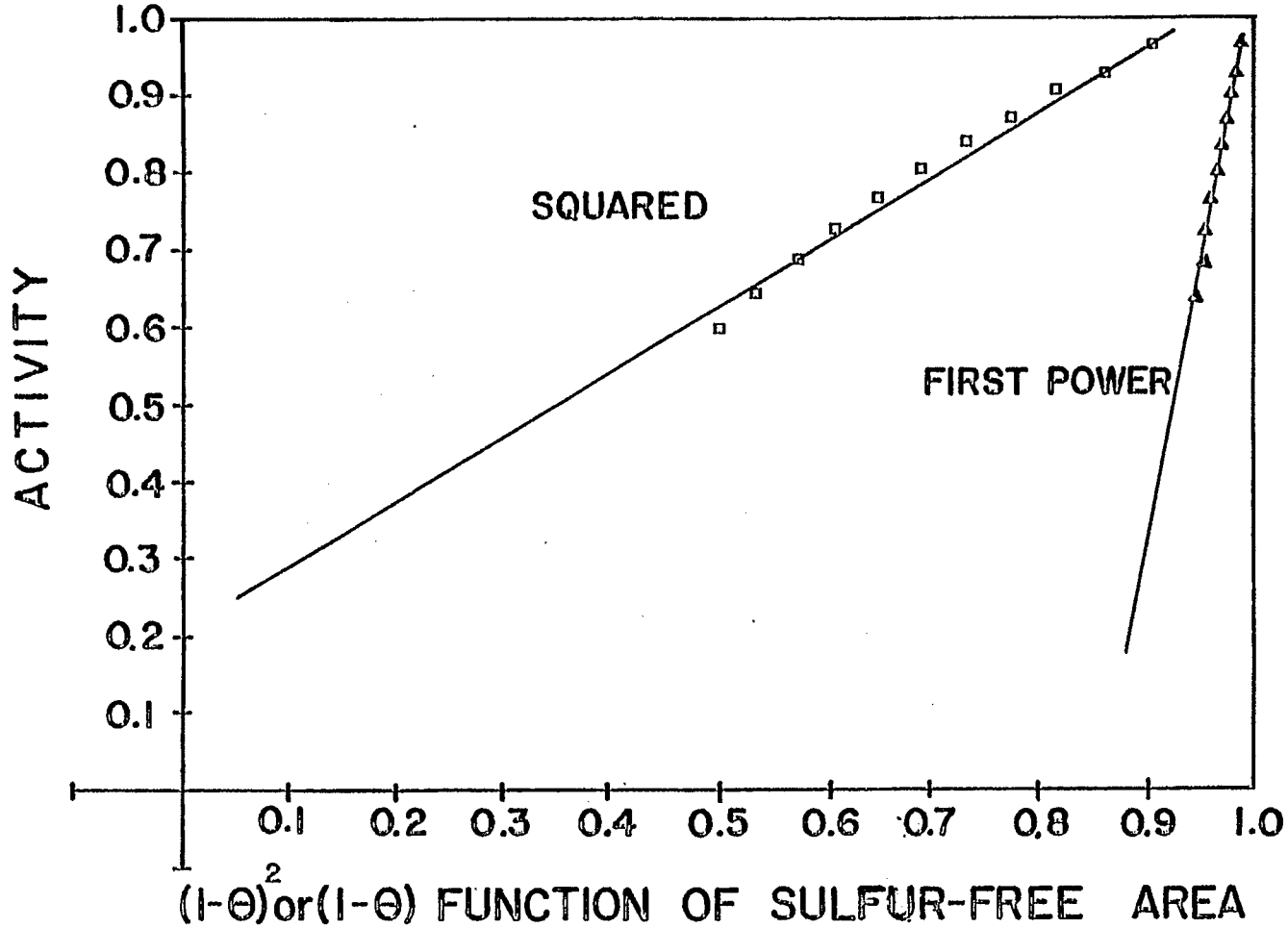

Figure 36. Activity vs. Sulfur-free Area to first and second powers for 0.1% Ni monolith. Test conditions: Quartz CFSTR, 153 x 10^{-6} m^3/min, 1 ppm H_2S, 1% CO in H_2, 100 kPa and 675 K.

against the square of the unsulfided surface area the activity data fit a straight line that passes very near the origin, corresponding to one H_2S molecule deactivating two active sites in good agreement with Fitzharris. Similar plots of data from tests run at 525 to 625 K indicate that the stoichiometry of deactivation is 1.5 at 625 K, and 1 at 575 and 525 K. Thus the SR data from the mixed flow experiments are in good agreement with the data from the fixed bed runs and with the high temperature data of Fitzharris. Collectively the data provide strong evidence that the number of nickel atoms deactivated per sulfur atom adsorbed increases with increasing temperature from 575 to 675 K.

One of the original objectives of our in situ H_2S poisoning investigation was to obtain a generalized deactivation model which would enable prediction of catalyst life at a specified reaction temperature and H_2S concentration. The data from this study do provide a basis for such estimates; however, the changes in sulfur adsorption stoichiometry with temperature, H_2S concentration and reactant concentrations are sufficiently complex to preclude the derivation of a generalized model. It appears that the Ablow-Bartholomew model is applicable at low temperatures since it assumes that one nickel site is deactivated per adsorbed sulfur atom.

Further details regarding this study including the derivation of the Ablow-Bartholomew model are treated in recently completed Ph.D. dissertation (27), were reported at the International Conference on Catalyst Deactivation (45), and will be discussed in a paper to be submitted to the Journal of Catalysis (46).

Task 5: Technical Interaction and Technology Transfer

Publications and presentations pertinent to this contract are summarized in Tables 35 and 36. Altogether six papers were published or accepted, one additional paper was submitted for publication, while six are in preparation (at the time this report was being compiled). Thirteen papers were presented at national and regional meetings while four seminars were presented at other universities and companies in connection with this contract work. The principal investigator visited 14 other laboratories (Table 37) and hosted 22 visitors (Table 38) during the contract period while maintaining close technical communication with 30-40 other engineers and scientists interested in this work, most of whose names are listed in the distribution list in Appendix A. Table 39 lists laboratories or companies to which we submitted catalyst samples developed as part of this contract, for high temperature or long term testing in various methanation processes. These many activities and communications, we feel, emphasize that technical interaction and technology transfer were important aspects of the contract work.

Another very important aspect of this contract work was the education and training of undergraduate and graduate chemical engineering students. Table 40 lists the students supported by

Table 35 Publications in Connection with this contract

1. C.H. Bartholomew, G.D. Weatherbee, and G.A. Jarvi, "Sulfur Poisoning of Nickel Methanation Catalysts, I. In Situ Deactivation by H_2S of Nickel and Nickel Bimetallics," J. Catal. 60, 257 (1979).

2. C.H. Bartholomew and E.J. Erekson, "Experience with an all Glass Internal Recycle Reactor," I and EC Fundamentals, 19, 131 (1980).

3. G.A. Jarvi, K.B. Mayo and C. H. Bartholomew, "Monolithic-Supported Nickel Catalysts, I. Methanation Activity Relative to Pellet Catalysts," Chem. Engr. Commun., 4, 325 (1980).

4. C.H. Bartholomew, G.D. Weatherbee, and G.A. Jarvi, "Effects of Carbon Deposits on the Specific Activity of Nickel and Nickel Bimetallic Catalysts," Chem. Eng. Commun. 5, 125 (1980).

5. C.H. Bartholomew and R.B. Pannell, "Sulfur Poisoning of H_2 and CO Adsorption on Supported Nickel," Preprints ACS Div. of Petr. Chem. 25(2), 319 (1980).

6. D.G. Mustard and C.H. Bartholomew, "Determination of Metal Crystallite-Size and Morphology in Supported Nickel Catalysts," J. Catal, in press.

7. C.H. Bartholomew and R.B. Pannell, "Sulfur Poisoning of H_2 and CO Adsorption on Supported Nickel," Manuscript in preparation.

8. E.J. Erekson, E.L. Sughrue, and C.H. Bartholomew, "Catalyst Degradation in High Temperature Methanation," Submitted to Fuel Processing Technology, 1980.

9. E.J. Erekson and C.H. Bartholomew, "Sulfur Poisoning of Nickel Methanation Catalysts II. Effects of H_2S Concentration, Temperature and Support on Deactivation Rates and Adsorption Stoichiometry," Manuscript in preparation, 1980.

10. E.L. Sughrue and C.H. Bartholomew, "Kinetics of CO Methanation on Nickel Monolithic Catalysts," Manuscript in preparation, 1980.

11. E.L. Sughrue and C.H. Bartholomew, "Effects of Carbon Deposits on Activity of Nickel Monolithic Catalysts," Manuscript in preparation, 1980.

12. R.M. Bowman, E.L. Sughrue, and C.H. Bartholomew, "Effects of Carbon Deposits on Activity of Ruthenium Methanation Catalysts," "Note in preparation, 1980.

13. E.L. Sughrue and C.H. Bartholomew, "Models of CO Methanation in Ni/Al_2O_3-Coated Monolithic Catalysts, I. A Two Species Model Using Power Rate Law Kinetics," Manuscript in preparation, 1980.

Table 36 Technical Meeting Papers and Presentations in Connection with the Contract

Technical Meeting Papers

1. G. D. Weatherbee, G. A. Jarvi and C. H. Bartholomew, "In situ Poisoning of Alumina-Supported Ni and Ni Bimetallic Catalysts," Third Rocky Mountain Fuel Symposium, Albuquerque, Feb. 10-11, 1978.

2. G. D. Weatherbee, G. A. Jarvi, and C. H. Bartholomew, "In situ H_2S Poisoning of Alumina-Supported Ni and Ni Bimetallic Catalysts," Conference on Catalysts Deactivation and Poisoning, May 24-26, 1978, Lawrence Berkeley Laboratory.

3. G. D. Weatherbee, G. A. Jarvi, and C. H. Bartholomew, "Nickel Bimetallic Catalysts for Methanation of CO," 85th National AIChE Meeting, Philadelphia, June 4-8, 1978.

4. G. D. Weatherbee, R. W. Fowler, and C. H. Bartholomew, "Sulfur Poisoning of Nickel Methanation Catalysts," 71st Annual Meeting of the AIChE, Miami, Nov. 12-16, 1978.

5. E. Sughrue, E. J. Erekson, and C. H. Bartholomew, "High Temperature Degradation of Methanation Catalysts," Fourth Rocky Mountain Fuel Symposium, Salt Lake City, Feb. 9-10, 1979.

6. C. H. Bartholomew, G. D. Weatherbee, and D. C. Gardner, "Deactivation of Methanation Catalysts by Carbon Deposits," Sixth North American Meeting of the Catalysis Society, Chicago, Ill., March 18-22, 1979.

7. G. A. Jarvi, K. B. Mayo, and C. H. Bartholomew, "Monolithic-Supported Nickel Catalysts: I. Methanation Activity Relative to Pellet Catalysts," 86th National AIChE Meeting, Houston, Texas, April 1-5, 1979.

8. E. L. Sughrue, and C. H. Bartholomew, "Kinetic Studies of Nickel Methanation Catalysts," Fifth Rocky Mountain Fuel Symposium, Salt Lake City, Utah, Feb. 21-22, 1980.

9. C. H. Bartholomew and D. G. Mustard, "Determination of Metal Crystallite Size in Supported Nickel Catalysts," Spring Meeting of the California Catalysis Society, Berkeley, CA, March 13-14, 1980.

10. C. H. Bartholomew, R. B. Pannell, J. L. Butler, and D. G. Mustard, "Nickel-Support Interactions: Their Effects on Particle Morphology, Adsorption and Activity/Selectivity Properties, 179th Meeting of the ACS, Houston, March 25-27, 1980.

11. C. H. Bartholomew and R. B. Pannell, "Sulfur Poisoning of CO and H_2 Adsorption on Supported Nickel," 179th Meeting of the ACS, Houston, March 25-27, 1980

12. E. L. Sughrue and C. H. Bartholomew, "Kinetics of CO Methanation on Nickel Monolithic Catalysts," 73rd National Meeting of the AIChE, Chicago, Ill., Nov. 16-20, 1980.

13. C. H. Bartholomew and James R. Katzer, "Sulfur Poisoning of Nickel in CO Hydrogenation," International Symposium on Catalyst Deactivation," Antwerp, Belguim, Oct. 13-15, 1980.

Presentations at Universities and Companies

1. C. H. Bartholomew, "Kinetics of Methanation Alloy Catalysts," Institute for Mining and Mineral Research, University of Kentucky, Lexington, Kentucky, October 10, 1977.

2. C. H. Bartholomew, "H_2, CO and O_2 Adsorption on Nickel," Norton Chemical Company, Akron, Ohio, May 15, 1978.

3. C. H. Bartholomew, "Molybdenum-Based Methanation Catalysts," Climax Molybdenum Co. of Michigan, Ann Arbor, Mich., June 5, 1978.

4. C. H. Bartholomew, "Sulfur Poisoning of Nickel Methanation Catalysts," Gulf Research and Development, Pittsburgh, Penn., September 25, 1978.

Table 37 Laboratories Visited by Principal Investigator During Contract Period

	Laboratory Visited	Host(s)	Date Visited
1.	University of Kentucky & Institute for Mining and Minerals Research	Prof. Phil Reucroft Dr. John Hahn, Assoc. Director	Oct. 10, 1977
2.	Division of Photochemistry Los Alamos Scientific Lab	Dr. Reid Jensen	May 3, 1978
3.	Norton Chemical Co. Akron, Ohio	Dr. Joseph Kiovsky	May 15, 1978
4.	Climax Molybdenum Co. Ann Arbor, Michigan	Dr. Robert Ference	June 5, 1978
5.	Gulf Research Co. Pittsburgh, Penn.	Dr. Thadeous Kobylinski Dr. Richard Pannell	Sept. 25, 1978
6.	Institute of Gas Technology	Mr. Tony Lee	June 13, 1979
7.	Chemicals Division Ventron Corp. Beverly, Mass.	Dr. Larry Guilbault Dr. Robert Wade	June 22, 1979
8.	Dept. of Chem Eng. Univ. of Delaware	Prof. James Katzer	June 29-30 1979
9.	Process Sciences & Engineering Div. Pittsburgh Energy Technology Center	Dr. Richard Schehl	Oct. 31, 1979
10.	Cornell University	Prof. Robert Merrill	Feb. 14, 1980
11.	Dept. of Chem Eng. Univ. of Delaware	Dr. Glen Schraeder Dr. James Katzer	April 9-12, 1980
12.	Catalytica Associates	Dr. Robert Garten Dr. Ralph Dalla Belta Dr. Richards Levy	April 15, 1980
13.	Lawrence Berkeley Lab University of California	Dr. Heinz Heinemin	April 16, 1980
14.	Refinery Research Science & Technology Union Oil Research Brea, California	Dr. Kess Alley Dr. Dennis McArthur Dr. David Mears	Summer 1980

Table 38 Visitors and Speakers, BYU Catalysis Laboratory, During Contract Period

Prof. Henry Dou	Le Centre National de la Recherche Scientifique France	Nov. 8, 1977
Dr. Robert Ference Technical Specialist	Catalyst Development Climax Molebdenum Co. of Michigan	Mar. 17, 1978
Mr. William Boyer Technical Specialist	Ceramic Products Corning Glass Works	July 19, 1978
Dr. Larry Guibault Mr. Fred Hoover Mr. James Grayer	Chemical Research Ventron Corp. Hercules	July 26, 1978
Dr. Donald LaRue Dr. Victor Kelsey	Idaho International Lab	Oct. 12, 1978
Dr. Frank Massoth Mr. Kyung Sup Chung	University of Utah	Dec. 6, 1978
Dr. Frank Williams Associate Professor	University of New Mexico	Feb. 8, 1979
Dr. William Thomson Associate Professor	University of Idaho	Feb. 13, 1979
Dr. Wayne Pretzer	Catalysis Research Gulf Res. & Dev. Co.	Mar. 1, 1979
Dr. Richard Pannell	Catalysis Research Gulf Res. & Dev. Co.	Mar. 26, 1979
Dr. Francis Hanson Associate Professor	Department of Fuels Eng. University of Utah	Mar. 29, 1979
Dr. Steven Fong	Analytical Research Corning Glass Works	May 17, 1979
Dr. Robert Ference Technical Specialist	Catalyst Development Climax Molybdenum Co. of Michigan	Oct. 1-2, 1979
Prof. M. Albert Vannice Associate Professor	Dept. of Chemical Eng. Penn. State U.	Oct. 2, 1979
Professor Robert Merrill	Dept. of Chemical Eng. Cornell Univ.	Oct. 8, 1979

Dr. P. Govind Menon	Laboratory for Petrochem. Eng. State University of Ghent, Belgium	Oct. 26, 1979
Dr. Perry Maxfield	Department of Chemistry Brigham Young University	Nov. 6, 1979
Dr. Richard Pannell	Catalysis Research Gulf Res. & Dev. Co.	Feb. 26, 1980

Table 39 Companies Or Laboratories to which Catalyst Samples were Submitted for Testing

	Companies	Samples Submitted
1.	Northwest Battelle	Ni/Al_2O_4 pellets Ni/Al_2O_3/Monoliths
2.	Conoco	Ni/Al_2O_4/Monolith Samples
3.	Unilever Research Netherlands	$Ni\text{-}MoO_3$ Catalysts

Table 40 Students Supported by this Contract

Name	Degree	
Erek J. Erekson	Ph.D.	Completed May, 1980 Employed by Gulf Research
Edward L. Sughrue	Ph.D.	Completed July, 1980 Employed by Phillips Research
George A. Jarvi.	M.S.	Completed April, 1978 Employed by Engelhard
Donald G. Mustard	M.S.	Completed June, 1980 Employed by Arco, Houston
Gordon D. Weatherbee	M.S.	Completed August, 1979 Pursuing Ph.D. work at BYU
Richard Bowman	B.S.	Working on B.S. Plans M.S. work
Clair James	B.S.	Will Finish B.S. 1980
Paul Moote	B.S.	Finished April 1980 Employed by Conoco
Kevin Mayo	B.S.	Finished August 1978 Employed by Dupont
John Watkins	B.S.	Finished August 1979 Employed by Exxon

this contract and Table 41 summarizes the thesis and dissertations obtained in connection with this contract. We feel, in fact, that the education of these students was the most important accomplishment even though we consider some of the technical accomplishments to be significant.

Table 41 M.S. Thesis and Ph.D. Dissertations Supported by this Contract

Author	Title
Dr. Erek J. Erekson	Sulfur Poisoning of Nickel Methanation Catalysts
Dr. Edward L. Sughrue II	Kinetic and Carbon Deactivation Studies of Nickel Methanation Catalysts
George A. Jarvi	Monolithic-Support Nickel and Nickel Bimetallic Catalysts: Methanation Activity and Deactivation of
Donald G. Mustard	Metal Particle Size Determination of Supported Nickel Catalysts
Gordon Weatherbee	Methanation Activity and Deactivation of Alumina Supported Nickel and Nickel Bimetallic Catalysts

IV. CONCLUSIONS

1. H_2 adsorption on Ni/Al_2O_3 is decreased by presulfiding with H_2S in proportion to the fraction of surface covered with sulfur while CO adsorption is increased, apparently due to formation of $Ni(CO)_4$. Thus H_2 adsorption provides a good measure of the degree to which a catalyst has been poisoned.

2. H_2 adsorption is the most convenient, inexpensive method for measuring average crystallite diameter in Ni/SiO_2 and Ni/Al_2O_3 catalysts. X-ray diffraction and Transmission Electron Microscopy are recommended for measurement of nickel particle size in the case of Ni/TiO_2, since H_2 adsorption appears to be suppressed by strong metal-support interactions.

3. Carbon deposition during methanation at high temperatures, high space velocities and low H_2/CO ratios causes significant loss of nickel catalyst activity. For example, Ni/Al_2O_3 loses 20-60% of its activity within 10-15 hours treatment at 673 K, presumably as a result of encapsulation of metal crystallites. Platinum and cobalt promoted nickel are more resistant to deactivation than nickel while molybdenum promoted nickel is less resistant.

4. Nickel and nickel bimetallic catalysts are very sensitive to poisoning by H_2S as evidenced by the complete deactivation during methanation within 2-3 days in the presence of 10 ppm H_2S. Ni-Mo is more resistant to sulfur poisoning than is Ni. The gradual breakthrough of H_2S in in situ runs suggests that less than equilibrium H_2S adsorption occurs under reaction conditions. H_2S apparently competes for adsorption sites with other reacting species. Attempts to regenerate the in situ poisoned catalysts with H_2, H_2/CO and even air are not promising. During treatment with H_2 or H_2/CO at high temperature, there is probably a surface reconstruction or a phase transformation to a totally inactive metal sulfide. Treatment of poisoned catalysts with O_2 partially restores catalyst activity however upon rereduction at high temperatures it is completely lost.

5. Monolithic nickel catalysts are clearly more active and selective for methane production than pellets of comparable nickel loading. The significantly better performance of monolithic catalysts can be attributed to their superior effectiveness and larger mass transfer rates. Accordingly monolithic nickel catalysts are recommended for use in high throughput methanators as they would enable significant savings in capital and operating costs.

6. The combined application of the internal recycle reactor and a washcoated monolithic catalyst enables intrinsic kinetics for an exothermic reaction to be obtained over a relatively wide range of experimental conditions. This powerful tool enabled the kinetics of methanation to be obtained over a wider range of conditions than heretofore studied.

7. The kinetics of CO methanation are not adequately described by a simple power rate law model. A complex Langmuir-Hinshelwood rate expression derived from a sequence of elementary steps involving CO dissociation and hydrogenation of carbon successfully correlates available data.

8. The principal mechanism of catalyst deactivation in high temperature methanation is carbon deposition. This is particularly true in regions of reactant gas compositions that are predicted by thermodynamics to deposit carbon. Addition of steam significantly lowers the rate of deactivation but shifts selectivity in favor of CO_2 at the expense of CH_4 formation. $Ni/NiAl_2O_4$ and $Ni\text{-}MoO_3/Al_2O_3$ are apparently more thermally stable than nickel and comparable with available commercial high temperature catalysts.

9. Rates of poisoning by H_2S of Ni catalysts vary with temperature, H_2S concentration, reactant concentration, and steam concentration. Hence the modeling of sulfur poisoning is difficult, but nevertheless possible under carefully limited conditions.

10. The work described in this report indicates that technical success was largely realized in meeting the objectives of this study. Nevertheless, the most important accomplishment was the training and education of 10 students, including two Ph.D. and three M.S. students.

V. REFERENCES

1. M. Greyson, "Methanation" in "Catalysts" Vol. IV, ed. P. H. Emmett, Rheinhold Pub. Corp., New York (1956).

2. G. A. Mills and F. W. Steffgen, "Catalytic Methanation," Catalysis Review 8, 159 (1973).

3. C. H. Bartholomew, "Alloy Catalysts with Monolith Supports for Methanation of Coal-Derived Gases," Final Technical Progress Report FE-1790-9 (ERDA), (Sept, 6, 1977).

4. W. D. Fitzharris and J. R. Katzer, Ind. Eng. Chem. Fund., 17, 130 (1978).

5. C. H. Bartholomew, "Alloy Catalysts with Monolith Supports for Methanation of Coal-Derived Gases," Quarterly Technical Progress Report FE-2729-1 (DOE), Jan. 5, 1978.

6. C. H. Bartholomew, "Alloy Catalysts with Monolith Supports for Methanation of Coal-Derived Gases," Quarterly Technical Progress Report FE-2729-2 (DOE), April 5, 1978.

7. C. H. Bartholomew, "Alloy Catalysts with Monolith Supports for Methanation of Coal-Derived Gases," Quarterly Technical Progress Report FE-2929-3; July 5, 1978.

8. K. S. Chung, "Effects of H_2S Poisoning on Hydrogen and Carbon Monoxide Adsorption for Alumina-Supported Alloys," M.S. Thesis, Brigham Young University, 1976.

9. D. E. Stowell, "Effects of H_2S Poisoning on Hydrogen and Carbon Monoxide Adsorption for Alumina-Supported Nickel and Ruthenium Alloys," M.S. Thesis, Brigham Young University, 1976.

10. C. H. Bartholomew, "Alloy Catalysts with Monolith Supports for Methanation of Coal-Derived Gases," Annual Report to DOE, FE-2729-4, October 5, 1978.

11. Ibid., Quarterly Report to DOE, FE-2729-5, January 5, 1979.

12. Ibid., Quarterly Report to DOE, FE-2729-6, April 5, 1979.

13. Ibid., Quarterly Report to DOE, FE-2729-7, July 5, 1979.

14. Ibid., Quarterly Report to DOE, FE-2729-8, October 5, 1979.

15. Ibid., Quarterly Report to DOE, FE-2729-9, January 5, 1980.

16. Ibid., Quarterly Report to DOE, FE-2729-10, April 5, 1980.

17. C. H. Bartholomew and R. B. Pannell, "Sulfur Poisoning of H_2 and CO Adsorption on Supported Nickel," Preprints ACS Division of Petr. Chem. 25 (2), 319 (1980).

18. D. G. Mustard, "Metal Particle Size Determination of Supported Nickel Catalysts," M.S. Thesis, Brigham Young University, 1980.

19. C. H. Bartholomew and D. G. Mustard, "Determination of Metal Crystallite Size in Supported Nickel Catalysts," Spring Meeting of the California Catalysis Society, Berkeley, CA, March 13-14, 1980.

20. D. G. Mustard and C. H. Bartholomew, "Determination of Metal Crystallite Size and Morphology in Supported Nickel Catalysts," J. Catalysis, in press.

21. C. H. Bartholomew, G. D. Weatherbee and G. A. Jarvi, "Effects of Carbon Deposits on the Specific Activity of Nickel and Nickel Bimetallic Catalysts," Chem. Eng. Commun. 5, 125 (1980).

22. J. L. Oliphant, R. W. Fowler, R. B. Pannell, and C. H. Bartholomew, "Chemisorption of Hydrogen Sulfide on Nickel and Ruthenium Catalysts, I. Desorption Isotherms," J. Catal. 51, 229 (1978).

23. G. D. Weatherbee, R. W. Fowler and C. H. Bartholomew, "Sulfur Poisoning of Nickel Methanation Catalysts," 71st Annual Meeting of the AIChE, Miami, Nov. 12-16, 1978.

24. C. H. Bartholomew, G. D. Weatherbee and G. A. Jarvi, "Sulfur Poisoning of Nickel Methanation Catalysts, I. In Situ Deactivation by H_2S of Nickel and Nickel Bimetallics, J. Catal. 60, 257 (1979).

25. G. A. Jarvi, K. B. Mayo, and C. H. Bartholomew, "Monolithic Supported Nickel Catalysts: I. Methanation Activity Relative to Pellet Catalysts," 86th National AIChE Meeting, Houston, April 1-5, 1979.

26. G. A. Jarvi, K. B. Mayo, and C. H. Bartholomew, "Monolithic-Supported Nickel Catalyst Nickel Catalysts: I. Methanation Activity Relative to Pellet Catalysts," Chem. Eng. Commun. 4, 325 (1980).

27. E. J. Erekson, "Sulfur Poisoning of Nickel Methanation Catalysts," Ph.D. Dissertation, Brigham Young University, 1980.

28. E. L. Sughrue, II, "Kinetic and Carbon Deactivation Studies of Nickel Methanation Catalysts," Ph.D. Dissertation, Brigham Young University, 1980.

29. J. H. Sinfelt, Chem. Eng. Sci., 23 1181 (1968).

30. D. C. Gardner and C. H. Bartholomew, "Kinetics of Carbon Deposition During Methanation of CO," I & EC Prod. Res. & Develop., in press.

31. D. C. Gardner and C. H. Bartholomew, "A Gravimetric Study of Adsorbed Intermediates in Methanation of CO," Submitted to I & EC Fundamentals, 1980.

32. S. Weller, "Analysis of Kinetic Data for Heterogeneous Reactions," AIChE Journal 2, 59 (1956).

33. V. Ponec, Cat. Rev. Sci. Eng., 11, 41 (1979).

34. E. L. Sughrue and C. H. Bartholomew, "Kinetics of CO Methanation on Nickel Monolithic Catalysts," 73rd National Meeting of the AIChE, Chicago, Ill., Nov. 16-20, 1980.

35. M. A. Vannice, J. Catal. 37, 449 (1975).

36. E. L. Sughrue, E. J. Erekson, and C. H. Bartholomew, "High Temperature Degradation of Methanation Catalysts," 4th Rocky Mountain Fuel Symposium, Salt Lake City, Utah, Feb. 9-10, 1979.

37. E. J. Erekson, E. L. Sughrue, and C. H. Bartholomew, "Catalyst Degradation in High Temperature Methanation," Submitted to Fuel Processing Technology, 1980.

38. J. G. McCarty and H. Wise, J. Catal., 57, 406 (1979).

39. E. L. Sughrue, and C. H. Bartholomew, "Kinetics of Deactivation by Carbon of Monolithic Nickel Catalysts," Paper in preparation, 1980.

40. R. M. Bowman, E. L. Sughrue, and C. H. Bartholomew, "Effects of Carbon Deposits on Activity of Ruthenium Methanation Catalysts," Note in preparation, 1980.

41. E. J. Erekson and C. H. Bartholomew, "Experience with an All-Glass Internal Recycle Reactor," I & EC Fund. 19, 131 (1980).

42. W. D. Fitzharris, "Sulfur Deactivation of Nickel Methanation Catalysts," Ph.D. Dissertation, Univ. of Delaware, 1978.

43. J. R. Rostrup-Nielsen and K. Pedersen, J. Catal. 59, 395 (1979).

44. R. W. Fowler, Jr. and C. H. Bartholomew, "Activity, Adsorption, and Sulfur Tolerance Studies of Fluidized Bed Methanation Catalysts," I & EC Prod. Res. & Devel. 18, 339 (1979).

45. C. H. Bartholomew and J. R. Katzer, "Sulfur Poisoning of Nickel in CO Hydrogenation," International Symposium on Catalyst Deactivation," Antwerp, Belgium, Oct. 13-15, 1980.

46. E. J. Erekson and C. H. Bartholomew, "Sulfur Poisoning of Nickel Methanation Catalysts, II. Effects of H_2S Concentration, Temperature and Support on Deactivation Rates and Adsorption Stoichiometry," Manuscript in Preparation, 1980.

*U.S. GOVERNMENT PRINTING OFFICE: 1980-740-145/882

SATISFACTION GUARANTEED

NTIS strives to provide quality products, reliable service, and fast delivery. Please contact us for a replacement within 30 days if the item you receive is defective or if we have made an error in filling your order.

▲▲ E-mail: info@ntis.gov
▲▲ Phone: 1-888-584-8332 or (703)605-6050

Reproduced by NTIS

National Technical Information Service
Springfield, VA 22161

This report was printed specifically for your order from nearly 3 million titles available in our collection.

For economy and efficiency, NTIS does not maintain stock of its vast collection of technical reports. Rather, most documents are custom reproduced for each order. Documents that are not in electronic format are reproduced from master archival copies and are the best possible reproductions available.

Occasionally, older master materials may reproduce portions of documents that are not fully legible. If you have questions concerning this document or any order you have placed with NTIS, please call our Customer Service Department at (703) 605-6050.

About NTIS

NTIS collects scientific, technical, engineering, and related business information – then organizes, maintains, and disseminates that information in a variety of formats – including electronic download, online access, CD-ROM, magnetic tape, diskette, multimedia, microfiche and paper.

The NTIS collection of nearly 3 million titles includes reports describing research conducted or sponsored by federal agencies and their contractors; statistical and business information; U.S. military publications; multimedia training products; computer software and electronic databases developed by federal agencies; and technical reports prepared by research organizations worldwide.

For more information about NTIS, visit our Web site at **http://www.ntis.gov**.

NTIS

Ensuring Permanent, Easy Access to U.S. Government Information Assets

U.S. DEPARTMENT OF COMMERCE
Technology Administration
National Technical Information Service
Springfield, VA 22161 (703) 605-6000